

**Dissertation zur Erlangung des Doktorgrades der Fakultät für Chemie und  
Pharmazie der Ludwig-Maximilians-Universität München**



**Characterization of novel NADPH oxidases in endothelial cells  
under basal and stress conditions**

Andreas Petry

aus

Berlin

2009

## Erklärung

Diese Dissertation wurde im Sinne von § 13 Abs. 3 bzw. 4 der Promotionsordnung vom 29. Januar 1998 von Frau Prof. Dr. Agnes Görlach betreut und von Frau Prof. Dr. Angelika Vollmar vor der Fakultät für Chemie und Pharmazie vertreten.

## Ehrenwörtliche Versicherung

Diese Dissertation wurde selbständig, ohne unerlaubte Hilfe erarbeitet.

München, am 25.09.2009

---

(Andreas Petry)

Dissertation eingereicht am	25.09.2009
1. Gutachter	Prof. Dr. Angelika Vollmar
2. Gutachter	Prof. Dr. Agnes Görlach
Mündliche Prüfung am	21.10.2009

On ne voit bien qu'avec le Coeur. L'essentiel est invisible pour les yeux.  
*Antoine de Saint-Exupery, Le petit prince*

*for my little godson Laurent-Miguel who shows me  
the beauty of the simple things*

<b>1</b>	<b>INTRODUCTION</b>	<b>1</b>
<b>1.1</b>	<b>Vascular remodeling</b>	<b>1</b>
1.1.1	Structure of the vessel wall	1
1.1.2	Characteristics of vascular remodeling	2
1.1.3	Examples for vascular remodeling	2
1.1.3.1	<i>Pulmonary hypertension</i>	2
1.1.3.2	<i>Atherosclerosis</i>	3
<b>1.2</b>	<b>Role of reactive oxygen species in the vasculature</b>	<b>4</b>
<b>1.3</b>	<b>Structure and function of NADPH oxidases</b>	<b>5</b>
<b>1.4</b>	<b>Endoplasmic reticulum stress and unfolded protein response</b>	<b>9</b>
<b>1.5</b>	<b>Aims</b>	<b>13</b>
<b>2</b>	<b>MATERIAL AND METHODS</b>	<b>14</b>
<b>2.1</b>	<b>Materials</b>	<b>14</b>
2.1.1	Equipment list	14
2.1.2	Chemicals	16
2.1.3	Cell culture reagents	19
2.1.4	Kits	19
2.1.5	Plasticware	19
2.1.6	Bacteria	20
2.1.7	Plasmids	21
2.1.7.1	<i>Overview</i>	21
2.1.7.2	<i>Expression vectors</i>	22
2.1.7.3	<i>Luciferase reporter plasmids</i>	23
2.1.7.4	<i>Gene silencing vectors</i>	24
2.1.8	Oligonucleotides	26
2.1.8.1	<i>Cloning primers</i>	26

2.1.8.2	<i>RT-PCR primers</i>	27
2.1.8.3	<i>qPCR primers</i>	27
2.1.8.4	<i>Sequencing primers</i>	28
2.1.9	DNA modifying enzymes	28
2.1.9.1	<i>DNA polymerase I, large (Klenow) fragment</i>	28
2.1.9.2	<i>Calf alkaline phosphatase</i>	28
2.1.9.3	<i>T4 DNA ligase</i>	28
2.1.10	TOPO cloning	29
2.1.11	Solutions	30
2.1.11.1	<i>Northern blot solutions</i>	30
2.1.11.2	<i>Western blot solutions</i>	32
2.1.11.3	<i>Solutions and media for molecular biology</i>	34
2.1.11.4	<i>Solutions for luciferase reporter gene assay</i>	35
2.1.11.5	<i>Solutions for immunofluorescence and immunohistochemistry</i>	36
2.1.11.6	<i>Solutions for cell culture</i>	36
2.1.12	Antibodies	36
2.1.12.1	<i>Primary antibodies</i>	37
2.1.12.2	<i>Secondary antibodies</i>	38
<b>2.2</b>	<b>Methods</b>	<b>39</b>
2.2.1	Cell biology methods	39
2.2.1.1	<i>Cells</i>	39
2.2.1.2	<i>Storage of the cells</i>	41
2.2.1.3	<i>Transfection of endothelial cells</i>	41
2.2.1.4	<i>Transfection of HEK293 and HeLa cells</i>	42
2.2.1.5	<i>Luciferase Assay</i>	43
2.2.1.6	<i>DCF fluorescence measurement</i>	44
2.2.1.7	<i>Dihydroethidium fluorescence measurement</i>	46
2.2.1.8	<i>Bimolecular fluorescence complementation (BiFC)</i>	46
2.2.1.9	<i>Proliferation assay with BrdU incorporation</i>	47
2.2.1.10	<i>In vitro matrigel angiogenesis assay</i>	48
2.2.1.11	<i>Immunofluorescence</i>	50

2.2.1.12	<i>Immunohistochemistry</i>	50
2.2.2	RNA-Methods	51
2.2.2.1	<i>Preparation of total RNA</i>	51
2.2.2.2	<i>Northern blot</i>	52
2.2.2.3	<i>cDNA synthesis from RNA</i>	53
2.2.3	DNA Methods	54
2.2.3.1	<i>Polymerase chain reaction (PCR)</i>	54
2.2.3.2	<i>Real time PCR</i>	57
2.2.3.3	<i>DNA Sequencing</i>	57
2.2.3.4	<i>Agarose gel electrophoresis</i>	60
2.2.3.5	<i>Restriction digest</i>	61
2.2.3.6	<i>DNA ligation</i>	62
2.2.3.7	<i>Preparation of chemical competent bacteria</i>	63
2.2.3.8	<i>Chemical transformation</i>	63
2.2.4	Protein methods	64
2.2.4.1	<i>Protein isolation</i>	64
2.2.4.2	<i>Subcellular cell fractionation</i>	65
2.2.4.3	<i>Protein quantification after Bradford</i>	65
2.2.4.4	<i>SDS-PAGE and Western blot analysis</i>	66
2.2.4.5	<i>Stripping and reprobing</i>	67
2.2.4.6	<i>Coimmunoprecipitation</i>	67
2.2.5	Statistical analysis	68
<b>3</b>	<b>RESULTS</b>	<b>69</b>
<b>3.1</b>	<b>Expression and localization</b>	<b>69</b>
3.1.1	Expression of NOX1, NOX2, NOX4, p22phox in endothelial cells	69
3.1.2	Expression of NOX5 variants in endothelial cells.	69
3.1.3	Expression of NOXA1 and NOXO1 in endothelial cells	74
3.1.4	Localization of NOX2, NOX4, NOX5, but not of NOX1 in the endoplasmic reticulum of endothelial cells	76

<b>3.2</b>	<b>Interaction of NOX2, NOX4, NOX5S and NOX5<math>\beta</math> with p22phox and contribution to basal endothelial ROS generation</b>	<b>79</b>
3.2.1	Interaction of NOX2, NOX4, NOXS and NOX5 $\beta$ with p22phox	79
3.2.2	Contribution of p22phox, NOX2, NOX4 and NOX5 to endothelial ROS generation	84
3.2.3	Contribution of NOX2, NOX4 and NOX5 to basal endothelial proliferation	89
3.2.4	The p38 MAP kinase contributes to the proliferative response mediated by NOX2 and NOX4	91
3.2.5	Influence on ROS generation and proliferation by NOX1 is limited in endothelial cells under basal conditions	92
<b>3.3</b>	<b>Function and regulation of NADPH oxidases in thrombin and endoplasmic reticulum stress activated endothelial cells</b>	<b>93</b>
3.3.1	Contribution of NOX2 and NOX5 to thrombin-induced endothelial ROS generation and cell proliferation	93
3.3.2	Regulation of NADPH oxidase subunits by endoplasmic reticulum stress	94
3.3.3	Regulation of p22phox upstream enhancer element activity by ATF4, XBP1 and ER-stress in endothelial cells	102
<b>4</b>	<b>DISCUSSION</b>	<b>105</b>
4.1	Expression of NOX2, NOX4, NOX5, p22phox in endothelial cells	105
4.2	Expression of NOX1, NOXA1 and NOXO1 in endothelial cells	108
4.3	NOX1, NOX2, NOX4 and NOX5 localization and interaction with p22phox	110
4.4	Contribution of p22phox, NOX2, NOX4 and NOX5 to endothelial ROS generation and proliferation	113
4.5	Regulation of NADPH oxidase subunits NOX2 and NOX5 by thrombin	117
4.6	Regulation of the NADPH oxidase subunit p22phox by ER-stress	118
4.7	Conclusion	123

<b>5</b>	<b>SUMMARY</b>	<b>125</b>
<b>6</b>	<b>REFERENCES</b>	<b>127</b>
<b>7</b>	<b>APPENDIX</b>	<b>134</b>
7.1	Abbreviations	134
7.2	List of figures	139
7.3	Curriculum vitae	142
7.4	Publications	145
7.5	Acknowledgements	149
7.6	Overview of used cloning PCR programs	151

# 1 Introduction

## 1.1 Vascular remodeling

The vessel wall is composed of the intima formed by the endothelial cells, the media built of vascular smooth muscle cells (VSMC) and the outer adventitia containing fibroblasts and extracellular matrix [1].

### 1.1.1 Structure of the vessel wall

The endothelial cells form the inner monolayer of a vessel, the intima. As the only cells of the vasculature, the endothelial cells have direct contact to the blood in the vessel. The endothelium not only provides a barrier between blood and underlying cell layers, but also plays a role in the regulation of the vascular tone. Endothelial cells secrete vasodilating substances such as nitric oxide (NO) or prostacyclin (PGI<sub>2</sub>) as well as vasoconstricting substances like platelet activating factor (PAF) and endothelin-1. The endothelium also regulates the traffic of the cellular elements in the blood, like erythrocytes, thrombocytes and leukocytes through interaction of these cells with endothelial cellular adhesion molecules at the surface of the endothelium.

VSMCs form the media of the vessel wall. They regulate the vessel tone, the blood pressure and the distribution of the blood flow. Although the VSMC have the ability to proliferate, under physiological conditions the proliferation as well as the metabolic rates are very low.

The outer layer of the vessel contains fibroblasts and extracellular matrix forming a very stable fibrous connective tissue. Its main function is the stabilization of the vessel under varying pressure.

### **1.1.2 Characteristics of vascular remodeling**

Structural changes in the three layers of the vessel wall are generally designated as vascular remodeling. Thereby, changes in cellular proliferation, in cell migration and apoptosis as well as changes in the composition of the extracellular matrix occur. Besides physiological vascular remodeling which takes place during embryonic development and vasculogenesis, vascular remodeling is also associated with a variety of diseases like atherosclerosis, ischemic diseases, systemic and pulmonary hypertension and tumor growth [2, 3].

One of the first events in pathophysiological vascular remodeling is an endothelial dysfunction which is associated with a decrease in NO availability leading to a change in the vascular tone due to increased contractility of the smooth muscle cells [4]. This change in the vascular tone can subsequently activate the endothelium resulting in the recruitment of leukocytes und inflammatory processes. Damage of the endothelium can lead to the coagulation cascade and the formation of thrombin. Subsequently VSMC become activated, which results in a change in their phenotype. They proliferate and synthesise growth factors and components of the extracellular matrix, which can lead to a thickening of the media.

### **1.1.3 Examples for vascular remodeling**

#### ***1.1.3.1 Pulmonary hypertension***

One pathological process accompanied by strong vascular remodeling is pulmonary hypertension [2]. Pulmonary hypertension is characterized by a thickening of the smooth muscle cell layer. Consequently, the vessels become stiff and show increased vasoconstriction. This eventually results in the elevation of pulmonary artery pressure and pulmonary vascular resistance and can subsequently cause heart right ventricle hypertrophy and failure. Pulmonary hypertension is also often

associated with the formation of so called plexiform lesions [5]. In this case disordered proliferation and migration of endothelial cells take place together with neoangiogenesis. Smooth muscle cells transdifferentiate into myofibroblasts altogether forming the plexiform lesions and finally resulting in luminal narrowing.

### 1.1.3.2 Atherosclerosis

Another disease accompanied by vascular remodeling is atherosclerosis characterized by a strong decrease of the vessel lumen due to the formation of an atherosclerotic plaque (Fig. 1). Rupture of this plaque can lead to thrombosis and subsequently to stroke or heart failure [6]. A lesion in the endothelium leads to recruitment of thrombocytes, T-lymphocytes and monocytes, the latter can transform into foam cells by uptake of low density lipoproteins (LDL) and oxidized LDL (oxLDL) [7]. Growth factors and cytokines released by foam cells as well as blood-borne factors like thrombin lead to VSMC proliferation and migration. Activated VSMC form together with foam cells then so called fatty streaks.

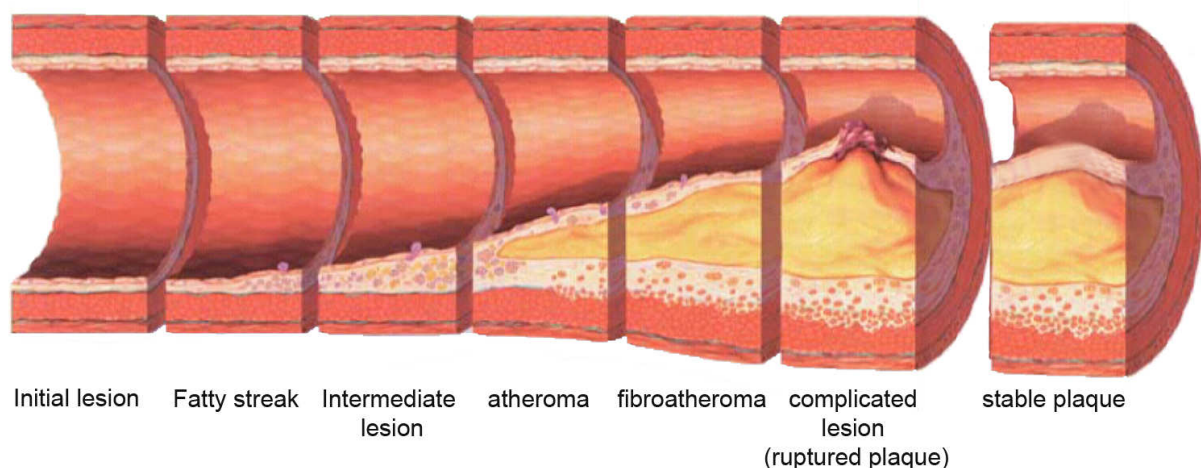


**Fig. 1 Schematic overview about the progression of atherosclerosis.**

Starting from early stages (fatty streaks) atherosclerosis progresses by continued inflammatory processes and lipid accumulation to early atherosclerotic lesions finally resulting into either rupture of the plaque or plaque stabilization (modified from [http://en.wikipedia.org/wiki/File:Endo\\_dysfunction\\_Athero.PNG](http://en.wikipedia.org/wiki/File:Endo_dysfunction_Athero.PNG), used under the GNU Free Documentation License).

Continued lipid uptake and proliferation then finally result in advanced lesions with a fibrous cap sealing off the plaque. The cap can either become thick, stabilizing the plaque, or can rupture, exposing the plaque content to the blood and resulting in a platelet aggregation and clot formation.

## 1.2 Role of reactive oxygen species in the vasculature

Reactive oxygen species (ROS) have been originally described as cytotoxic molecules responsible for bacterial killing in host defense produced by phagocytic cells including neutrophils, monocytes and macrophages [8, 9]. These species include superoxide anion radicals ( $O_2^{\cdot-}$ ), hydrogen peroxide ( $H_2O_2$ ) and hydroxyl radicals ( $OH\cdot$ ). Single electron reduction of molecular oxygen results in superoxide anion radical formation. Although this highly reactive molecule is membrane impermeable, it can use anion channels in the cell membranes for transmigration [10, 11]. Spontaneously or catalyzed by the superoxide dismutase (SOD), superoxide anion radicals are transformed into  $H_2O_2$ , which is less reactive than superoxide anion radicals. On the other hand,  $H_2O_2$  diffuses more easily and has a longer half life time than  $O_2^{\cdot-}$ .  $H_2O_2$  is then either enzymatically metabolized by catalase or glutathione-peroxidase (GPx) or is converted in a Fenton reaction with transition metals like ferrous ions ( $Fe^{2+}$ ) into highly reactive hydroxyl radicals. Superoxide anion radicals can also react with NO, which is produced in endothelial cells by NO synthase, forming peroxynitrite leading to a decrease in the NO bioavailability (Fig. 2). More recently, it has been appreciated that also non-phagocytic cells, including vascular cells, can produce ROS at low levels which play a role as signaling molecules in a wide spectrum of physiological and pathophysiological responses [12], including endothelial dysfunction, vascular remodeling and atherosclerosis. In endothelial cells, low levels of ROS appeared to be required for proliferation and

growth and to be implicated in tube formation and angiogenesis [13, 14]. Exposure to higher doses of ROS can also elicit an apoptotic response, modulate vascular tone, impair the endothelial barrier functions, promote thrombosis and mediate vascular remodeling processes [15-17]. Increased and sustained production of ROS is associated with the pathogenesis of various cardiovascular diseases including diabetes, hypertension, atherosclerosis, heart failure and ischemia reperfusion [16-18].

### 1.3 Structure and function of NADPH oxidases

The structure and function of the NADPH oxidase were primarily described in neutrophils, where it is composed of the two membrane-bound subunits p22phox and NOX2 – previously known as gp91phox forming the flavocytochrome b558 as the catalytic core of the NADPH oxidase [8, 19, 20]. Other important components are the cytosolic subunits p40phox, p47phox, p67phox and the small GTP-binding protein Rac. Dormant in resting neutrophils, p47phox becomes phosphorylated after stimulation with pathogens like bacterial lipopolysaccharids [20, 21]. This phosphorylation leads to a change in their conformation and subsequently

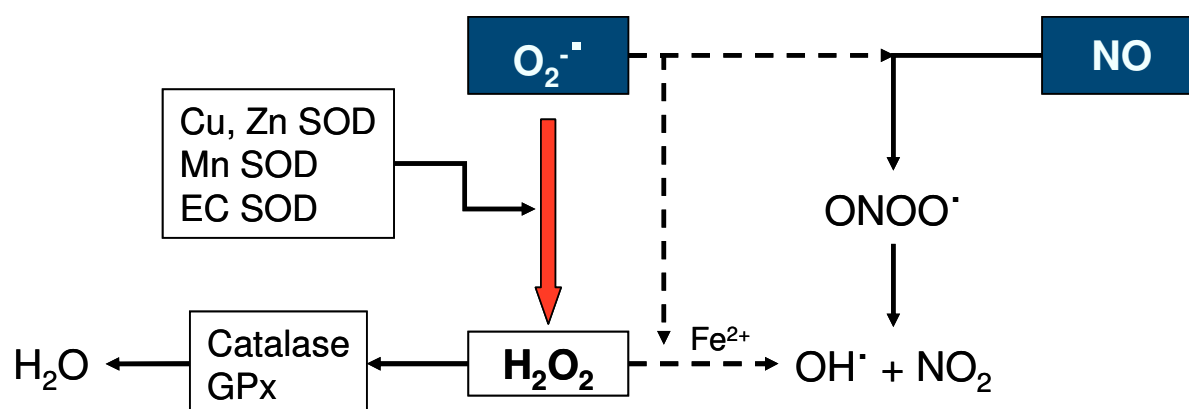


**Fig. 2** Reactive oxygen and reactive nitrogen species in vascular cells.

Schematic overview of reactive oxygen and nitrogen species in the vasculature. SOD: superoxide dismutase. Cu (II): Copper II ions as cofactor for SOD. GPx: Glutathione peroxidase. Fe(II) Iron II ions as cofactor for the GPx. (adapted from [22])

translocation and association with the flavocytochrome b558 at the membrane. In addition, loading of Rac with GTP and interaction of active Rac with p47phox and p67phox triggers the translocation of Rac to the flavocytochrome b558 at the flavocytochrome b558 in the right direction for electron transfer [23, 24]. The finally activated oxidase releases large amounts of superoxide in the well characterized respiratory burst (Fig. 3).

The physiological significance of the phagocytic NADPH oxidase is illustrated by chronic granulomatous disease (CGD) caused by mutations in any of the genes encoding gp91phox, p22phox, p47phox or p67phox subunits of the NADPH oxidase. Phagocytes of patients suffering from CGD are unable to produce  $O_2^-$ , and these patients are therefore highly susceptible to bacterial and fungal infections. The other membrane-bound component of the flavocytochrome b558, p22phox, is a 22-kDa membrane protein. As described, p22phox forms together with NOX2 the catalytical core of the phagocytic NADPH oxidase [25, 26]. Moreover, upon stimulation,

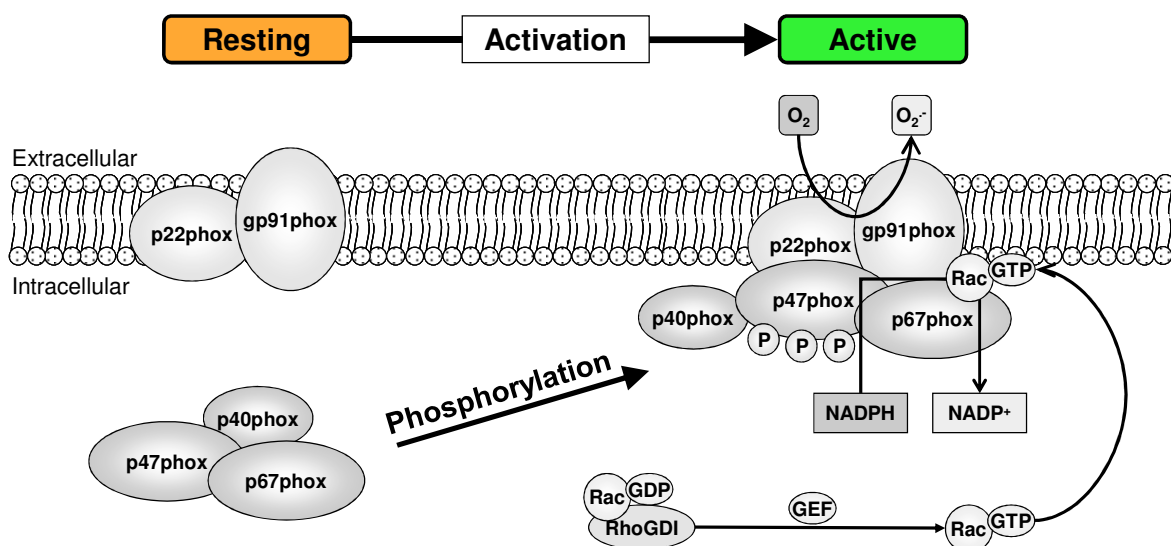


**Fig. 3 Schematic overview of the structure and activation of the phagocytic NADPH oxidase.**

In resting phagocytic cells, gp91phox forms together with p22phox a membrane bound flavocytochrome b558. The cytosolic factors p40phox, p47phox and p67phox form a cytosolic complex. In activated phagocytic cells, the cytosolic complex translocates to the membrane upon phosphorylation of p47phox. Activation of Rac leads to the fully activation of the NADPH oxidase.

p22phox binds to p47phox to assemble the active oxidase [20]. Expression of p22phox is ubiquitous and has been shown in all vascular cell types underlining the essential function of this component for the assembly and activation of NADPH oxidases. Interestingly, several polymorphisms in the p22phox gene were identified. A polymorphism in the p22phox promoter revealed higher promoter activity and has been associated with hypertension [27]. Furthermore, increased levels of p22phox and other NADPH oxidase subunits have been identified in the vascular wall after balloon angioplasty, as well as in atherosclerosis, hypertension, diabetes and other disorders and have been associated with elevated ROS levels in these disorders [18, 28-31].

Recently, a NOX2-containing NADPH oxidase has been described to be functionally active in endothelial cells together with the other components of the neutrophil enzyme, which have also been identified in these cells [32, 33]. In contrast to neutrophils, endothelial cells produce ROS already under basal conditions. Exposure of endothelial cells to different stimuli including endothelin-1 (ET-1), angiotensin-II (AngII), tumor necrosis factor  $\alpha$  (TNF $\alpha$ ), thrombin, platelet-derived growth factor (PDGF), insulin growth factor-1 (IGF-1), interleukin-1  $\alpha$  (IL1- $\alpha$ ), vascular endothelial growth factor (VEGF), transforming growth factor- $\beta$  (TGF- $\beta$ ), LDL or oxLDL, results in ROS production [34-37]. However, ROS levels achieved in vascular cells are significantly lower than in leukocytes, suggesting that important differences exist between neutrophil and endothelial NADPH oxidases, for example expression levels or functional regulation [32]. In recent years, homologues of NOX2 (NOX1-NOX5) as well as homologues of p47phox (p41nox or NOXO1) and p67phox (p51nox or NOXA1) were discovered to be expressed in different cell types including vascular cells suggesting the presence of different NADPH oxidase forms in these cells (Fig. 4, 5) [8, 38, 39]. In addition to the NOX2-containing NADPH oxidase, NOX4 has

been recently found to be expressed in certain types of endothelial cells suggesting that it may play a role in endothelial ROS generation [40]. Interestingly, high levels of NOX2 mRNA have been found in veins whereas the amount of NOX4 mRNA was found to be elevated in arteries compared to veins suggesting that the abundance and the potential functional role of the NOX proteins may also differ in different vascular beds [29]. Only very recently, NOX1 has been detected in certain endothelial cells [41, 42]. However, it is unclear whether its cofactors NOXO1 and NOXA1 are expressed in endothelial cells. So far, NOX3 has been only found in the inner ear [43, 44] and fetal tissue. NOX5 has been described to contain an amino terminal calmodulin-like domain with four binding sites for calcium (EF hands) [45]. In addition, two related proteins, called DUOX1 and DUOX2, mainly expressed in thyroid tissue, have NOX-homologous regions as well as regions with peroxidase activity [20, 46]. It has been suggested for NOX5 that calcium-binding induces a conformational change to intramolecular interactions between the N-

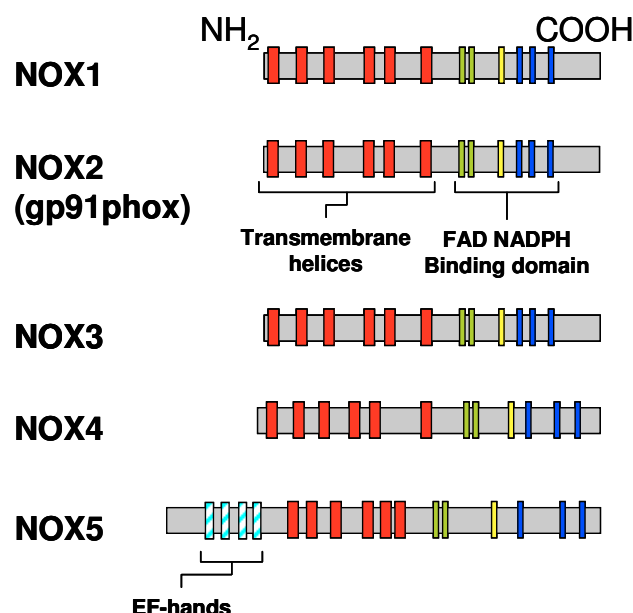


**Fig. 4 Schematic overview of the NOX homologues NOX1 to NOX5.**

Simplified structures of the NOX homologues NOX1 to NOX5 showing homologue domains. Red: transmembran helix. Green: FAD binding domain. Blue: NADPH binding domain. EF-hands: calcium-binding motives.

terminus and the C-terminal catalytic domain which may result in enhanced ROS production upon addition of free calcium or ionomycin [45, 47]. To date four splice variants named NOX5 $\alpha$ , NOX5 $\beta$ , NOX5 $\gamma$  and NOX5 $\delta$  (GenBank<sup>TM</sup> AF353088, AF325189, AF353089 and AF325190, respectively) which differ in the sequence of their EF hands, have been described [45]. NOX5 $\alpha$  was found in spleen and NOX5 $\beta$  in testis [45] whereas the cellular presence of NOX5 $\gamma$  and NOX5 $\delta$  has not been shown, yet. In addition, expression of NOX5 protein has been described in a prostate carcinoma cell line [48] and in malignant B-cell hairy leukemic cells [49], while NOX5 mRNA was found in the stomach [50] as well as in cardiac fibroblasts [51].

#### 1.4 Endoplasmic reticulum stress and unfolded protein response

Most of the newly discovered homologues to NOX2 (NOX1 - 5) have been associated with intracellular membrane systems, especially the endoplasmic reticulum (ER) [52-56]. There is evidence for the interaction between NOX1 and NOX4 with the protein disulfide isomerase (PDI), an ER-localized thiol oxidoreductase assisting in redox protein folding [56-58].

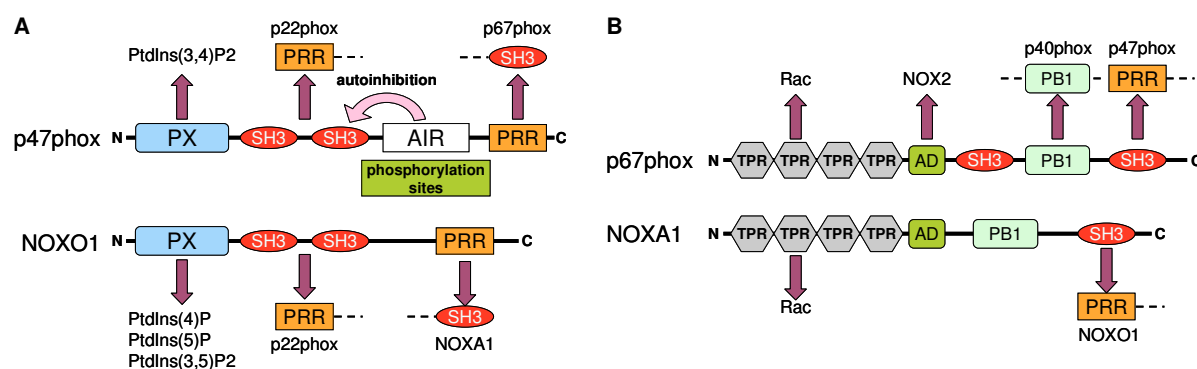


**Fig. 5 Schematic overview of NOXO1 and NOXA1 in comparison with their homologues p47phox and p67phox.**

A. Schematics of p47phox and NOXO1. NOXO1 is lacking the autoinhibitory region (AIR) of p47phox. B. Schematics of p67phox and NOXA1. NOXA1 is lacking the N-terminal located SH3 domain. PX: phosphoinositide binding domain; SH3: Src homology 3 domain; AIR: autoinhibitory region; PRR: proline rich region; TPR: tetratricopeptide repeat; AD: activating domain; PB1: Phox and Bem1 domain (adapted from [59]).

Pathophysiological processes such as atherosclerosis are associated with the accumulation of oxysterols which induces ER-stress, which is characterized by a disturbance in the normal ER function leading to an accumulation of mis- or unfolded proteins, and triggers the unfolded protein response (UPR) (Fig. 6) [16, 55, 60]. The UPR is characterized by a general attenuation in protein synthesis with a simultaneous increase in UPR genes such as specific transcription factors, chaperones and proteins of the protein degradation machinery for an increased ER-associated degradation of proteins. Prolonged UPR results finally in apoptosis [61, 62]. ER-stress is associated with an accumulation of misfolded proteins. This accumulation results in an increased binding of the binding protein (BiP or GRP78) to these proteins. Under physiological conditions, BiP is bound to the PRKR-like endoplasmic reticulum kinase (PERK), the ER-membrane located inositol requiring element 1 (IRE1) and the activating transcription factor 6 (ATF6) inhibiting their

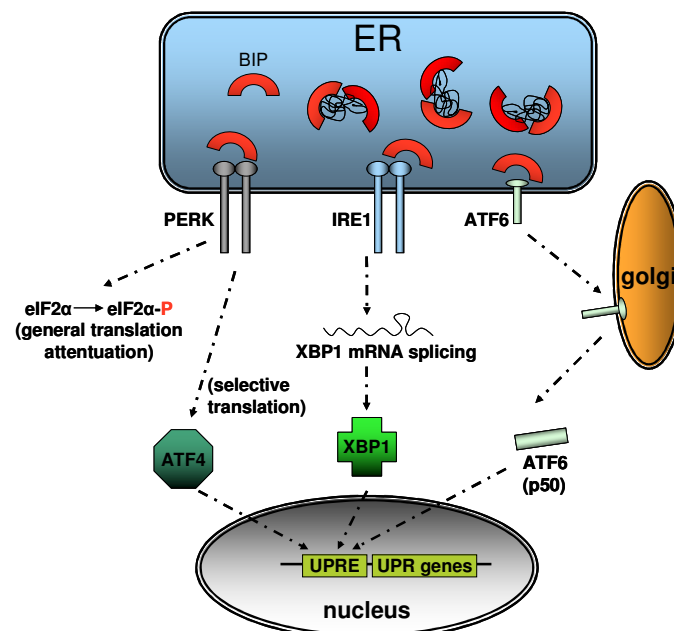


**Fig. 6 Schematic overview of the unfolded protein response (UPR).**

Accumulation of unfolded proteins leads to higher requirement of BiP leading to the activation of the kinase PERK, IRE1 and ATF6. PERK activation leads to increased ATF4, IRE1 activation to increased XBP1 activation. ATF4, XBP1 and ATF6 binds to UPR elements in UPR-gene promoters (adapted from <http://biochemistry.utoronto.ca/volchuk/images/UPR.jpg>).

activation. Dissociation of BiP activates PERK, IRE1 and ATF6. Under non-stress conditions, ATF6 is anchored in the ER-membrane by an N-terminal transmembrane domain. Upon ER-stress, ATF6 translocates to the Golgi compartment, where the active cytosolic part is released. It travels to the nucleus activating the transcription of UPR genes including the X-box binding protein 1 (XBP1) [62]. The ER-transmembrane glycoprotein IRE1 contains both kinase and RNase activities in the cytoplasmic domain. ER-stress leads to autophosphorylation and activation of IRE1 RNase activity which initiates the splicing of XBP1 mRNA generating a mature XBP1 mRNA to be translated (Fig. 7A). This splice variant of XBP1 is a potent transcription factor whereas the product of the unspliced mRNA has been suggested to inhibit transcription [61, 62]. XBP1 induces UPR genes including PDI. The ER transmembrane protein kinase PERK phosphorylates the  $\alpha$ -subunit of the translation initiation factor 2 (eIF2 $\alpha$ ) leading to reduced formation of translation initiation complexes and subsequently general attenuation of translation.

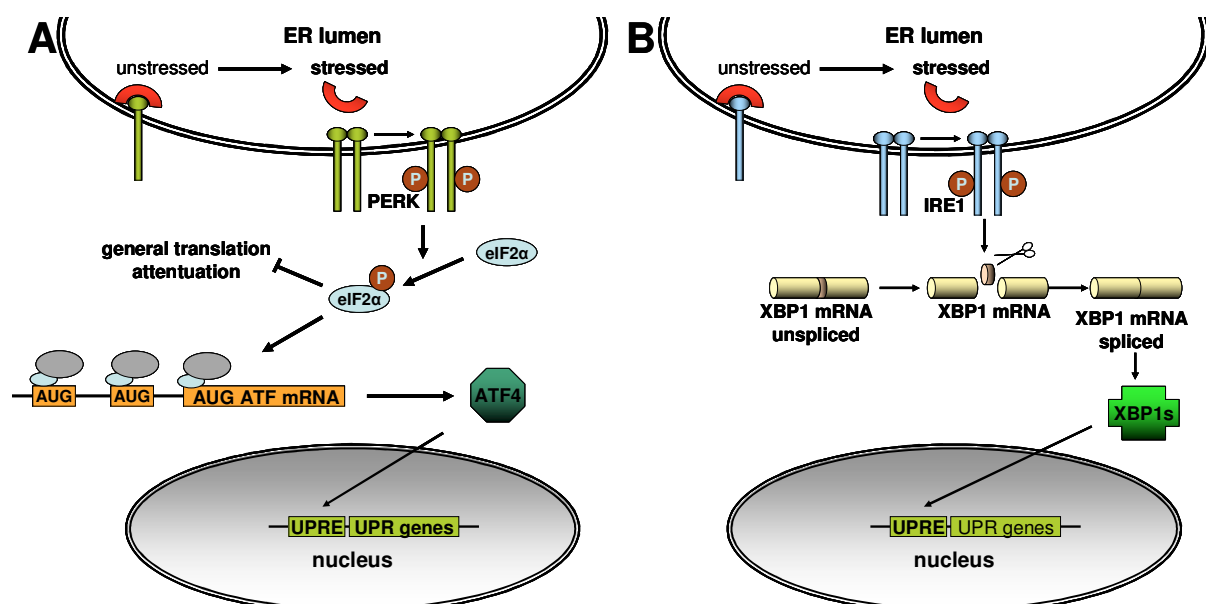


**Fig. 7** Activation of ATF4 and XBP1 by unfolded protein response.

A. Activation of ATF4 expression by ER-stress. PERK getting activated and phosphorylates eIF2 $\alpha$  leading to an increase in ATF4 translation. B. ER-stress leads to activation of IRE1. IRE1 processes specifically the mRNA of XBP1. Spliced XBP1 mRNA is translated into the active form of XBP1 whereas unspliced XBP1 mRNA is translated into an inactive protein (adapted from [63]).

Paradoxically, translation of mRNAs having a lower requirement for eIF2 $\alpha$  and the translational initiation complex are enhanced including the activating transcription factor ATF4 which induces UPR genes (Fig. 7B) [62]. Prolonged ER-stress leads to a phosphorylation cascade initiated by IRE1 resulting in activation of JNK and mitochondria/Apaf1-dependent caspases ending in apoptosis. This process has been associated with ROS and NOX4 expression has been recently associated with this response in SMCs [55].

## 1.5 Aims

Although initial evidences have been provided that a NOX2 containing NADPH oxidase is expressed and functionally active in endothelial cells, the differential expression and potential functions of the novel NOX homologues have not been fully understood. Thus the overall aim of this study was to better characterize the expression, regulation and function of NOX homologues (NOX1 – NOX5) in different endothelial cell models. The hybridoma cell line Ea.Hy926 which is derived from human umbilical vein endothelial cells fused with the lung carcinoma cell line A549 was used as a model for endothelial cells from larger vessels. In contrast, human microvascular endothelial cells HMEC1 were used as a model for endothelial cells from smaller, capillary vessels.

Hereby, specific aims were formed:

1. It was aimed to analyze the expression levels of NOX1, NOX2, NOX4 and NOX5 and their interaction with p22phox as well as the expression levels of the p47phox and p67phox homologues NOXO1 and NOXA1 in human endothelial cells.
2. It was aimed to characterize the functional role of the NOX homologues in endothelial cells, specifically to analyze their contribution to the basal ROS production and proliferation.
3. Since ER-stress and thrombin induced cellular stress have been associated with increased ROS generation, it was aimed to investigate whether NOX1, NOX2, NOX4, NOX5 as well as p22phox participate in cellular stress induced by thrombin, tunicamycin or thapsigargin.

## 2 Material and Methods

### 2.1 Materials

#### 2.1.1 Equipment list

<u>Device</u>	<u>Product name</u>	<u>company</u>
Analytical balance	B 301 S	Sartorius
Autoclave big	KSG 116-2-ED	KSG
Autoclave small	KSG 25-2-3	KSG
Balance	BP 4100 S	Sartorius
Bunsen burner	Vulcan	Heraeus
Centrifuges	Biofuge fresco	Heraeus
	Biofuge pico	Heraeus
	Biofuge stratos	Heraeus
	Megafuge 1.0 R	Heraeus
	Varifuge 3.0 R	Heraeus
Deep-freezer (-70 °C)	Hera freeze	Heraeus
Fluorescence microscope	IX50	Olympus
	Hg-Lamp U-RFL-T	Olympus
	Camera Controller	Hamamatsu
	Filtermodule improvisation	improvisation
	Orbit	
	Hg-Lamp U-RFL-T	Olympus
Liquid-N <sub>2</sub> -Dewar	Locator 6 Plus	Thermolyne
Freezer (-20 °C)	comfort	Liebherr
Freezer big (-20 °C)	comfort	Liebherr
Fridge big	profi line	Liebherr
Fridge small	Premium	Liebherr
Fridge-freezer combination		Liebherr
Gel documentation system	Gel Doc 2000	BioRad
Heating block	Thermomixer comfort	Eppendorf
Heatingplate	CM1850	Leica

Hybridization oven	Herahybrid 12	Heraeus
Hypoxia bench	Hypoxia Workstation	IUL Instruments
Incubator	Hera Cell	Heraeus
Incubator	Binder	WTC Binder
Isopropanol freezing box	Qualifreeze	Qualilab
Laboratory dishwasher	G7783CD Mielabor	Miele
laminar airflow cabinet (hood)	Hera Safe	Heraeus
Luminometer	AutoLumat plus	Berthold Technologies
Magnetic stirrer with heater	MR3001	Heidolph
Magnetic stirrer without heater	MR3000	Heidolph
Microscope	HAL 100	Zeiss
Microscope	Axiovert 25	Zeiss
Microwave		Whirlpool
Millipore water supply	Milli-Q synthesis	Millipore GmbH
Mini-table-top-centrifuge	Capsulefuge PMC-060	TOMY
pH Meter	pH 540 GLP	WTW
Photometer	U-2001	Hitachi
	Spectrophotometer	
Platereader	Tecan Safire	Tecan
Power supplies	Power Pac 200	BioRad
	Power PAC 300	BioRad
	Power Pac 3000	BioRad
Pump	CVC 2000	vacuubrand
Roller mixer	RM5 Assistent	Karl Hecht KG
Rotator		Fröbel Labortechnik GmbH
SDS-PAGE hardware	Mini-Protean 3	BioRad
Shaker	Duomax 1030	Heidolph
	IKA-Schüttler MTS2 electronic	IKA-Werke
	Polymax 1040	Heidolph
Shaker-incubator	C24 Incubator Shaker	New Brunswick

Stand-dewar		Scientific
Thermocycler	iCycler	KGW Isotherm
	PCR System 9700	BioRad
	Rotor-Gene 6000	PE Applied Biosystems
	SDS 7700	Corbett
Transfer hardware	Mini Protean 3	Applied Biosystems
UV-Stratalinker	Stratalinker 1800	BioRad
Vacuum pump		Stratagene
Vortexer		Neuberger
	Reax top	Heidolph
	Vortex-Genie 2	Scientific Industries
Water bath	Grant	SUB
	“no name”	Memmert

### 2.1.2 Chemicals

<b><u>Name</u></b>	<b><u>Company</u></b>
Acetic acid	Carl Roth GmbH
Actinomycin D	Sigma
Agar	Carl Roth GmbH
Agarose NEEO Ultra quality	Carl Roth GmbH
Alamar Blue	Biosource
Ammonium persulfate	Carl Roth GmbH
Ampicillin	Calbiochem
Amidoblack	Carl Roth GmbH
BAPTA	Sigma
Bovine serum albumin	Sigma
Brilliant Blue G250	Carl Roth GmbH
Calciumchlorid-Dihydrate	Merck
Chloroform	Merck
Coumaric acid	Sigma
DCF	MoBiTec /Invitrogen
Diethylpyrocarbonate (DEPC)	Carl Roth GmbH
diaminobenzidine	Sigma

Dihydroethidium (DHE)	MoBiTec /Invitrogen
Dimethylsulfoxide (DMSO)	Carl Roth GmbH
Dithiothreitol (DTT)	Carl Roth GmbH
Ethylene diamine tetraacetic acid (EDTA)	Carl Roth GmbH
Ethylene glycol tetraacetic acid (EGTA)	Carl Roth GmbH
Ethanol	Merck
Ethidium bromide	Carl Roth GmbH
Formaldehyde 37%	Merck
D-(+)-glucose	Sigma
Glycine	Carl Roth GmbH
Glycerol	Carl Roth GmbH
Guanidinethiocyanate	Carl Roth GmbH
Hank's balanced salt solution (HBSS)	Gibco
Hydrochloric acid	JT Baker
Hydrogen peroxide	Merck
Igepal CA-630	Sigma
Ionomycine	Sigma
Isoamylalcohol	Merck
Isopropanol	JT Baker
Kanamycine sulfate	Calbiochem
Lucigenin	Sigma
Luminol	Sigma
Magnesium carbonate hydroxide	Sigma
Magnesium chloride-hexahydrate	Carl Roth GmbH
Magnesiumsulfat-heptahydrat	Applichem
Maleic acid	Sigma
Manganese-(II)-chloride	Merck
Mayer's hemalum solution	Merck
$\beta$ -mercaptoethanol	Carl Roth GmbH
3-(N-morpholino)propanesulfonic acid (MOPS)	Carl Roth GmbH
N-nitro-L-arginine	Calbiochem
Non-fat dry milk powder	Merck
PBS-tablettes	GibCo /Invitrogen
Phenylmethanesulfonyl fluoride (PMSF)	Sigma

Ponceau S	Carl Roth GmbH
Potassium acetate	Merck
Potassium carbonate	Merck
Potassium chloride	Merck
Potassium dihydrogene Phosphate	Merck
Potassium hydrogencarbonate	Merck
Potassium hydroxide	Carl Roth GmbH
Phorbol 12-myristate 13 Acetate	Sigma
Roti-aqua-phenol	Carl Roth GmbH
Rotiphorese gel 30%	Carl Roth GmbH
P38 MAP kinase inhibitor (SB202190)	Calbiochem
SDS ultra pure	Carl Roth GmbH
Sodium acetate	Merck
Sodium chloride	Carl Roth GmbH
Sodium citrate	Carl Roth GmbH
Sodium dihydrogen phosphate	Sigma
Sodium fluoride	Merck
Sodium orthovanadate	Merck
Sucrose	Sigma
Sulfuric acid	Carl Roth GmbH
TEMED	Carl Roth GmbH
Thapsigargin	Sigma
Thrombin	Haemochrom Diagnostik
Tricine	Carl Roth GmbH
Trifluoroacetic acid	Sigma
Tris ultra	Carl Roth GmbH
Triton <sup>®</sup> X-100	Sigma
Trypan blue (C.I. 23850)	Merck
Tryptone	Carl Roth GmbH
Tunicamycin	Sigma
Tween <sup>®</sup> 20	Sigma
Vitamin C	Sigma
Xylenecyanol	Carl Roth GmbH
Yeast extract	Carl Roth GmbH

### 2.1.3 Cell culture reagents

#### **Cell culture media and additives**

	<b><u>Company</u></b>
Dulbecco's Modified Eagle Medium (DMEM)	Gibco, PAA
Fetal calf serum (FCS)	Pan Biotech
HAT supplement	Gibco
MCDB 131 medium	Gibco
Endothelial basal medium	PAA
Penicillin / streptomycin	Gibco
SmBm-2 medium	Cambrex / Lonza
SmGm-2 single Quot	Cambrex / Lonza
Trypsin-EDTA	Gibco, PAA
PBS	PAA
HBSS with Mg/Ca	Gibco, PAA

### 2.1.4 Kits

<b><u>Name</u></b>	<b><u>Company</u></b>
ABI PRISM BigDye Terminator v1.1 Cycle Sequencing Kit	Applied Biosystems
BrdU proliferation assay	Roche
Jetstar Plasmid Maxi Kit	Genomed
Nucleo Seq sequencing clean-up kit	Macherey-Nagel
Qiagen RNeasy Mini Kit	Qiagen
Qiagen Plasmid Maxi Kit	Qiagen
siSTRIKE™U6 Hairpin Cloning System (Human)-Neomycin	Promega
SuperScript™III Reverse Transcriptase	Invitrogen
Expand High FidelityPLUS PCR System	Roche
Phusion™ High-Fidelity DNA Polymerase	NewEngland Biolabs
qPCR MasterMix (Plus) for SYBR® green I	Eurogentec

### 2.1.5 Plasticware

<b><u>Item</u></b>	<b><u>Company</u></b>
T75 flasks	Greiner

10 and 6 cm dishes	Sarstedt
6-, 24- and 96-well plates	Greiner
2, 5, 10 and 25 ml pipettes	Sarstedt
1.5 and 2 ml reaction tubes	Sarstedt
15 ml and 50 ml tubes	Sarstedt
Cryovials	Greiner

### 2.1.6 Bacteria

For amplification of plasmids, chemical transformation was performed with competent bacteria of the following stems:

#### **Subcloning**

Bacteria stem	Genotype
DH-5 $\alpha$	<i>F-<math>\phi</math>80lacZ<math>\Delta</math>M15 <math>\Delta</math>(lacZYA-argF)U169 recA1 endA1 hsdR17(rk-, mk+) phoA supE44 thi-1 gyrA96 relA1 <math>\lambda</math>-</i>
XL-1 Blue	<i>recA1 endA1 gyrA96 thi-1 hsdR17 supE44 relA1 lac [F' proAB lacIqZ<math>\Delta</math>M15 Tn10 (Tetr)]</i>
JM109	<i>(e14-(McrA-) recA1 endA1 gyrA96 thi-1 hsdR17 (rk- mk+) supE44 relA1 <math>\Delta</math>(lac-proAB) [F' traD36 proAB lacIqZ<math>\Delta</math>M15])</i>

#### **Mutagenesis**

XL-10 Ultracompetent cells	<i>(TetrD(mcrA)183 D(mcrCB-hsdSMR-mrr)173 endA1 supE44 thi-1 recA1 gyrA96 relA1 lac Hte [F' proAB lacIqZDM15 Tn10 (Tetr) Amy Camr])</i>
TOP10F'	<i>F' {lacIq Tn10 (TetR)} mcrA <math>\Delta</math>(mrr-hsdRMS-mcrBC) <math>\Phi</math>80lacZ<math>\Delta</math>M15 <math>\Delta</math>lacX74 recA1 araD139 <math>\Delta</math>(ara-leu)7697 galU galK rpsL (StrR) endA1 nupG</i>

## 2.1.7 Plasmids

### 2.1.7.1 Overview

The following vectors and plasmids were used:

<u>Plasmid name</u>	<u>Reference</u>
<b>Cloning vectors</b>	
pCR2.1-Topo-TA	Invitrogen
<b>Expression vectors</b>	
pcDNA3.1-	Invitrogen
pcDNA3.1p22phoxS	Djordjevic et al. 2005
psDNA6.1ECFP	Djordjevic et al. 2005
pcDNA6.1hp22phoxECFP	Djordjevic et al. 2005
pcDNA3.1NOX4S	Djordjevic et al. 2005
pFLAG-p22YN	Petry et al. 2006
pCMV-NOX4YC	Petry et al. 2006
pcDNA3.1-NOX2YC	Petry et al. 2006
pcDNA3.1-NOX2	Petry et al. 2006
pcDNA3.1-YC	Petry et al. 2006
pcDNA3.1-YN	Petry et al. 2006
pCDNA3.1-NOX5 $\beta$	Banfi et al. 2004
pcDNA3.1-NOX5S	BelAiba, Djordjevic, Petry et al. 2007
pCMV-NOX5 $\beta$ -YC	BelAiba, Djordjevic, Petry et al. 2007
pCMV-NOX5S-YC	BelAiba, Djordjevic, Petry et al. 2007
pCMVSPORT6-ATF4	RZPD
pCMVSPORT6-XBP1	RZPD
pEF/myc/ER/YFP	Petry et al. 2006
pER-CFP	Petry et al. 2006
pER-DsRed	T.Kietzmann, Kaiserslautern
pCMV-hPDI	T.Kietzmann, Kaiserslautern
pCMV-hPDI <sub>mut</sub>	T.Kietzmann, Kaiserslautern
<b>Gene silencing plasmids</b>	
pSTRIKE-None	Petry et al. 2006
pSTRIKE-p22phox	Petry et al. 2006
pSTRIKE-NOX2	Petry et al. 2006

pSTRIKE-NOX4	Petry et al. 2006
pSTRIKE-NOX1	Petry et al. 2006
pSTRIKE-NOX5	BelAiba, Djordjevic, Petry et al. 2007
pSTRIKE-ATF4	Unpublished
pSTRIKE-XBP1	Unpublished
<b>Reporter gene constructs</b>	
pGL3B-p22phox1.2Kluc	M. Weitnauer
pGL3P-p22phox-XBPluc	M. Weitnauer, K. Diemer
pGL3-Promoter	Promega Corporation
pGL3-Basic	Promega Corporation

### 2.1.7.2 Expression vectors

To obtain pcDNA3.1p22phoxS (p22S) the full length cDNA fragment encoding human p22phox derived from pBShp22phox (provided by Dr. M. Dinauer, Indianapolis, USA) was digested with *EcoRI*, blunt-ended with mung bean nuclease and the fragment was ligated into pcDNA3.1 in sense and antisense direction resulting in p22S. The human NOX4 full length cDNA was cut out from pCMV4-SPORT-NOX4 (RZPD, Accession number NM-016931) by *AvaI*, and blunted using Klenow fragment. It was then inserted into pcDNA3.1 linearised with *EcoRV* resulting in pcDNA3.1NOX4 sense construct (NOX4S).

The plasmid pCMVERCFP encoded for an endoplasmatic localization sequence fused to the cyan fluorescent protein (CFP) and the pEFERYFP plasmid were a gift from Dr. M. Grez (Frankfurt a. M., Germany). For the p22phoxYN and the YFP-p22phox constructs, polymerase chain reaction (PCR) with primers adding appropriate restriction sites was performed on the pcDNA3.1- p22phoxS plasmid to amplify the human p22phox coding sequence and cloned either into the pCMV-FLAG-bJunYN vector (kindly provided by Dr. T. Kerppola, Ann Arbor, MI) or pEYFP-C1 (BD Biosciences Clontech), resulting in pCMV-FLAG-p22phoxYN, encoding for a FLAG-p22phoxYN chimera, and pEYFP-C1-p22phox plasmid encoding for the YFP-p22phox

chimera, respectively. The pcDNA3.1-YN was created by cutting the YN-fragment from pCMV-FLAG-bJunYN with BamHI and subcloning it into pcDNA3.1. For the NOX4YC and the YFP-NOX4 fusion constructs, the cDNA encoding for human NOX4 was amplified by PCR from pcDNA3.1-NOX4S using specific primers for adding appropriate restriction sites and cloned into the pCMV-HA-bFosYC vector (kindly provided by Dr. T. Kerppola) or pEYFP-C1 resulting in pCMV-NOX4YC encoding for NOX4YC and in pEYFP-C1-NOX4 encoding for YFP-NOX4. The full-length human NOX2 cDNA was derived from pBShgp91phox and subcloned into pcDNA6.1CFP resulting in pcDNA6.1hgp91phoxCFP encoding for CFP-NOX2. For the NOX2YC fusion construct, the YC-fragment was cut from pCMV-HA-bFosYC and subcloned into pcDNA3.1, resulting in pcDNA3.1-YC. For NOX2YC and for NOX2 expression vectors, NOX2 was amplified from pcDNA6-ECFP-NOX2 by PCR using primers adding appropriate restriction sites and subcloned either in pcDNA3.1 or into pcDNA3.1-YC, resulting in pcDNA3.1-NOX2 and pcDNA3.1-NOX2YC, respectively. All other expression plasmids were already in the lab or purchased from the company listed in the table above.

### **2.1.7.3 Luciferase reporter plasmids**

The plasmid containing the full p22phox-promoter (pGL3B-p22phox1.2Kluc) was based on the pGL3-Basic vector containing a multiple cloning site adjacent upstream to the luciferase coding sequence, whilst the plasmids containing only small part upstream of the putative promoter sequence were based on the pGL3-Promoter plasmids containing a SV40 promoter driving the transcription of the luciferase gene (Fig. 8). Both the pGL3B-p22phox1.2Kluc and the pGL3P-p22phox-XBPluc were already present in the lab, and were cloned from HEPG2 genomic DNA using polymerase chain reaction with primers attaching appropriate restriction sites at the 5'-

end and at the 3'-prim end and were subcloned into the pGL3-Basic or pGL3-Promoter.

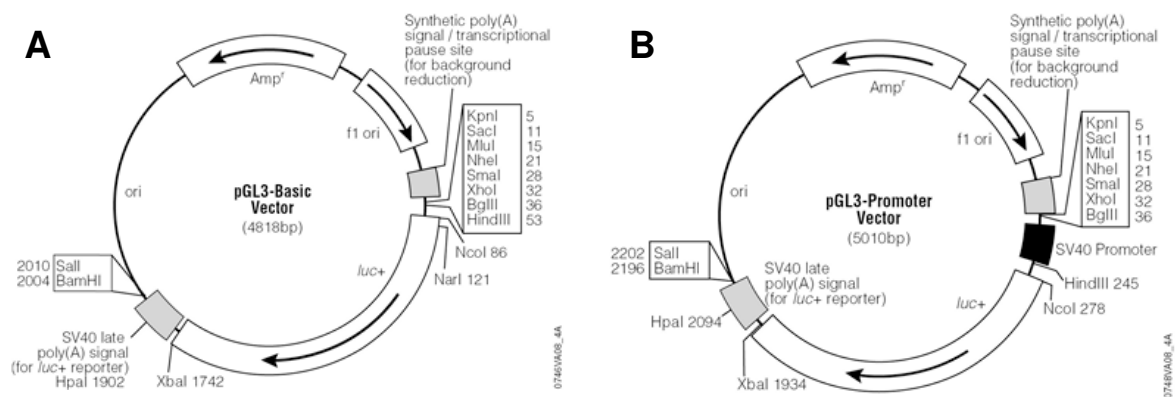


**Fig. 8 Luciferase reporter plasmid maps.**

For luciferase reporter gene assay, two types of vectors were used: pGL3-Basic (A) contained a multiple cloning site 5' to the luciferase coding sequence to enable the analysis of full promoters whilst the pGL3-Promoter (B) vector had a multiple cloning site in front of an SV40 promoter 5' to the luciferase gene thus enabling analysis of enhancer sequences (©Promega Cooperation, www.promega.com, used with permission).

#### 2.1.7.4 Gene silencing vectors

Selective gene silencing can be achieved by using short double stranded interfering RNAs (siRNA) which match the sequence of the gene to be silenced. This is done by either direct transfecting siRNA duplexes into the cell or via endogenous production of siRNA. In this study, *in vivo* expression of siRNA was conducted by the transfection of an expression vector (psiSTRIKE, Promega) which produced siRNA as fold-back stem-loop structures (short hairpin RNA, shRNA) that were transcribed from a U6 promoter thanks to a linker sequence (5'- TTC AAG AGA -3') joining the sense to the antisense sequence. The oligos also had terminal *Pst*I sites which enabled sticky end ligation to the psiSTRIKE vector (supplied linearised with *Pst*I). This enzyme was later used for confirmation of insert. Two oligonucleotides with the same sequence as the target siRNA sequence were synthesized and annealed to form a DNA insert containing the hairpin siRNA target sequence. Upon annealing, the oligonucleotides formed ends that were compatible with the ends of the linearised psiSTRIKE vector thus facilitating a "sticky end" ligation (Fig. 9). The oligonucleotides were designed

using the siRNA Target Designer program on the Promega website and a random sequence was used as control siRNA.

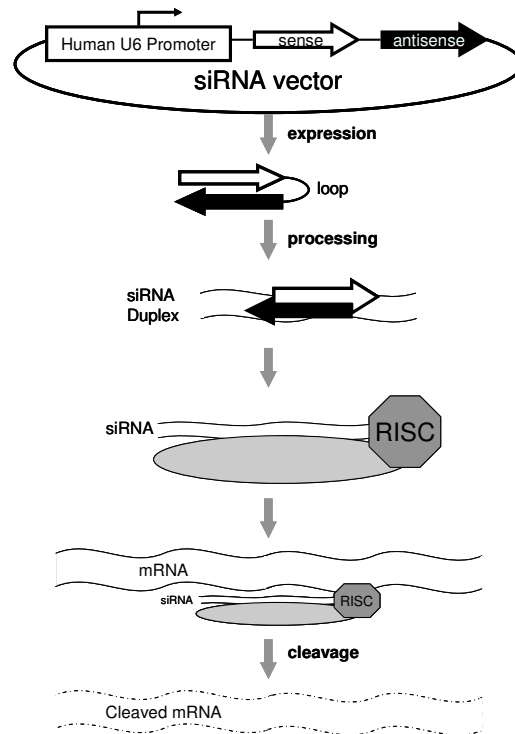


**Fig. 9 Principle of gene silencing using the siStrike system.**

A double stranded oligonucleotide containing the sense and antisense of the to be silenced target RNA is linked into the target psiSTRIKE vector under the control of the human U6 promoter. After transfection, RNA polymerase III produces short hairpin RNA (shRNA) which is then processed to short interfering RNA (siRNA) with the effect of silencing mRNA homologous to the target sequence in the RISC complex (adapted from <http://www.abcam.com>)

The following oligonucleotides were generated:

<b>Name</b>	<b>Sequence (5' -&gt; 3')</b>
siCtr-F	ACCGTCTCCGAACGTGTCACGTTTTCAAGAGAACGTGACACGTTCCGGAGAATTTTTTC
siCtr-R	TGCAGAAAAATTCTCCGAACGTGTCACGTTCTCTTGAAACGTGACACGTTCCGGAGA
siNOX4-F	ACCGCCTCTACATATGCAATAATTTGTGTAGTTATTGCATATGTAGAGGCTTTTTTC
siNOX4-R	TGCAGAAAAAGCCTCTACATATGCAATAACTACACAAATTATTGCATATGTAGAGG
sip22-F	ACCGGCCCTTTACCAGGAATTATTTGTGTAGTAATTCCTGGTAAAGGGCCTTTTTTC
sip22-R	TGCAGAAAAAGGCCCTTTACCAGGAATTACTACACAAATAATTCCTGGTAAAGGGC
siNOX2-F	ACCGAATCTCACCTTTTCATAAATTTGTGTAGTTTATGAAAGGTGAGATTCTTTTTTC
siNOX2-R	TGCAGAAAAAGAATCTCACCTTTTCATAAACTACACAAATTTATGAAAGGTGAGATT
siNOX1-R	TGCAGAAAAAGCACCGGTCATTCTTTTATACTACACAAATATAAAGAATGACCGGTG
siNOX1-F	ACCGCACCGGTCATTCTTTTATATTTGTGTAGTATAAAGAATGACCGGTGCTTTTTTC

siXBP1-F	ACCGAAGTAGACATGGAATTTATTTGTGTAGTAAATTCATGTCTACTTCTTTTTTC
siXBP1-R	TGCAGAAAAAGAAGTAGACATGGAATTTACTACACAAATAAATTCATGTCTACTT
siATF4-F	ACCGGTGGCCAAGCACTTCAAATTTGTGTAGTTTGAAGTGCTTGGCCACCTTTTTTC
siATF4-R	TGCAGAAAAAGGTGGCCAAGCACTTCAAACCTACACAAATTTGAAGTGCTTGGCCAC

## 2.1.8 Oligonucleotides

### 2.1.8.1 Cloning primers

Restriction sites underlined

<u>Name</u>	<u>Restriction enzyme</u>	<u>Sequence (5' -&gt; 3')</u>	<u>AT(°C)</u>
<b>BiFC vectors</b>			
p22phoxYN	F (EcoRI)	AT <u>GAATTC</u> AGGGCAGATCGAGTGGGCC	55
	R (Xbal)	CCTCTAGACACGACCTCGTCGGTCACC	
p47phoxYC	F (EcoRI)	AG <u>GAATTC</u> GATGGGGGACACCTTCATCCGTC	58
	R (KpnI)	TCGGT <u>TACCG</u> ACGGCAGACGCCAGCTTC	
p47phoxYN	F (EcoRI)	AT <u>GAATTC</u> GATGGGGGACACCTTCATCCG	58
	R (Xbal)	TATCTAGAGACGGCAGACGCCAGCTTC	
p67phoxYC	F (EcoRI)	AT <u>GAATTC</u> GGATGTCCCTGGTGGAGGCCATC	58
	R (KpnI)	TAGGT <u>TACCG</u> ACTTCTCTCCGAGTGCTTTCC	
gp91phoxYC	F (XhoI)	ATCTCGAGGCCACCATGGGGA <u>ACTGGGCTGTGAATG</u>	59
	R (XhoI)	TACTCGAG <u>cGAAGTTTTTCCTTGTTGAAAATGAAATG</u>	
Nox5SYC	F (EcoRI)	AT <u>GAATTC</u> CAAATGGAGAACCTGACCATCAGGGCTG	59
	R (KpnI)	TAGGT <u>TACCG</u> AAATCTCTTGAAAAATCTGAAGCCG	
Nox4YC	F (ApaI)	ATGGG <u>CCCCGCC</u> CATGGCTGTGTCTGGAGGAGC	59
	R (KpnI)	CCGGT <u>TACCG</u> CTGAAAGACTCTTTATTGTATTC	

**Expression vectors**

F-N4-Sacl-w/oATG F (Sacl)	AAGAGCTCGGGCTGTGTCCTGGAGGAGC	59
R-Nox4-KpnI-STP R (KpnI)	TTGGTACCTCAGCTGAAAGACTCTTTATTGTATTC	

**2.1.8.2 RT-PCR primers**

<u>Target</u>	<u>Sequence (5'→3')</u>	<u>AT(°C)</u>	<u>P 1roduct length</u>
p22phox	CAGATCGAGTGGGCCATGT TCGTCGGTCACCGGGATG	57	571
NOX1	GTCTTCTGGTATACTCACCACC GAATGACCGGTGGAAGGATCCAC	54	228
NOX2	CATGTTTCTGTATCTCTGTGA GTGAGGTAGATGTTGTAGCT	57	614
NOX4	CCATGGCTGTGTCCTGGAGGAGCTG AGTTGAGGGCATTACCAGATGGGC	57	389
GAPDH	TATGACAACAGCCTCAAGAT AGGTCACCACCTGACACGTT	58	316
NOX5	ATGAGTGGCACCCTTCACCATCAG TTCGAGTGGTTTGTGAGCCTGCTGAC	65	501
NOX5 $\alpha$ /NOX5 $\gamma$	GGCCCTGAAGGCTGTAGAGGCA GCGCAGCTCATCCGGGTCAATG	65	326/451
NOX5 $\beta$ / NOX5 $\delta$	CAGGACGGTACTCCGCTGACACCTT GCGCAGCTCATCCGGGTCAATG	65	577/661

**2.1.8.3 qPCR primers**

<u>Target</u>	<u>Sequence (5'→3')</u>	<u>Product length</u>
NOX1	CACCCCAAGTCTGTAGTGGGAG CCAGACTGGAATATCGGTGACA	91
GAPDH	GAAGGTGAAGGTCGGAGTC GAAGATGGTGATGGGATTTTC	226

#### 2.1.8.4 Sequencing primers

<u>Primer-Name</u>	<u>Sequence (5'→3')</u>
R-YC-Seq	CCCGCGGCCGCTTACTTGTACAG
Sp6	CATACGATTTAGGTGACACTATAG
M13 Forward (-20)	GTAAAACGACGGCCAG
M13 Reverse	CAGGAAACAGCTATGAC
CMV-F	CGCAAATGGGCGGTAGGCGTG
BGH-R	TAGAAGGCACAGTCGAGG

#### 2.1.9 DNA modifying enzymes

##### 2.1.9.1 DNA polymerase I, large (Klenow) fragment

DNA polymerase I, Large (Klenow) Fragment is a DNA polymerase that contains 3'5' exodeoxyribonuclease activity. It is used to fill-in 5' overhangs to make blunt-ended vectors and/or inserts.

##### 2.1.9.2 Calf alkaline phosphatase

Alkaline phosphatases catalyse the dephosphorylation of 5' phosphates from DNA and RNA. Once dephosphorylated, the 5'-hydroxyl end cannot be ligated to a 3'-hydroxyl end of double-stranded DNA. In this way, dephosphorylated ends can be prevented from religating to themselves or to other dephosphorylated DNA molecules, increasing the efficiency of the ligation reaction.

##### 2.1.9.3 T4 DNA ligase

T4 DNA ligase can be used to join DNA fragments with staggered or blunt ends and to repair nicks in double-stranded DNA having 3'-hydroxyl and 5'-phosphate ends. The enzyme is isolated from *E. coli* lambda lysogen NM989. It catalyzes the formation of a phosphodiester bond between adjacent nucleotides only if one nucleotide carries a 5'-

phosphate residue and the other carries a 3'-hydroxyl terminus. It was therefore used to clone inserts into the multiple cloning sites of cloning vectors.

### 2.1.10 TOPO cloning

For some clonings the TOPO-TA cloning kit (Invitrogen) was used in accordance to the manual (Fig. 10). The target vector pCR2.1-TOPO is supplied linearized with the following characteristics:

- Single 3'-thymidine (T) overhangs for TA Cloning
- Topoisomerase I covalently bound to the vector (referred to as "activated" vector)

The PCR itself was performed with *the Taq* polymerase containing Expand High FidelityPLUS PCR System (Roche). The Taq polymerase has a nontemplate-dependent terminal transferase activity that adds a single deoxyadenosine (A) to the 3' ends of PCR products. The pCR2.1-TOPO vector contains a single overhanging 3' deoxythymidine (T) residue which allows PCR inserts to ligate efficiently with the vector. Topoisomerase I from *Vaccinia* virus binds to duplex DNA at specific sites and cleaves the phosphodiester backbone after 5'-CCCTT in one strand [64-67]. The energy from the broken phosphodiester backbone is conserved by formation of a covalent bond between the 3' phosphate of the cleaved strand and a tyrosyl residue (Tyr-274) of topoisomerase I. The phospho-tyrosyl bond between the DNA and enzyme can subsequently be attacked by the 5' hydroxyl of the originally cleaved strand, reversing the reaction and releasing topoisomerase [68]. The TOPO-TA cloning was used as a first cloning step of the NOX5 and NOX4 for the pCMV-NOX5SYC and pEGFP-NOX4.

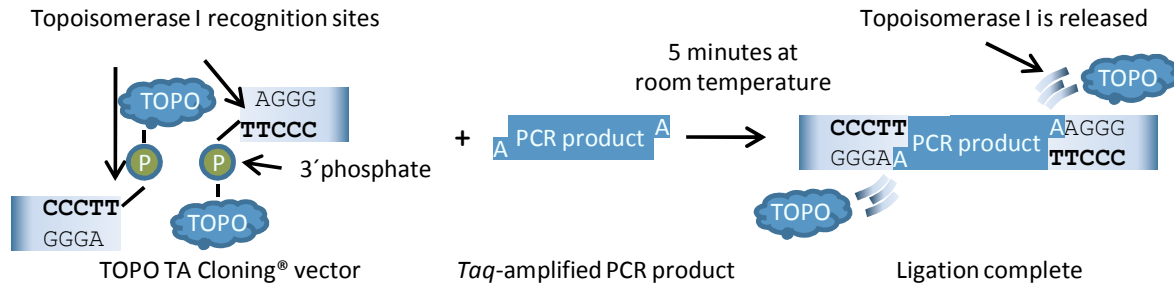


**Fig. 10 Schematic overview over the TOPO cloning principle.**

The TOPO target pCR2.1-TOPO vector contains a single 3'-T-overhang covalently bound to the Topoisomerase I. Adding of a PCR product or other DNA-sequence containing a single 3'-A-overhang and incubation results in a ligation of the PCR product and the pCR2.1-TOPO vector and a release of the Topoisomerase I (adapted from [www.invitrogen.com](http://www.invitrogen.com)).

### 2.1.11 Solutions

All solutions were prepared with double distilled water if not otherwise stated.

#### 2.1.11.1 Northern blot solutions

##### DEPC Water

500 µl DEPC were added to 900 ml dH<sub>2</sub>O and left overnight with slightly opened lid at room temperature. The solution was then autoclaved.

##### GT

Guanidine thiocyanate	4 M
Na-citrate	25 mM
N-Lauryl Sarcosine	0.3%

##### MOPS buffer (10x)

MOPS	0.2 M
Sodium acetate	80 mM
EDTA	10 mM

The pH were adjusted to 7.0. 500 µl DEPC was added to 900 ml 10x MOPS buffer and left overnight with slightly opened lid. The solution was then autoclaved.

##### SSC (20x)

NaCl	3 M
Sodium citrate	0.3 M

500 µl DEPC were added to 900 ml 20X SSC and left overnight with slightly opened lid. The solution was then autoclaved.

**Premix for RNA probes**

Formamid	10 ml
Formaldehyd 37%	3.5 ml
10 X MOPS	2.0 ml
Ethidium Bromide	0.03 µg

The solution was aliquoted and stored at - 20°C.

**Blue marker for RNA probes (10x)**

Glycerine	1 ml
Bromphenolblue	1.6 mg
Xylenecyanol	1.6 mg
EDTA pH 8.0	1 mM
DEPC H <sub>2</sub> O	2 ml

The solution was stored at 4 °C.

**Hybridisation solution**

20 X SSC	25%
Formamid	50%
10 X Blocking reagent	20%
N-Lauryl Sarcosinate	0.01%
SDS	0.02%

**Washing solution**

Maleic acid	0.10 M
NaCl	0.15 M

The pH was adjusted to 7.5.

**Blocking****solution**

10X Blocking solution (Roche) was diluted 1:9 in washing solution.

**Detection solution**

Tris	0.1 M
NaCl	5 M

The pH was adjusted to 9-9.5.

**2.1.11.2 Western blot solutions****Running gel (volume for one gel)**

<u>Percentage</u>	<u>8%</u>	<u>10%</u>	<u>12%</u>
H <sub>2</sub> O (ml)	3.4	2.8	2.1
30% acrylamid (Rotiphorese gel) (ml)	2.7	3.3	4
1M Tris pH 8.8 (ml)	3.7	3.7	3.7
10% SDS (µl)	100	100	100

For polymerization, 80 µl ammoniumpersulfate and 10 µl of TEMED were added.

**Stacking gel**

<u>Percentage</u>	<u>5%</u>
H <sub>2</sub> O (ml)	2.14
30% acrylamid (ml)	0.488
1M Tris pH 6.8 (ml)	0.375
10% SDS	30

For polymerization, 15 µl ammoniumpersulfate and 3 µl of TEMED were added.

**Laemmli buffer (3x)**

Tris pH 6.8	187 mM
SDS	6%
Glycerol	30%
Bromphenol blue	0.06%
DTT	15 mM
EDTA	60 mM

**Running buffer**

Tris	25 mM
Glycine	200 mM
SDS	0.5%

**Transfer buffer**

Tris	25 mM
Glycine	200 mM
Methanol	20%

**Stripping buffer**

SDS	2%
Tris pH 6.8	62.5 mM
β-	0.07%
Mercaptoethanol	

**Enhanced chemiluminescent reagent 1 (ECL1)**

Tris pH 8.8	100 mM
Luminol	2.5 mM
Coumaric acid	0.4 mM

**Enhanced chemiluminescent reagent 2 (ECL2)**

Tris pH 8.8	100 mM
H <sub>2</sub> O <sub>2</sub>	0.15%

**Phospho-buffer**

Tris pH 7.4	50 mM
NaCl	300 mM
10% Triton 100	1%
500mM EDTA	2 mM
500mM EGTA	2 mM
125 mM Na <sub>4</sub> P <sub>2</sub> O <sub>7</sub>	10 mM
100mM Na <sub>3</sub> VO <sub>4</sub>	0.5 mM
chymostatin, antipain, leupeptin, pepstatin, and aprotinin	2μg / ml each
PMSF	1mM

**2.1.11.3 Solutions and media for molecular biology**

<b><u>SOC medium</u></b>	<b><u>Final (%) in H<sub>2</sub>O</u></b>
Yeast extract	0.5%
Tryptone	2%
NaCl	0.05%

After dissolving in 950 ml of water, 10 ml of 250 mM KCl solution (final concentration 2.5 mM) were added and pH was adjusted to 7.0. The solution was then autoclaved and thereafter 20 ml of sterile 1 M solution of glucose (final concentration 5 mM) and 5 ml of sterile 2 M MgCl<sub>2</sub> (final concentration 0.5 mM) were added.

**LB medium**

Yeast Extract 0.5 %	0.5%
Tryptone	1%
NaCl	1%

The pH was adjusted to 7.2 and the solution autoclaved.

**LB plates**

Agar	1.5%
Antibiotic (Ampicilin or Kanamycin)	1%

Agar was added to LB medium prior to autoclaving. After cooling to 45-50 °C antibiotic was added, mixed and plates were poured.

**TSS**

NaCl	1% (w/v)
Tryptone	1% (w/v)
Yeast Extract	0.5% (w/v)
MgCl <sub>2</sub>	30 mM
PEG 4000	10%
DMSO	5%

The pH was adjusted to 6.5 with NaOH, buffer sterile filtered and stored at 4 °C.

**TAE (50x stock in 1 litre H<sub>2</sub>O)**

Tris	242 g
Glacial acetic acid	57.1 ml
EDTA 0.5M pH 8.0	100 ml
Water	Add 1000ml

In the 1x working solution was 40mM Tris acetate and 1mM EDTA.

**6x Gel loading dye (in H<sub>2</sub>O)**

Bromophenol blue	0.25% (w/v)
Sucrose	40 % (w/v)

**2.1.11.4 Solutions for luciferase reporter gene assay****Luciferase lysis buffer**

Tris pH 7.8	5 mM
trans-CDTA	0.4 mM
99.5% Glycerol	50%
DTT	2 mM
Triton-X 100	5%

DTT and Triton-X 100 were added after autoclaving and buffer was stored at -20 °C.

**Luciferase substrate**

Tricine pH 7,8	20 mM
(MgCO <sub>3</sub> ) <sub>4</sub> · Mg(OH) <sub>2</sub> · 5H <sub>2</sub> O	1.07 mM
MgSO <sub>4</sub>	2.67 mM
EDTA	0.1 mM
DTT	33.3 mM
D-Luciferin	460 mM
ATP	580 mM

The pH was adjusted to 7.8. The solution was stored in 12 ml aliquots at -70 °C.

Before use the solution was warmed to 37 °C and protected from light at all times.

**2.1.11.5 Solutions for immunofluorescence and immunohistochemistry****M/A solution**

Methanol	50%
Acetone	50%
Store at -20 °C.	

**Blocking solution**

BSA	5%
In PBS	

**Citrate buffer**

Citric acid pH 6.0	0.01 M
in water.	

**2.1.11.6 Solutions for cell culture****HEPES-buffered phosphate (HBSS)**

HEPES	25 mM
NaCl	140 mM
Na <sub>2</sub> HPO <sub>4</sub>	0.75 mM

The solution was adjusted to pH 7.5 and sterilised by filtration.

**2.1.12 Antibodies**

Primary antibodies were prepared in 5% non-fat dry milk powder or 5% BSA diluted in Tris buffered salt solution containing 0.3% Tween 20 (TBS-T).

**TBS-T**

Tris pH 7.5	50 mM
NaCl	150 mM
HCl (37%)	0.3%
Tween	0.3%

**2.1.12.1 Primary antibodies**

<b><u>Antibody</u></b>	<b><u>Isotype</u></b>	<b><u>Company</u></b>	<b><u>Dilution</u></b>	
			WB (in 5% milk)	IF (in 5% milk)
$\beta$ -Actin	Goat polyclonal	Santa Cruz	1/1000	
$\alpha$ -Actin	Mouse monoclonal	Dako	IHC: 1:100	
f-actin	Alexa Fluor488-coupled phalloidin	Molecular Probes		1:1000
ARNT	Mouse monoclonal	Abcam	1:1000	
ATF4	Rabbit polyclonal	Santa Cruz	1:500	
Calnexin	Mouse monoclonal	BD Biosciences	1:1000	
Calreticulin	Mouse monoclonal	Upstate	1:1000	1:1000
eIF2 $\alpha$	Mouse monoclonal	Cell Signaling	1:2000	
Flag	Mouse monoclonal	Sigma	1:4000	
GFP	Rabbit polyclonal	Molecular Probes	1:1000	1:200
GFP	Mouse monoclonal	Roche	1:1000	1:200
gp91phox/NOX2	Rabbit polyclonal	upstate	1:500	1:100
HA	Mouse monoclonal	Roche	1:1000	
NOX1	Rabbit polyclonal	Eurogentec, peptide: CAESFEMWDDDRSH	1:1000	1:100
NOX1	Goat polyclonal	Santa Cruz	1:500	
NOX2 (cl. 49)	Mouse monoclonal	Kindly provided by Dr. D. Roos, Amsterdam	1:500	
NOX4	Rabbit polyclonal	Eurogentec, peptide: CSYGTRFEYNKESFS	1:500	1:100
NOX4	Goat polyclonal	Santa Cruz	1:500	
NOX5	Rabbit polyclonal	Davids Biotechnologie GmbH; peptide: QTRTQPGRPDWSKVF	1:500	1:100
NOX5	Rabbit polyclonal	Eurogentec, peptide: TRAYWHNHRSQLFC	1:500	1:50
p22phox	Rabbit polyclonal	Eurogentec, peptides: CEQWTPIEPKPRERPQ YPRGKRKKGSTMERWC	1:500	1:100
p22phox (cl. 449)	Mouse monoclonal	Kindly provided by Dr. D. Roos, Amsterdam	1:250	

Phospho-p38 MAP Kinase	Rabbit monoclonal	Cell Signaling	1:1000	
p38 MAP Kinase	Rabbit monoclonal	Cell Signaling	1:1000	
PDI	Mouse monoclonal	Stressgene	1:10000	1:2000
p-eIF2 $\alpha$	Rabbit monoclonal	Cell Signaling	1:1000	
XBP1	Rabbit polyclonal	Santa Cruz	1:500	

### 2.1.12.2 Secondary antibodies

#### Western blot

<u>Antibody</u>	<u>Company</u>	<u>Dilution</u>
Goat anti mouse HRP conjugated	Calbiochem	1:10000
Goat anti rabbit HRP conjugated	Calbiochem	1:10000
Rabbit anti goat HRP conjugated	Calbiochem	1:10000

#### Immunofluorescence

<u>Antibody</u>	<u>Company</u>	<u>Dilution</u>
Mouse IgG Alexa Fluor 488	Molecular Probes/Invitrogen	1:200
Mouse IgG Alexa Fluor 594	Molecular Probes/Invitrogen	1:200
Rabbit IgG Alexa Fluor 488	Molecular Probes/Invitrogen	1:200
Rabbit IgG Alexa Fluor 594	Molecular Probes/Invitrogen	1:200
Goat IgG Alexa Fluor 488	Molecular Probes/Invitrogen	1:200
Goat IgG Alexa Fluor 568	Molecular Probes/Invitrogen	1:200
Goat IgG Alexa Fluor 594	Molecular Probes/Invitrogen	1:200

#### Immunohistochemistry

LSAB2 Systems HRP	Dako
-------------------	------

## 2.2 Methods

### 2.2.1 Cell biology methods

#### 2.2.1.1 Cells

##### 2.2.1.1.1 *Ea.Hy926*

The human endothelial cell line Ea.Hy926 (kindly provided by Dr. U. Foerstermann, Mainz, Germany) is a permanent cell line established by hybridization of human umbilical vein endothelial cells with the permanent human cell line A549 [69]. This cell line is well characterized for its endothelial phenotype and biology, and expresses markers of highly differentiated vascular endothelium, including factor VIII-related antigen, which is maintained for more than 100 cumulative populations. Cells were grown in DMEM medium with 1 g/l glucose, containing 10% FCS, 100 U/ml penicillin and 100 µg/ml streptomycin. Since Ea.Hy926 cells need to be cultured in selective medium to maintain the endothelial phenotype, medium was supplemented with 1.5x Hypoxanthine, Aminopterin, Thymidine (HAT) and cells were maintained at 37°C under the humidified atmosphere of 5% CO<sub>2</sub>. Cells were cultured in T75 flasks and passaged twice a week by trypsinisation. First, cells were briefly rinsed and then incubated with 2 ml of 0.05% trypsin containing 0.53 mM EDTA•4Na for 1-2 minutes at 37°C. The digestion was stopped by adding complete medium and cells were subcultured in the ratio 1:3 in T75 flasks or were appropriately seeded in dishes or plates. Prior to stimulation cells were starved from serum in DMEM medium containing 1.5x HAT, 100 U/ml penicillin and 100 µg/ml streptomycin for 16 h.

### **2.2.1.1.2 HMEC-1**

The permanent endothelial cell line, HMEC-1 is derived from human dermal microvascular endothelial cells transfected with a pBR-322-based plasmid containing the coding region of the simian virus 40 A gene product, large T antigen. They are immortalised cells which have retained all the morphological, phenotypic and functional characteristics of normal human microvascular endothelial cells [70].

The cells were grown at 37°C, 5% CO<sub>2</sub> in MCDB or EBM medium supplemented with 10% FCS, 100 U/ml penicillin, 100 U/ml streptomycin, 10 mM L-glutamine, 0.5 µg hydrocortisone and 50 pg epidermal growth factor. The culture medium was changed every two days and the cells were trypsinised at 90% confluency to prevent senescence as described before.

### **2.2.1.1.3 Other cell lines**

The human cervix carcinoma cell line HeLa (ATCC CCL-2), the human embryonic kidney cell line HEK293 (ATCC CRL-1573) and the colon carcinoma cell line CaCo2 (ATCC HTB-37) were cultured in DMEM with 1 g/l glucose, 10% fetal calf serum, 100 U/ml penicillin, and 100 µg/ml streptomycin. The human hepatocellular carcinoma cell line HepG2 (ATCC HB-8065) cultured in DMEM with 4.5 g/l glucose, 10% fetal calf serum, 100 U/ml penicillin, and 100 µg/ml streptomycin. Pulmonary artery smooth muscle cells (PASMC) were purchased from Lonza and grown in the provided SmBm medium supplemented with 5% foetal bovine serum and the “SmGm-2 Single Quot” supplement containing insulin, human fibroblast growth factor-B and epidermal growth factor. PASMC were used only up to passage 12 in order to maintain the phenotypic characteristics of PASMC. All cells were grown at 37°C and 5% CO<sub>2</sub> and passaged twice a week.

### **2.2.1.2 Storage of the cells**

To store the cells in liquid nitrogen, confluent cells were detached by trypsinisation and centrifuged at 1000 rpm for 5 minutes. Cells were then resuspended in precooled culture medium containing 10% DMSO and transferred to cryovials. To allow gradual freezing, vials were then placed in a cold isopropanol freezing box and kept for one day at -70 °C. Thereafter, cells were frozen at -70 °C and kept for at least 24 h to acclimate to extreme cold. Finally, cells were transferred to and stored in liquid nitrogen (-196 °C).

### **2.2.1.3 Transfection of endothelial cells**

Ea.Hy926 cells were transfected using the Effectene transfection reagent. The Effectene reagent is a non-liposomal lipid formulation that spontaneously forms micelle structures that show no variations in size or batch. In the first step of transfection, DNA is highly condensed by interaction with DNA-condensation buffer (Buffer EC) with the help of the Enhancer solution in a ratio 1:8 (DNA : Enhancer). Then, Effectene reagent is added in a ratio 1:10 (DNA : Effectene) in order to coat condensed DNA molecules and produce Effectene-DNA complexes, thus allowing transfer of DNA into eukaryotic cells. When performing transfections, Ea.Hy926 cells were seeded one day before the experiments in 96-well plates or 10 cm dishes to achieve 50-70% confluency on the following day. Per one well of 96 well plates 0.3 µg of plasmid DNA was diluted in DNA-condensation buffer EC to a total volume of 5 µl, 2.4 µl Enhancer solution and 3.0 µl of Effectene reagent was used. For a 10 cm dish 4.5 µg of DNA were mixed with 180 µl of EC buffer and 36 µl Enhancer solution and incubated for 3 minutes. Then 45 µl Effectene reagent was added, the mixture vortexed for 10 seconds and incubated for 8 minutes at room temperature to allow the formation of the transfection complex. Thereafter, the growth medium from

the plate was gently aspirated, 100  $\mu$ l of serum containing media per one well of a 96 well plate or 5 ml per 10 cm dish was added to the cells. The transfection complex was filled up to a total volume of either 50 or 500  $\mu$ l, mixed by pipetting and immediately added to the cells. The transfection efficiency was about 60%.

HMEC-1 were transfected using the SuperFect reagent. SuperFect transfection reagent is an activated dendrimer with a defined spherical architecture, with branches radiating from a central core and terminating at positively charged amino groups. Net positive charge allows them to bind to negatively charged receptors on the surface of eukaryotic cells (e.g. sialylated glycoproteins). Once inside the cell, SuperFect reagent buffers the lysosome after it has fused with the endosome, leading to pH inhibition of lysosomal nucleases and stability of SuperFect–DNA complexes. For transfection experiments, cells were plated one day before transfection. A ratio of a total of 1  $\mu$ g of DNA to 5  $\mu$ l Superfect per well was used in each transfection. After 2 h of incubation with the transfection complex, the medium was changed, and the cells were further cultured. Before stimulation, cells were serum-starved 16 h prior to stimulation.

#### **2.2.1.4 Transfection of HEK293 and HeLa cells**

The calcium phosphate method was used to transfect HEK293 and HeLa cell lines. This method is based on the method described in the Maniatis' laboratory manual [71].

A precipitate containing calcium phosphate and DNA is formed by slowly mixing a HEPES-buffered phosphate solution with a solution containing 2.5 M calcium chloride and DNA. These DNA precipitates are then taken into eukaryotic cells by an endocytic-type mechanism.

DNA was diluted to the required concentration with water and calcium chloride was added. The solution was mixed well and centrifuged down. HEPES was then added while vortexing the mixture vigorously. After spinning down, it was incubated for 10 minutes. Then, medium of the cells were changed against fresh medium and transfection mixture was added to the cells.

#### **2.2.1.5 Luciferase Assay**

The luciferase reporter gene assay makes use of the firefly luciferase enzyme gene to catalyse the chemiluminescent redox reaction of luciferin to oxyluciferin. By placing the luciferase gene under the control of a promoter or enhancer sequence, it can be used to study gene activation under different stimuli or to investigate the effect of a protein on the activity of a particular promoter or enhancer. The procedure described here is based on the Promega manual for Luciferase activity.

Cells were transfected with a plasmid containing the luciferase gene which is under control of the promoter under investigation. After cell lysis, the proteins are mixed with a substrate containing luciferin and ATP. Firefly luciferase is a monomeric, 61 kDa-enzyme that catalyzes luciferin oxidation using ATP  $Mg^{2+}$  as a cosubstrate. Light is produced by converting chemical energy of luciferin oxidation through an electron transition, forming oxyluciferin. The light produced is directly proportional to the amount of luciferase present and is therefore a measure of promoter activity in the luciferase vector.

Cells (HEK293 or Ea.Hy926 cells) were plated in 24-well plates at 50-60% confluency and transfected the next day. After transfection the cells were left in serum supplemented medium for 24 hours. Then the cells were stimulated with either Tunicamycin (2  $\mu$ g/ml) or Thapsigargin (2.5 nM) for 8 hours or left unstimulated. The medium was aspirated and passive lysis buffer optimised for luciferase extraction

was then added (HEK293: 500  $\mu$ l, Ea.Hy926: 400  $\mu$ l). The plates were placed on a shaker for 30 minutes and centrifuged at 500 g for 5 minutes at 4°C to deposit cell debris to the bottom of the wells. Then 150  $\mu$ l lysed cells were transferred to measuring tubes or the lysate was stored at -20°C for later analysis.

To measure the luciferase activity, samples were loaded on a luminometer (Berthold Technologies, Pforzheim, Germany). The luminometer was programmed to inject 100  $\mu$ l of luciferase substrate and to measure average luminescence for 5 s at 37°C. Finally, protein content of the total lysate was determined by performing Bradford assay.

#### **2.2.1.6 DCF fluorescence measurement**

The generation of reactive oxygen species (ROS) was measured using the fluoroprobe 5-(and-6)-chloromethyl-2',7'-dichlorodihydrofluorescein diacetate, acetyl ester (CM-H<sub>2</sub>DCFDA (DCF)). Fluorescent dyes, like fluorescein, are chemically reduced to colorless, nonfluorescent products easily reoxidized in the presence of ROS to fluorescent compounds. Dichlorodihydrofluorescein diacetate passively diffuses into the cells where its diacetate groups are cleaved by cellular esterases, giving a more polar compound that stays trapped in the cells. The carboxylated analogue of H<sub>2</sub>DCFDA passes even easier through the membranes and has better retention in the cells, since it has two negative charges at physiological pH. Moreover, thiol-reactive chloromethyl groups react with glutathione and other thiols, further preventing the leakage of the dye from the cells (Fig. 12).

Subsequent oxidation of DCF gives a fluorescent product that remains trapped in the cells and indicates ROS production. DCF is sensitive to H<sub>2</sub>O<sub>2</sub>, but it also detects peroxynitrite (ONOO<sup>-</sup>) that is formed in a reaction between NO<sup>•</sup> and O<sub>2</sub><sup>-•</sup>. Endothelial cells express eNOS and produce high amounts of NO<sup>•</sup>. Therefore, when measuring

ROS in endothelial cells, the contribution of ONOO<sup>-</sup>-dependent DCF oxidation was excluded by preincubating the cells for 30 minutes with the eNOS inhibitor N- $\omega$ -nitro-L- arginine methyl ester (L-NAME, 10  $\mu$ M), and by adding L-NAME to HBSS. To determine DCF fluorescence in a microplate reader (Tecan), endothelial cells were grown in 96-well plates to 80% confluence, or transfected as described above, and made quiescent in serum free medium for 16 h. Cells were then treated, washed with HBSS and incubated in the dark with DCF (8.5  $\mu$ M) dissolved in HBSS for 10 minutes at 37°C. Cells were then washed with HBSS to remove excess dye, and fluorescence was monitored using 480 nm excitation and 540 nm emission wavelength. In some experiments, cells were preincubated with various inhibitors or antioxidants for 30 minutes and then exposed to stimuli. To evaluate ROS levels, background fluorescence of unloaded cells was subtracted from DCF fluorescence. Moreover, DCF fluorescence was standardized to the number of viable cells using the alamarBlue test. Continued cellular growth maintains a reduced environment in the cells, and therefore causes the redox indicator from alamarBlue to change from the oxidized, nonfluorescent, blue form to the reduced, fluorescent, red form. Therefore, to determine the number of viable cells, cells were incubated with alamarBlue in

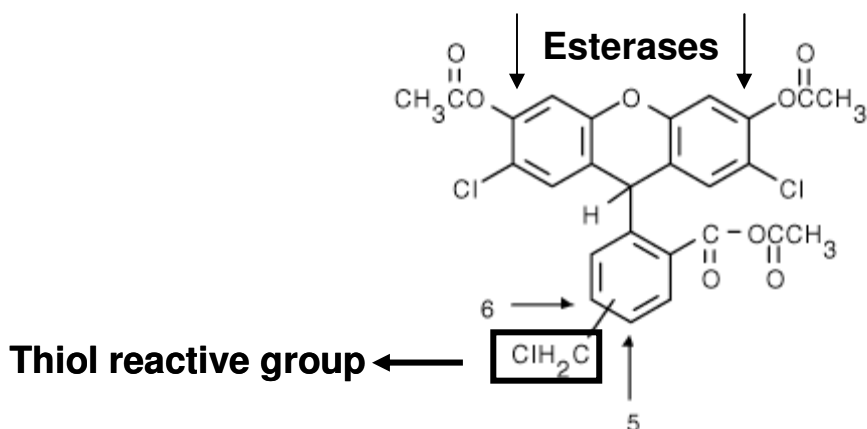


**Fig. 11** Structure of 5-(and-6)- chloromethyl-2',7'- dichlorodihydrofluorescein diacetate, acetyl ester (CM-H2DCFDA).

Explanations are given in the text.



fragments, YC and YN which are fused to the coding sequence of the protein of interest. As a result a fusion protein of the protein and the YC or YN fragment is encoded. When two interacting YC/YN-fusion proteins are expressed in one cell, the original YFP fluorophore is reconstituted upon interaction of the two binding partners in a finally irreversible manner and the interaction can be monitored using fluorescence microscopy.

For the BiFC experiments HeLa cells were used. The cells were seeded on glass-bottom dishes (Willco Wells, Berlin, Germany) before transfection to achieve 50% confluency. Then the cells were cotransfected with NOX2YC/p22phoxYN, NOX4YC/p22phoxYN, NOX5 $\beta$ YC/p22phoxYN and NOX5SYC/p22phoxYN or NOX5 $\beta$ YC/YN, NOX5SYC/YN, NOX2YC/YN and NOX4YC/YN as negative controls. The cells were grown for 24 h, then the media was changed for a HEPES-buffered DMEM (Gibco) and the cells were cooled down several hours to promote fluorophore formation. The fluorescence complementation was then monitored in a fluorescence microscope (Olympus, Hamburg, Germany) and images were obtained using the Openlab Modular Software for Scientific Imaging (Improvision, Tübingen, Germany).

### **2.2.1.9 Proliferation assay with BrdU incorporation**

Cellular proliferation requires DNA replication. Therefore, monitoring of DNA synthesis is an indirect marker of the rate of proliferation in response to different stimuli. To assess proliferative activity of endothelial cells we used 5-bromo-2'-deoxyuridine (BrdU) labeling. BrdU is an analogue of the DNA nucleoside thymidine, and is incorporated in newly synthesized DNA of proliferating cells. The incorporated BrdU is detected by an immunoassay, using a peroxidase-conjugated antibody that specifically recognizes BrdU bound to denatured DNA. The bound antibody is detected by a peroxidase-catalysed colorimetric reaction, using

tetramethyl-benzidine (TMB) as a substrate. Cells were seeded in 96-well plates to achieve 50% of confluency. In the experiments where DNA synthesis of transfected cells was investigated, cells were transfected on the following day with corresponding vectors, and starved from serum overnight 24 h after transfection. On the following day, cells were exposed to stimuli as described in the figure legends.

To assess proliferation, cells were then incubated with BrdU (10  $\mu$ M) for 16 h. Thereafter, cells were fixed for 30 minutes and then incubated for one hour with the peroxidase-conjugated antibody against BrdU. Immunodetection was performed by adding the colorimetric substrate TMB. When the blue color developed, the reaction was stopped with 1 M  $H_2SO_4$ . Absorbance was measured in an ELISA reader (Tecan Safire) at 450 nm with a reference wavelength at 690 nm.

#### **2.2.1.10 *In vitro matrigel angiogenesis assay***

To determine the capability of endothelial cells to form capillaries, BD matrigel (BD Biosciences) was used. BD Matrigel Basement Membrane Matrix is a solubilized basement membrane preparation extracted from the Engelbreth-Holm-Swarm (EHS) mouse sarcoma, a tumor rich in extracellular matrix proteins. Its major component is laminin, followed by collagen IV, heparan sulfate proteoglycans, entactin and nidogen. It also contains TGF- $\beta$ , fibroblast growth factor, tissue plasminogen activator, and other growth factors which occur naturally in the EHS tumor, however, in this study we used growth factor-reduced Matrigel. When plated onto matrigel, endothelial cells spontaneously form capillary-like structures which are a measure of angiogenic activity. Since the matrigel matrix gels rapidly between 22°C and 35°C, all plates and pipette tips were kept at -20°C and all work was performed on ice. The matrigel itself was thawed overnight on ice at +4°C.

Matrigel (150  $\mu$ l) was added to each well of a 48-well plate by tilting the plate to one side and pipetting slowly and continuously to avoid air bubbles from forming inside the gel. Any bubbles were removed immediately with a hot needle. The plate was then tilted slightly in all directions to cover the bottom of the well completely. When all wells were coated with matrigel, the plate was warmed to 37°C for 20 minutes.

The cells were plated out in 6 cm dishes and transfected the next day. After 24 h the cells were trypsinised and counted. They were then suspended at 24000 cells/250  $\mu$ l medium without FCS in the case cells were stimulated or with FCS otherwise for each well. They were then added to the polymerised matrigel and the plate tilted gently in all directions to ensure a uniform cell cover over the entire matrigel surface. The cells were then incubated at 37°C and 5 % CO<sub>2</sub> for 30 minutes to let the cells settle down. Cells were stimulated and were incubated for 4 h to allow capillary structure formation.

After the experiment, calcein AM staining was used to visualise the tube-like structures, since it gives a strong fluorescence signal with minimal background staining. The medium was removed from the plates by placing them upside down on a stack of paper towels and tapping gently to avoid disturbing the tube structures. The wells were then washed twice with warm (37°C) HBSS. Calcein AM solution (8  $\mu$ g/ml in HBSS) was then added to each well (100  $\mu$ l) and the plates were incubated for 30 minutes at 37°C, 5% CO<sub>2</sub>. The labeling solution was then removed and the plates washed twice with warm HBSS. The washing solution was then removed and the plates were viewed under a fluorescence microscope at 40X magnification. Pictures were taken and analyzed using ImageJ software. Total tube length was then measured and used as a measure of angiogenesis.

### **2.2.1.11 Immunofluorescence**

The cellular localization of proteins can be visualized by using specific antibodies against the proteins of interest, which are detected by secondary antibodies conjugated with a fluorescent label which can be visualized under a fluorescent microscope. This method is based on the one in the Maniatis laboratory manual [71]. Cells were plated out to ~50 % confluency onto glass coverslips inside a 24-well plate. After stimulation, they were washed twice with PBS (5 minutes each time) and then fixed with cold methanol/acetone (MA) solution at -20 °C for 10 minutes. The MA solution was then aspirated and the plates left to dry at room temperature for 5 minutes. The coverslips were then blocked with blocking solution (5% BSA in PBS) for 1 hour at room temperature. Primary antibody (35 µl) diluted in blocking solution was then pipetted onto parafilm and the coverslips placed face-down over the droplet. Incubation was carried out in a humidified chamber overnight at 4 °C. The cover slips were then placed into the 24-well plate and washed 3 times with PBS for 5 minutes each. As negative control, one coverslip was incubated in blocking solution alone. The secondary antibody (30 µl) was pipetted onto parafilm and the coverslips placed face down onto it. Incubation with secondary antibody was carried out for 1 h at room temperature in the dark. The samples were then washed 3 times with PBS for 5 minutes and checked under the fluorescence microscope. They were then fixed onto glass slides with fluorescent mounting medium.

### **2.2.1.12 Immunohistochemistry**

To localize proteins in tissue sections, immunohistochemistry was performed on tonsil sections using LSAB2 Systems HRP (Dako) in accordance with the manufacture's manual with specific antibodies against NOX5, p22phox and smooth muscle cell actin.

The samples were deparaffinised by subsequent treatment with 100% xylol, 100% ethanol, 96% ethanol, 70% ethanol, 50% ethanol. They were then washed for 3 times with PBS and then washed with citrate buffer in a pressure cooker for 4 minutes. The samples were then washed in cold water and then 3 times in PBS, 5 minutes each time. To block endogenous peroxidase activity, the samples were then treated with 3% H<sub>2</sub>O<sub>2</sub> for 5 minutes and washed again 3 times with PBS.

Blocking was performed using 4% BSA for 30 minutes at room temperature. Then the slides were left to drip the excess solution. Incubation was performed with the primary antibody diluted in 1% BSA. As negative control, one sample was incubated in 1% BSA alone. The samples were then washed for 3 times with PBS and incubated in streptavidin-HRP conjugated secondary antibody for 30 minutes at room temperature. The samples were then washed for 3 times in PBS and incubated with diaminobenzidine (DAB) for 10 minutes. After washing with PBS for 3 times, the samples were counterstained with Mayer's Hämalaun solution. The samples were then washed with tap water before taking pictures with a light microscope.

## **2.2.2 RNA-Methods**

### ***2.2.2.1 Preparation of total RNA***

Total RNA from endothelial cells was purified using guanidine thiocyanate-acid phenol extraction. For RNA extraction, cells were plated in 10 cm dishes. At the end of the experiment, cells were washed with ice cold PBS and plates were frozen on liquid nitrogen. Thereafter, cells were lysed in 800 µl GT-DTT buffer, which denatures cellular and nucleoprotein complexes and releases RNA. The lysate was incubated for 30 minutes on ice with 800 µl phenol and 200 µl chloroform-isoamyl alcohol (24:1) to remove contaminating chromosomal DNA from the RNA preparation. Moreover, 80 µl of 2 M sodium-acetate buffer (pH 4) was added to maintain the pH of the

denatured cell lysate during acid extraction and to provide the salt necessary for RNA precipitation with isopropanol. After centrifugation for 30 minutes at 13000 rpm, DNA and proteins remained in the lower organic phase, while RNA was present in the upper aqueous phase. After separation of phases, RNA was purified by two isopropanol precipitations at -20 °C for 2 h. Finally, the pellet of RNA was diluted in DEPC treated H<sub>2</sub>O, heated at 65 °C for 10 minutes and RNA concentration was measured in a Hitachi spectrophotometer model U-2001. Alternatively, total RNA was purified using the RNeasy Mini Kit (Qiagen) in accordance with the manufacturer's manual.

#### ***2.2.2.2 Northern blot***

10 to 15 µg of total RNA were mixed with RNA Premix (containing ethidium bromide) in a 1:1 ratio and 10x RNA blue marker was added to the mix. Samples were heated at 65°C for 10 minutes and loaded on 1.3% denaturing agarose gels containing 1.1% formaldehyde. The gel was run in 1X MOPS buffer on 40 V for 4 h. After separation, loading of the gel was confirmed by staining the gel with ethidium bromide and checking the 18S band under the UV light. Then, RNA was transferred from the gel to a nylon membrane (Porablot, Macherey Nagel) for 24 h using capillary transfer in 20X SSC buffer. After the transfer was controlled by UV detection of incorporated ethidium bromide, transferred RNA was cross-linked by UV irradiation in Stratalinker 1800 (Stratagen). Northern membranes were then incubated in hybridization solution for 2 h at 65°C. Northern hybridizations were carried out with digoxigenin(DIG)-labeled antisense RNA for human p22phox at 65°C for 16 h which was present in the lab [72]. Then, membranes were washed 2 times in 2X SSC solution containing 0.1% SDS and then 2 times in 0.1 SSC solution containing 0.1% SDS at 65°C. Membranes were blocked for 30 minutes in 1X blocking solution and

then incubated for 1 h with anti-DIG antibody conjugated with alkaline phosphatase (Roche) diluted 1:10000 in blocking solution. After washing the membranes in washing solution, detection was performed by using the chemiluminescent substrate CDP-Star (Roche) diluted 1:100 in detection buffer. Blots were scanned and analyzed using GelDoc software (BioRad).

### **2.2.2.3 cDNA synthesis from RNA**

Reverse transcriptase (RT) reaction involves the use of an RNA-dependent DNA polymerase to produce a library of cDNA from mRNA extracted from cultured cells or tissue. The technique is based on RNA denaturation and hybridisation to short non-specific DNA sequences (random hexamers). The cDNA thus produced can be used to clone genes or to analyze the mRNA expression of a specific gene by PCR or quantitative PCR. Reverse transcription was performed on 1 to 5 µg total RNA using random hexamers. After addition of dNTPs, the reaction mixture was warmed to 65°C to denature any RNA secondary structures. After cooling on ice a mix consisting of reverse transcriptase buffer, DTT and Superscript III<sup>®</sup> was added to the reaction tubes. The tubes were vortexed and spun down. They were then incubated at 25°C for 5 minutes to allow the hexamer primers to hybridize with the RNA. This was followed by incubation at 55°C for 60 minutes to allow the reverse transcriptase

**Table 1 Reverse transcription mixes for Superscript III (Invitrogen)**

Primer hybridization mix

RNA	1 - 5 µg
pdN6 (100 ng/µl)	1 µl
dNTP mix (10mM)	1 µl
H <sub>2</sub> O-DEPC up to	13 µl

Reverse transcriptase master mix

5X RT Buffer	4 µl
DTT (100 mM)	1 µl
Superscript III (200 U/µl)	1 µl

to work. The enzyme was then inactivated at 70°C for 15 minutes. The RNA was destroyed by incubation with RNase H at 37°C for 20 minutes. The cDNA thus produced was then stored at -21°C. As negative control, RT reaction for each sample was performed without adding reverse transcriptase.

## **2.2.3 DNA Methods**

### ***2.2.3.1 Polymerase chain reaction (PCR)***

Polymerase chain reaction (PCR) is a technique used to produce a large number of copies of a specific DNA sequence. The technique relies on oligonucleotide complementary hybridization.

First, the template DNA is denatured at high temperature to get single strands at the initiation denaturation step, followed by the annealing of two short oligonucleotides (~25 bp), so called primers, to the DNA sequence flanking the region of interest at a lower temperature. This annealing step is followed by the elongation of the strands by the DNA polymerase starting at the 3' site of each primer. This leads to an extension of the 3' end of the primer resulting in a complementary strand of the template. This step is followed by another denaturation step and the newly synthesized strands act as templates for the next cycle of elongation (Fig. 11). As the number of products is doubled with each cycle, the number of PCR products increase in a logarithmic manner.

The precision with which PCR amplifies the selected DNA sequence is known as fidelity. The fidelity of a PCR reaction depends primarily on the annealing temperature (TA) at which the primers hybridise to the template and magnesium concentration.

A temperature higher than the optimal TA reduces the hybridisation rate of the primers to the template, resulting in a reduced product yield. On the other hand, if the

temperature is too low the specificity of the primers decreases resulting in an unspecific binding and subsequently amplification of unspecific PCR products. The TA of a primer sequence depends on the length of the primer and number of GC nucleotides. It can be calculated using the following formula:

$$T_a = 64.9^{\circ}\text{C} + 41^{\circ}\text{C} \times (\text{number of G's and C's in the primer} - 16.4)/N$$

N = number of nucleotides.

However, the predicted TA is just an indication and often the best working TA has to be found by heuristic testing of different annealing temperatures. The magnesium concentration in the reaction is another important factor since the polymerase requires magnesium to function. Lower magnesium concentrations give higher fidelity than high concentrations. Since each PCR product incorporates both primers, modification of the primers by attaching fluorescent tags or short DNA sequences, results in the same modification being present in all the PCR products. For this reason PCR can be used to prepare DNA sequences for cloning by attaching a DNA sequence which will be recognised by a restriction enzyme as well as inserting a mutation in the PCR product by changing the primer sequence. The type of polymerase being used is also important since not all enzymes contain a so called proof reading function for the correction of misincorporation of nucleotides which results in single base pair changes. This can be a critical factor to be considered when cloning a coding sequence for overexpression experiments as one base pair change can result in the production of a mutated protein or a prematured STOP codon. Polymerase derived from *Thermophilus aquaticus* (Taq) has an error rate of  $2.4 \times 10^{-5}$  whilst polymerase derived from *Pyrococcus furiosus* (Pfu), has a much lower error rate ( $0.2 \times 10^{-5}$ ) due to its proof reading capability. For this reason Pfu is a much slower enzyme than Taq. Hybrid enzymes based on the Pfu polymerase also exist. They possess the proofreading properties of Pfu but are as fast as Taq. In this study,

PCR was used to detect the expression of different genes (by using cDNA obtained from a reverse transcription of isolated RNA), attaching linkers to a specific sequence for cloning purposes and introducing site-specific mutations in a DNA sequence. Verification of the PCR target was done by sequencing. The reactions were performed in a thermal cycler (ABI Prism 3700). The optimal TA was found using a temperature gradient thermal cycler (iCycler) and identifying which temperature gave the highest yield with lowest amount of unwanted products. When error-free or mutagenesis PCRs were performed, Pfu-based polymerases (Pfu, Bioron; Pfx, Invitrogen) or a hybrid system (Expand High FidelityPLUS PCR System, Roche; Phusion, NEB) were used with an extension temperature of 72 °C.

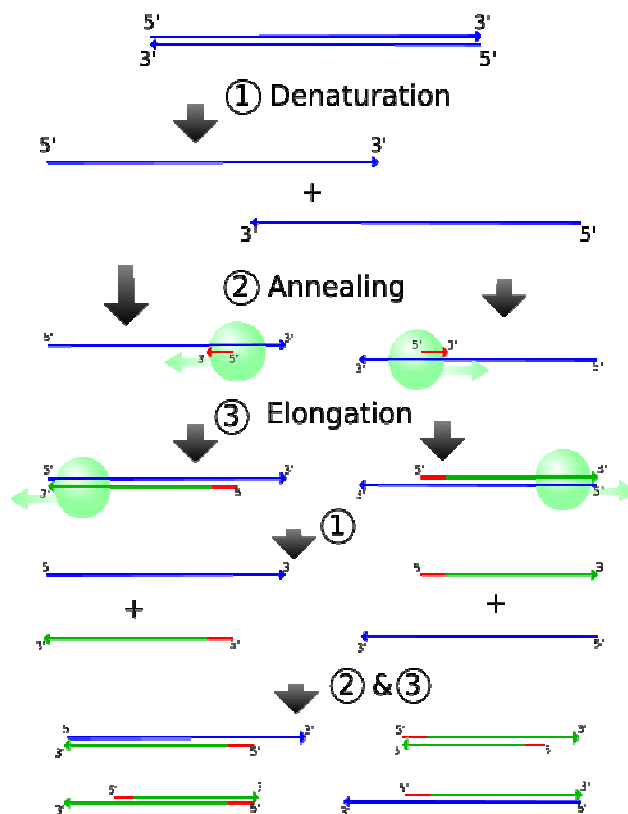


**Fig. 13** Schematic overview of the working principle of the polymerase chain reaction (PCR).

PCR starts with the initial denaturation (1) followed by the annealing step (2) and the elongation (3) in which the template is amplified. Steps 1-3 are repeated in circles for an exponential amplification. (modified from <http://en.wikipedia.org/wiki/File:PCR.svg>, used under the GNU Free Documentation License)

### **2.2.3.2 Real time PCR**

The real time PCR is a variation of the PCR in which the amplification of the PCR products is monitored during the amplification process. This can be done by several techniques, here the incorporation of a dye, SYBR green, in the PCR products were used. SYBR green, similar to ethidium bromide, becomes fluorescent after incorporation in double-stranded DNA. Subsequently, as the amounts of PCR products increase after each PCR cycle, also the SYBR green fluorescence increases and can be measured after each cycle. The SYBR green fluorescence can then be drawn as an amplification graph and the cycle number from which the PCR enters the exponential phase (CT value) can be determined. The CT value correlates antiparalel with the amount of PCR template and in the case of a cDNA in the end with the amount of RNA, meaning the lower the CT value, the higher is the RNA content of the sample. The PCR was performed with the following settings. First a heating to 95°C for 10 minutes was performed as a hot-start. As the polymerase used is blocked by a specific antibody to prevent unspecific amplifications at not-optimized conditions, the PCR-mix was heated to 95°C for 10 minutes to denaturate the antibody and releasing the polymerase. Then 44 cycles were performed with a denaturation step at 95°C for 15 seconds followed by a annealing/elongation step at 60°C for 1 minute.

### **2.2.3.3 DNA Sequencing**

Automated fluorescent sequencing utilizes a variation of the Sanger chain-termination protocol. In this method, the DNA to be sequenced acts as a template molecule to which a primer will anneal to begin enzymatic extension and amplification of a specific region of double-stranded DNA. The newly created fragments will be complementary to the template DNA. This process takes place during the cycle

sequencing reaction which works after the same principle as a PCR described before. As the reaction mix contains a mixture of deoxynucleotides (dNTPs) and dideoxynucleotides (ddNTPs), at concentrations that create a statistical probability that a dideoxynucleotide will be incorporated instead of a deoxynucleotide at each nucleotide position in the newly generated fragments, the chain termination occurs during the extension step. When a dNTP is incorporated, the new fragment will continue to grow. A ddNTP contains a hydrogen atom instead of a hydroxyl group at its 3' end and cannot participate in further extension. Therefore, when a ddNTP is incorporated, further chain elongation is blocked and this results in a population of truncated products of varying lengths. When separated by electrophoresis, a "ladder" of these truncated products will form, each differing in size by one nucleotide, with the smallest terminated fragments running fastest on the gel. There are four different ddNTPs that correspond to each of the four DNA nucleotides, and each ddNTP has a different color. Thus, each truncated fragment will contain a fluorescently labelled ddNTP at its 3' end, and the sequencing ladder will be composed of colored bands. The sequence can then be determined by correlating the color of a band on the gel with its specific ddNTP, and the order in which they ran on the gel. So, the first and smallest band visualized will correspond to the first labeled nucleotide incorporated immediately adjacent to the primer. The second band will be the fragments that consist of 1 unlabeled dNTP and 1 labeled ddNTP that terminated those particular growing chains. The third band will be made up of 2 unlabeled dNTPS followed by 1 labeled ddNTP, and so on up the gel. Once the sample has been amplified and labeled, it must be electrophoresed for separation and visualization of the labeled fragments. The dyes attached to ddNTPs are energy transfer dyes and consist of a fluorescein energy donor dye linked to an energy acceptor dichlororhodamine dye. This energy transfer system is much more sensitive than a single dye system. The

dye-labeled fragments are loaded onto the sequencers to allow capillary electrophoresis, through a liquid polymer. At the end of the capillary, a laser is placed which excites the fluorescent dyes attached to the fragments inducing them to emit light. The wavelength of the emitted light is specific for each dye. Wavelength separation occurs by a spectrograph onto a cooled, charge-coupled device (CCD). The data collection software collects these light intensities from the CCD camera at particular wavelength bands and stores them onto the sequencer's computer as digital signals for processing. The analysis software then interprets the fluorescent intensity at each data point. For cycle sequencing, the reagents were added, vortexed briefly and centrifuged down before placing them into the thermal cycler. The PCR products were cleaned from unincorporated dye using the Nucleo Seq sequencing clean-up kit (Macherey-Nagel). To prepare the spin columns, the powdered silica was collected at the bottom of the tube by centrifugation at 380 g for 1 minute. The silica powder was hydrated with water and incubated for 30 minutes at room temperature. The tubes were then centrifuged again to remove excess water. The sequencing PCR product was applied to the silica by pipetting in the middle of the tube. The cleaned product was collected by centrifugation at 380 g for 5 minutes

**Table 2 Sequencing mix and sequencing program for the ABI3100 Genetic Analyser and the BigDye Terminator v1.1**

Sequencing mix

DNA template 100 ng	~100ng
BigDye Terminator v1.1	3.0 µl
Sequencing Primer (10 mM)	1 µl
Add water	10 µl

Sequencing program

temperature	Time (min)	Cycles
96 °C	1:00	1x
96 °C	0:10	25x
50 °C	0:05	
60 °C	4:00	

and loaded onto a 96-well sequencing plate. The samples were then run on an ABI 3100 Genetic Analyser.

#### ***2.2.3.4 Agarose gel electrophoresis***

Agarose gel electrophoresis is used to separate DNA strands according to their size/weight ratio. The DNA is loaded onto an agarose gel and a current is passed through. Since DNA is negatively charged it moves from the negatively charged cathode towards the positively charged anode through the pores created by the polymerised agarose. As it moves through the gel, the different DNA strands start separating according to size with the smallest strands migrating faster than the longer strands. The resolution of the gel is determined by size of the pores which are in turn determined by the agarose concentration. The gel was prepared by melting agarose powder in electrophoresis buffer (1x TAE) until a clear transparent solution was achieved. The concentration of agarose depended on the size of the DNA strands to be separated. The open ends of the plastic tray supplied with the electrophoresis apparatus was sealed and set up horizontally. A comb containing the appropriate number of sample slots was chosen and positioned around 0.5 mm above the bottom of the gel casting tray. When the gel solution had cooled down to around 55°C, ethidium bromide was added to a final concentration of 0.5 µg/ml. The solution was then poured into the gel casting tray and allowed to harden for 30 minutes. The electrophoresis tank was then filled with electrophoresis buffer (1x TAE). The DNA samples were mixed with 0.2 volumes of 6X DNA loading buffer and then loaded onto the gel. A size standard was used to determine the approximal DNA fragment size. The lid of the electrophoresis tank was closed and the electrodes attached such that the DNA would migrate from the cathode to the anode. The power supply was set to 100 or 120V. After separation, the gel was removed from the tank and viewed

using a UV transilluminator connected to a camera. The picture of the gel was then printed and labelled.

**Table 3 Agarose gels concentration and their resolution for DNA separation**

<u>Agarose Concentration Gel (% [w/v])</u>	<u>Range of Separation of Linear DNA Molecules (kb)</u>
0.3	5-60
0.6	1-20
0.7	0.8-10
0.9	0.5-7
1.2	0.4-6
1.5	0-2-3
2.0	0.1-2

### ***2.2.3.5 Restriction digest***

Restriction digest is the process by which DNA molecules are cut into smaller pieces by enzymes called restriction endonucleases or restriction enzymes. These enzymes recognise a specific DNA sequence and cleave it wherever it occurs inside a DNA molecule. In most cases, the recognition sites are short (4-8 nucleotides) and are usually palindromic sequences, although also other non-palindromic recognition sites are known. Since both strands have the same sequence running in opposite directions, the enzymes make a double-stranded break, which, if the site of cleavage is off centre, generates fragments with short single stranded tail known as overhangs. These tails can hybridise to the tails of other fragments and are thus called “sticky ends”. On the other hand, when the cleavage site is in the centre of the palindrome no overhangs are generated and the fragments are said to be “blunt”.

Each enzyme requires particular conditions such as temperature, NaCl and MgCl<sub>2</sub> concentrations and pH. For this reason the right buffer has to be chosen for every enzyme.

DNA was digested with restriction endonucleases by incubating it in the presence of the desired enzyme and the appropriate buffer at 37°C for 1 h. After digestion, the DNA was visualised by agarose gel electrophoresis and/or purified for further processes such as cloning. The enzymes mentioned are all from New England Biolabs (Frankfurt am Main, Germany).

**Table 4 Reaction mix for NEB enzymes**

Restriction Reaction Mix

DNA up to	1 µg
Enzyme	0.25 units
10X Buffer	3.0 µl
Water up to	30 µl

### **2.2.3.6 DNA ligation**

DNA ligation was used to clone inserts into eukaryotic expression vectors. T4 DNA ligase (New England Biolabs) was used for this reaction. Around 50 ng of linearised, dephosphorylated vector were added to a 3-fold molar excess of insert and the volume adjusted to 10 µl with water. The following formula was used to calculate the molarity ends:

$$\text{Molarity of ends: Molarity} = [(\mu\text{g}/\mu\text{l}) \div (\text{base pairs} \times 650 \text{ Daltons})] \times 2 \text{ ends}$$

For convenience, usual 2 µl of vector and 6 µl of insert were used. Then 1 µl of 10x ligation buffer was added and the reaction mixed and centrifuged down. After adding of T4 DNA ligase (1 µl) the reaction was mixed, centrifuged down and incubated for 25 minutes at room temperature or for 16 h at 16°C and used directly for transformation.

### **2.2.3.7 Preparation of chemical competent bacteria**

To produce large amounts of plasmids, bacteria are used to replicate the DNA. For this purpose, so called “competent” bacteria are used which make it easy for plasmid DNA to be inserted into them. The technique used was based on the one described in the Maniatis’ laboratory manual [71].

A LB plate was streaked with XL-1 Blue or JM109 bacteria from a stock glycerol solution stored at -70°C and then incubated overnight at 37°C. Then a colony was picked and grown overnight in 5 ml LB medium. The next day, this volume was grown in 500 ml LB medium at 37°C for 3 to 4 h until its OD<sub>550</sub> was between 0.3 and 0.4. The culture then was centrifuged at 1500 g for 15 minutes at 4°C. The supernatant was decanted and the pellet resuspended in 5 ml ice cold TSS solution. Aliquots of 100 µl were then prepared on an ice/ethanol bath and the bacteria stored at -70°C until use.

The quality of new stocks of competent bacteria was checked by transforming an ampicillin-resistant plasmid into them and plating on to an LB-Amp plate. The number of colonies was counted after 16 h incubation at 37°C.

### **2.2.3.8 Chemical transformation**

The bacteria were thawed from -70°C on ice and 0.1 µg of DNA or 1/3 of ligation mix was added whilst stirring gently with the pipette tip. Then, bacteria were incubated on ice for 30 minutes and heated to 42°C for 90 seconds in a water bath. They were cooled on ice for 1 minute and 400 µl preheated (42°C) SOC medium was added. The bacteria were shaken at 225 rpm at 37°C for 60 minutes. The culture was then plated onto LB plates coated with the appropriate selective antibiotic (ampicillin 10 µg/ml or kanamycin 10 µg/ml) and grown for 16 h at 37°C.

The next day, at least one colony was chosen and inoculated in 2 ml LB medium and grown for 6 h at 37°C whilst shaking at 225 rpm, after which 1.5 ml of culture was used to perform a plasmid mini preparation. After confirming the presence of the right plasmid by restriction digest or sequencing, 200 µl of culture was grown in 200 ml of LB medium for 16 h at 37°C whilst shaking at 225 rpm. Plasmid maxi preparation was performed using the Qiagen Plasmid Maxi kit.

## **2.2.4 Protein methods**

### ***2.2.4.1 Protein isolation***

Proteins were extracted from cultured cells using different techniques. The guanidinium thiocyanate-acid phenol extraction used here has the advantage that one can obtain RNA and proteins from the same experiment and is based on the procedure described in the Maniatis laboratory manual [71].

Cells were washed with ice cold serum free medium and plates were frozen on liquid nitrogen. Cells were then lysed in GT-DTT buffer and total proteins from endothelial cells were purified using guanidine thiocyanate-acid phenol extraction, as described for purification of total RNA. The proteins which remained in the lower organic phase were precipitated overnight at 4°C by addition of 3 ml isopropanol and 600 µl of ethanol. Thereafter, the protein pellet was washed in 70% ethanol and dissolved in PBS containing 1% SDS and 1 mM NaF.

Alternatively, to detect phosphorylated proteins, cells were lysed in freshly prepared phospho-buffer. After scraping of the cells, samples were incubated for 30 minutes on ice, centrifuged for 10 minutes at 16000 g to remove cellular debris and stored at -20°C or -70°C until use.

As second alternative, cells were scraped directly in 1.5x Laemmli loading buffer, boiled at 95°C for 5 minutes and directly used for western blot analysis.

#### **2.2.4.2 Subcellular cell fractionation**

Microsomal membrane fraction was isolated as described with some modifications [73]. Briefly, cells were harvested in phosphor buffer without detergent and homogenized by sonification (5x 10 seconds burst). The cell homogenate was centrifuged at 1000g for 10 minutes at 4°C and the supernatant was further centrifuged at 12000g for 15 minutes at 4°C. Subsequently, the supernatant was centrifuged at 40.000g for 30 minutes at 4°C to receive the microsomal membrane fraction. The pellet was resuspended in 1.5X Laemmli buffer and applied for Western blot analysis.

#### **2.2.4.3 Protein quantification after Bradford**

Total protein quantification was performed after Bradford [74] using the Roti-Quant (Carl Roth GmbH) containing Coomassie Brilliant Blue Dye-G250. This dye appears in three different states which absorb at varying wavelengths (cationic 470 nm, neutral 650 nm, anionic 595 nm). By binding the dye with a protein it changes from a cationic to an anionic state and changes its absorption level to 595 nm. This absorption change is proportional to the protein concentration over a wide range. Coomassie Brilliant Blue-G250 binds primarily to basic amino acids. This accounts for the difference in the level of absorption of varying proteins. Therefore we used a BSA protein standard for quantification (0, 5, 10, 20, 30, 40, 50, 60 µg/ml). Protein cell lysates were diluted 1:100 to 1:300 and 80 µl of protein standard and samples were added to the wells of a 96-well microtiterplate. The Roti-Quant solution was diluted 1:5 and 200 µl were added to the samples and standard. Absorbance of the proteins was analyzed using a microplate reader (Tecan) and protein concentration was calculated performing a standard curve from the standard and linear regression analysis.

#### **2.2.4.4 SDS-PAGE and Western blot analysis**

Western blot is used to detect protein levels. After protein extraction, the proteins are loaded onto a denaturing polyacrylamide gel where they are separated according to size. They are then blotted onto a membrane which is hybridized with an antibody specific for the protein of interest (the primary antibody). The membrane is then incubated with another antibody which recognizes the primary antibody (the secondary antibody). The secondary antibody is tagged with horseradish phosphatase so the protein levels are detected by exposure of photographic films to the chemoluminescence given off by the secondary antibody.

Before performing the electrophoresis, samples were mixed with 3x Laemmli loading buffer and boiled at 95°C for 5 minutes. Proteins (50 µg) were separated by 8-12% SDS polyacrylamide gel electrophoresis (PAGE) in running buffer in a Mini-Protean 3 System (Biorad) and transferred to nitrocellulose Protran membranes (Schleicher & Schuell) using the Mini Trans-blot System (Biorad) in ice cold transfer buffer. After transfer, membranes were rinsed in water and incubated in Ponceau S solution for several minutes. The membranes were then washed in water to reduce background staining and the membranes were scanned for documentation and loading control. For reversing the Ponceau S staining, membranes were washed with TBS-T and then blocked for 60 minutes in TBS-T containing 5% non-dry milk or 5% BSA and then overnight at 4°C with specific antibodies. After incubation with primary antibodies, the membranes were washed 3 times for 10 minutes with TBS-T and incubated with a horseradish peroxidase-conjugated secondary antibody for 1 h. After washing the membranes 3 times for 10 minutes with TBS-T, protein bands were visualized by performing luminol-enhanced chemiluminescence. Blots were analyzed and quantified using ImageJ software (NIH, USA).

#### ***2.2.4.5 Stripping and reprobing***

To remove bound antibodies, membranes were incubated in stripping buffer for 30 minutes at 50°C. Thereafter, membranes were washed 2 times for 30 minutes in TBS-T, blocked for 2 h in TBS-T containing 5% non-dry milk and then incubated with the appropriate primary antibody.

#### ***2.2.4.6 Coimmunoprecipitation***

Coimmunoprecipitation was used to detect protein-protein interactions [71]. This technique can be used to detect interaction of endogenous and/or overexpressed proteins. It relies on cellular lysis without denaturing the proteins and whilst maintaining all protein interactions. An antibody is then used to precipitate a specific protein, which can precipitate some of its interaction partner together with it. The precipitate is separated from the remaining lysis product by the addition of beads which have a high affinity for the antibody. The whole complex can thus be pelleted by centrifugation. Finally the precipitated proteins are denatured and detected by Western blot.

The cells were washed with PBS and scraped in phosphor-buffer supplemented with protease inhibitors and samples were incubated on ice for 20 minutes. Then samples were centrifuged at 16000 g at 4°C for 15 minutes and the supernatant was transferred to new 1.5 ml reaction tubes. After protein concentration determination 500 µg protein was used for each immunoprecipitation and the remaining protein samples were stored at -20°C.

For setting the immunoprecipitation mix, per precipitation mix 30 µl of a 50:50 slurry sepharose beads solution in PBS were washed 3 times with phospho-buffer and resuspended in phospho-buffer. Protein samples were added to the beads and the solution was filled up to 500 µl with phosphor-buffer. Finally 4 µg GFP-antibody

(Invitrogen) was added and the mixture was incubated overnight at 4°C slowly rotating. The samples were then centrifuged for 1 minute. The supernatant was dissolved in 2x Laemmli lysis buffer and loaded onto an SDS-PAGE gel for Western blot.

The immunoprecipitate was washed 5 times with phospho-buffer. After the last wash the pellets were dissolved in 2X Laemmli buffer and loaded onto an SDS-PAGE gel for Western blot.

### **2.2.5 Statistical analysis**

Values presented are means  $\pm$  standard deviation. Results were compared by ANOVA for repeated measurements followed by Student–Newman–Keuls *t* test.  $P < 0.05$  was considered statistically significant.

## 3 Results

### 3.1 Expression and localization

Function and expression of the novel NOX2 homologues NOX1, NOX4 and NOX5 are poorly understood in the vasculature. Their expression and subcellular localization were therefore firstly investigated.

#### 3.1.1 Expression of NOX1, NOX2, NOX4, p22phox in endothelial cells

As a model for endothelial cells, we used the endothelial cell line Ea.Hy926 and human microvascular endothelial cells (HMEC-1). In Ea.Hy926 cells, the expression levels of NOX1, NOX2, NOX4 and ,in addition, of the small NADPH oxidase subunit p22phox were analyzed by RT-PCR and Western blot analyzes. NOX2, NOX4 and p22phox were easily detectable in Ea.Hy926 cells at the mRNA (Fig. 14A) and protein levels (Fig. 14B). However, in polymorphonuclear neutrophils, which were used as known model cells for the phagocytic NADPH oxidase, NOX2 and p22phox proteins appeared to be the only detectable NADPH oxidase subunits (Fig. 14B). RT-PCR and Western blot analyzes showed that NOX1 was expressed in Ea.Hy926 cells (Fig. 14A, B), although detection of NOX1 mRNA levels required increased cycle numbers in Ea.Hy926 cells (Fig. 14A). Similarly, qPCR analysis of the NOX1 RNA level in HMEC-1 and CaCo2 cells, a colon carcinoma cell line known to highly express NOX1, showed a higher CT value (cycle of take off) for HMEC-1 cells (CT=32) than for CaCo2 cells (CT=25) (Fig. 14C).

#### 3.1.2 Expression of NOX5 variants in endothelial cells.

To investigate whether NOX5 is expressed in vascular cells, RT-PCR was performed with primers amplifying a region at the 3' end of the coding sequence which is

conserved in all NOX5 variants. A PCR product corresponding to the expected NOX5 sequence (501 bp) was detected in human microvascular endothelial cells (HMEC-1), human umbilical vein endothelial cells (HUVEC), pulmonary artery smooth

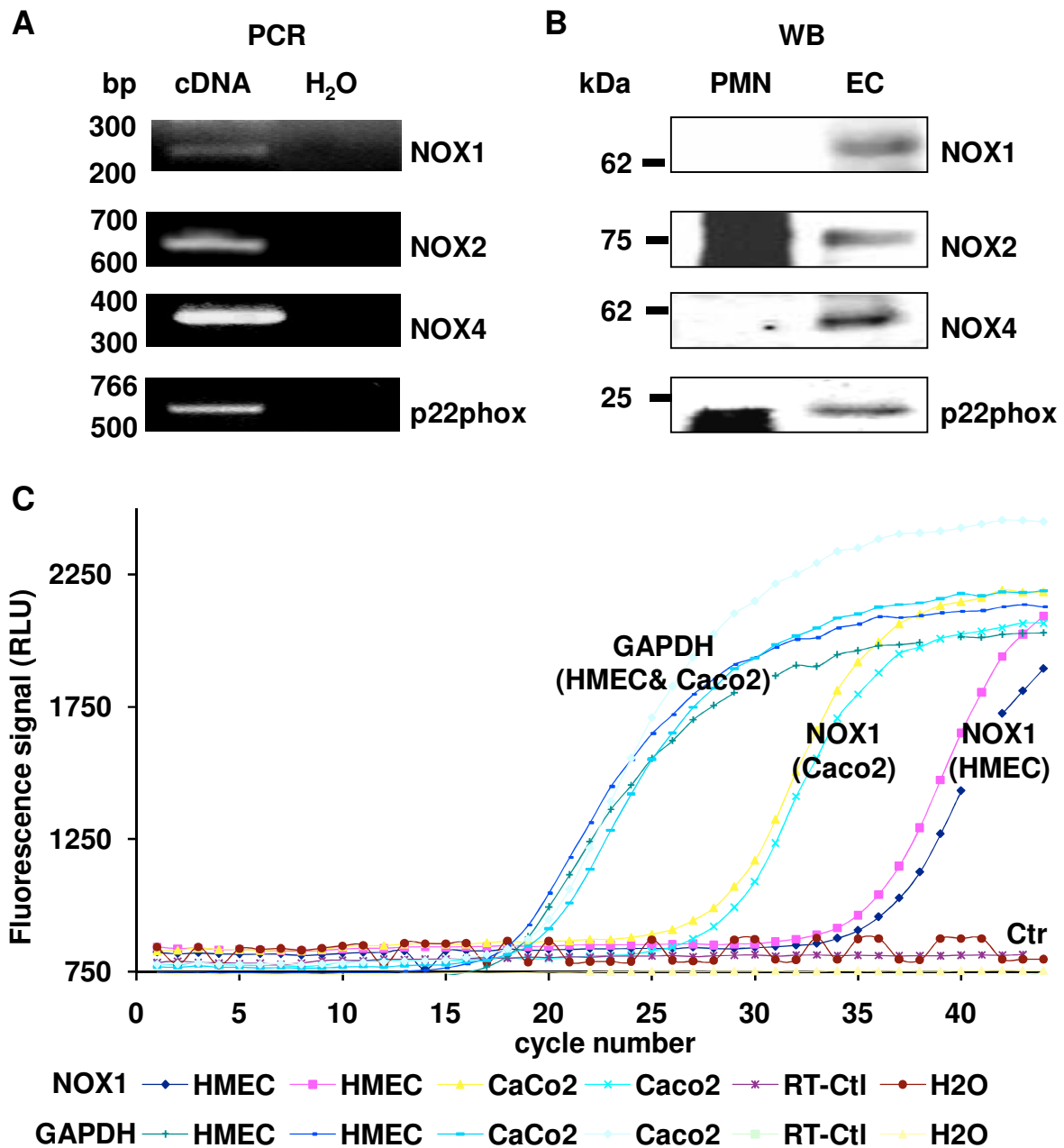


**Fig. 14** NOX1, NOX2, NOX4 and p22phox mRNA and protein are expressed in endothelial cells.

A. RT-PCR was carried out with cDNA reverse transcribed from mRNA derived from Ea.Hy926 cells using specific primers for p22phox, NOX1, NOX2, NOX4 (lane 1: cDNA derived from mRNA, lane 2: H<sub>2</sub>O as negative control). B. Western blot analysis was performed with Ea.Hy926 cells and polymorphonuclear neutrophils (PMN) lysates using antibodies against human p22phox, NOX1, NOX2, NOX4. C. Representative amplification graph for a qPCR analysis of the NOX1 RNA levels in HMEC-1 and CaCo2 cells. Amplification graph of GAPDH shown as indicator for equal amounts of cDNA for CaCo2 and HMEC-1 cells. All PCR products were confirmed by sequencing.

muscle cells (PASMC), and colon carcinoma cells (CaCo2) used as positive control (Fig. 15A). Four NOX5 variants have been described so far which differ in the sequences of their calcium-binding domains in the N-terminus [45]. To discriminate between the different variants and to analyze which of the NOX5 variants were present in vascular cells, primers were designed to specifically amplify the  $\alpha$ -,  $\beta$ -,  $\gamma$ -, and  $\delta$ -variants of NOX5. RT-PCR followed by sequence analysis of the respective PCR products revealed that endothelial cells (HMEC-1 and HUVEC) expressed NOX5 $\beta$  and NOX5 $\delta$ . In contrast, CaCo2 cells expressed NOX5 $\alpha$  and NOX5 $\gamma$  and PASMC expressed all four variants (Fig. 15B). For detection on protein level, an antibody against an epitope in the core region of NOX5 was designed in the lab and Western blot analysis of HMEC-1 cells was performed. In addition to a band of 75 kDa corresponding to NOX5, a band at around 60 kDa was detected whereas no corresponding bands were observed in lysates from polymorphonuclear neutrophils, which were reported not to express NOX5 (Fig. 16A). Furthermore, after preincubation of the antibody with the peptide used for immunization, these bands

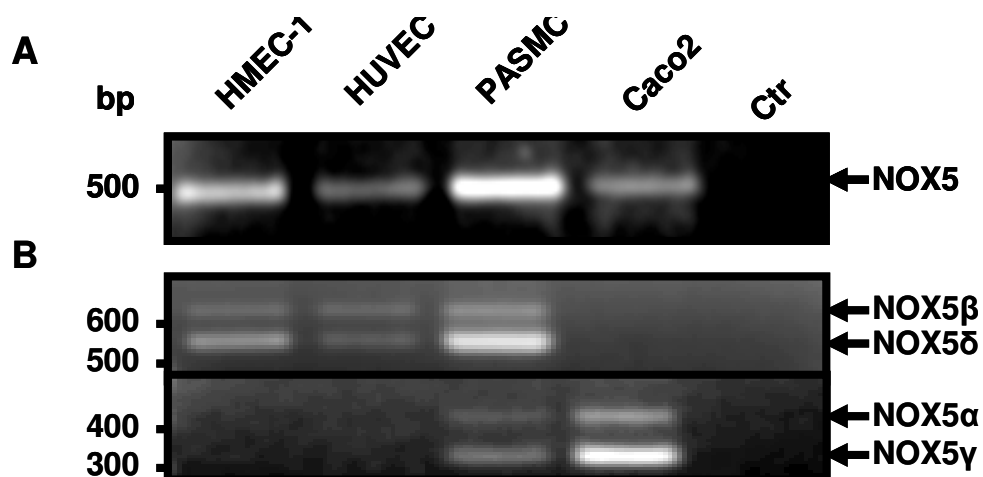


**Fig. 15** Different NOX5 splice variants are expressed in endothelial cells.

RT-PCR was carried out with mRNA derived from human microvascular endothelial cells (HMEC-1), human umbilical vein endothelial cell (HUVEC), pulmonary artery smooth muscle cells (PASMC) and colon carcinoma cells (CaCo2). A. PCR was performed using specific primer pairs to detect NOX5. PCR was performed using specific primer pairs for the calcium-binding domain containing regions of NOX5 $\alpha$ , NOX5 $\beta$ , NOX5 $\gamma$  or NOX5 $\delta$  (B).

were not detectable anymore suggesting the presence of two different NOX5 variants in HMEC-1 cells (Fig. 16A). Previously, a NOX5 variant lacking the calcium-binding domains and thus resembling other NOX homologues has been described [75]. To test whether the shorter NOX5 protein detected by our antibody resembles the reported NOX5 variant we cloned the full length coding sequence of this variant, which we termed NOX5S, from HMEC-1 and from CaCo2 cells. Sequence analysis confirmed the presence of the complete coding sequence of NOX5S (Genbank #DQ413001) leading to a predicted protein of 565 amino acids. To further confirm that NOX5 and NOX5S are present in HMEC-1 cells and detected by the antibody, NOX5S and NOX5 $\beta$  were overexpressed in HMEC-1 cells. Western blot analysis using the NOX5 antibody revealed bands at 60 and 75 kDa (Fig. 16B) similarly to non-transfected cells and confirming that the antibody recognized both NOX5 variants in HMEC-1 cells. In addition, NOX5S and NOX5 $\beta$  were fused to green fluorescent protein (GFP) and these fusion proteins were expressed in HMEC-1 cells. Western blot analyzes with antibodies against NOX5 and GFP revealed bands at 85 and 100 kDa corresponding to the respective NOX5 fusion proteins (Fig. 16D), further confirming that this antibody recognizes NOX5 and NOX5S and that HMEC-1 cells express both NOX5 proteins. Densitometric quantification further suggested that approximately one third of the total NOX5 content represented NOX5S in HMEC-1 cells (Fig. 16E). We further investigated the expression of NADPH oxidase subunits in the vasculature. Since NOX5 mRNA has been previously described to be expressed in spleen [45], immunohistochemistry was performed in archival tissue samples from spleen as a positive control and for testing our developed antibody. Indeed, positive NOX5 staining was observed in spleen tissue (Fig. 17A). In addition, strong staining for NOX5 was detected in spleen vessels in the smooth muscle cell layer which was positive for  $\alpha$ -actin (Fig. 17A) as well as in the endothelial cell layer

(Fig. 17A) which was positive for PECAM-1 [53] confirming the presence of NOX5 in the vasculature. To test whether NOX5 protein was present in vessels from non-lymphoid tissues immunohistochemistry was performed in lung tissue. Consistently with the situation in the spleen, NOX5 protein was indeed detected in the wall of pulmonary vessels in endothelial as well as in smooth muscle cells (Fig. 17B).

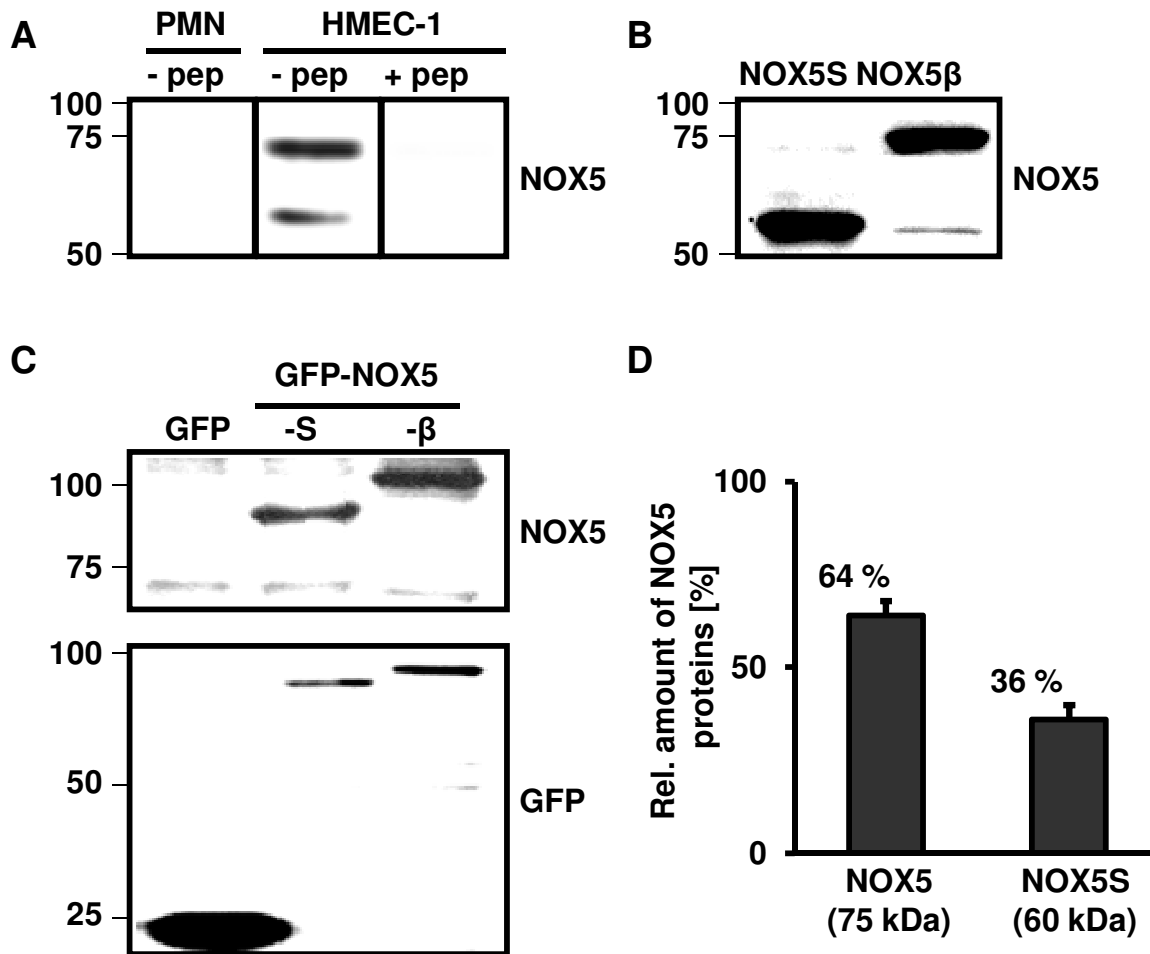


**Fig. 16** Different NOX5 proteins are expressed in endothelial cells.

A. Western blot analysis was performed in polymorphonuclear neutrophils (PMN) or in HMEC-1 cells using NOX5 antibody (-pep (without peptide)), or NOX5 preadsorbed with the antigenic peptide (+pep (with peptide)). B. HMEC-1 cells were transfected with plasmids encoding for NOX5S or NOX5β and Western blot analysis was performed using an antibody against NOX5. C. HMEC-1 cells were transfected with plasmids encoding GFP, GFPNOX5S or GFPNOX5β, and Western blot analysis was performed using antibodies against NOX5 or GFP. D. The relative levels of the 75 kDa band (NOX5) and the 60 kDa band (NOX5S) were determined from immunoblots by densitometry using GelDoc software. Data are presented as relative amount of NOX5 (75 kDa) and NOX5S (60 kDa) to total NOX5 (100%) (n=3).

### 3.1.3 Expression of NOXA1 and NOXO1 in endothelial cells

In the next step we investigated whether endothelial cells express the p47phox homologue NOXO1 and p67phox homologue NOXA1. RT-PCR studies were performed with Ea.Hy926 cells and HEPG2 cells, as NOXA1 and NOXO1 are known to be expressed in the liver [47], using specific primers for NOXA1 and NOXO1. Surprisingly, in both cases longer PCR products were detected. In addition to the expected fragments of 214 bp (NOXA1) or 159 bp (NOXO1) longer fragments of 326 bp (NOXA1) or 270 bp (NOXO1) were amplified. (Fig. 18A, 19A, red arrows).

Sequencing analysis revealed that both additional PCR products contained NOXA1

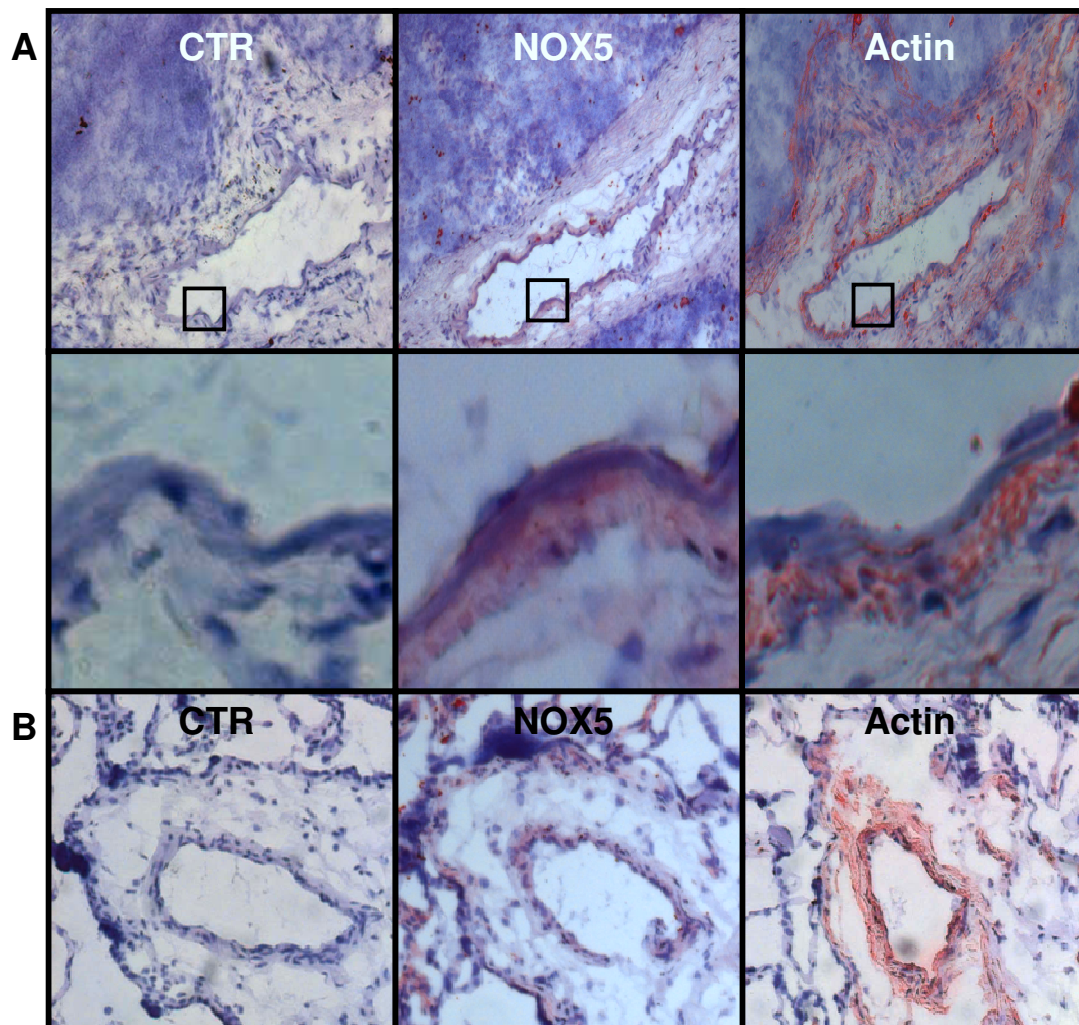


**Fig. 17** p22phox and NOX5 are expressed in the vessel wall.

NOX5 expression was detected in human spleen (A) or human lung (B) using an antibody against NOX5.  $\alpha$ -actin staining (Actin) was used to mark the smooth muscle cell layer. As negative control, the first antibody was omitted (CTR).

and NOXO1, respectively, but revealed potential new splice variants of NOXA1 and NOXO1. The primers used for NOXA1 were spanning from exon 2 to exon 4. The longer PCR product contained additional nucleotides from the intron upstream of exon 3 in accordance to the gene bank entry (NT\_078083). The transition between exon 2 and the novel nucleotides corresponded to the canonical GT-AG splicing rule indicating a novel splice variant of NOXA1 (Fig. 18B).

Assuming no other differences, the partial incooperation of intron 2 into the mRNA of NOXA1 would lead to a premature STOP codon at 307 bp resulting in a protein of 102 amino acids. The primers for NOXO1 were also spanning between exon 2 and exon 4 in accordance to the gene bank intron-exon structure (NT\_037887). Here, we found that the longer PCR product contained the intron between exon 3 and exon 4 which was not excised in the novel PCR product, whereas the intron between exon 2 and exon 3 was regularly spliced (Fig. 19B). Therefore this amplificate may be either

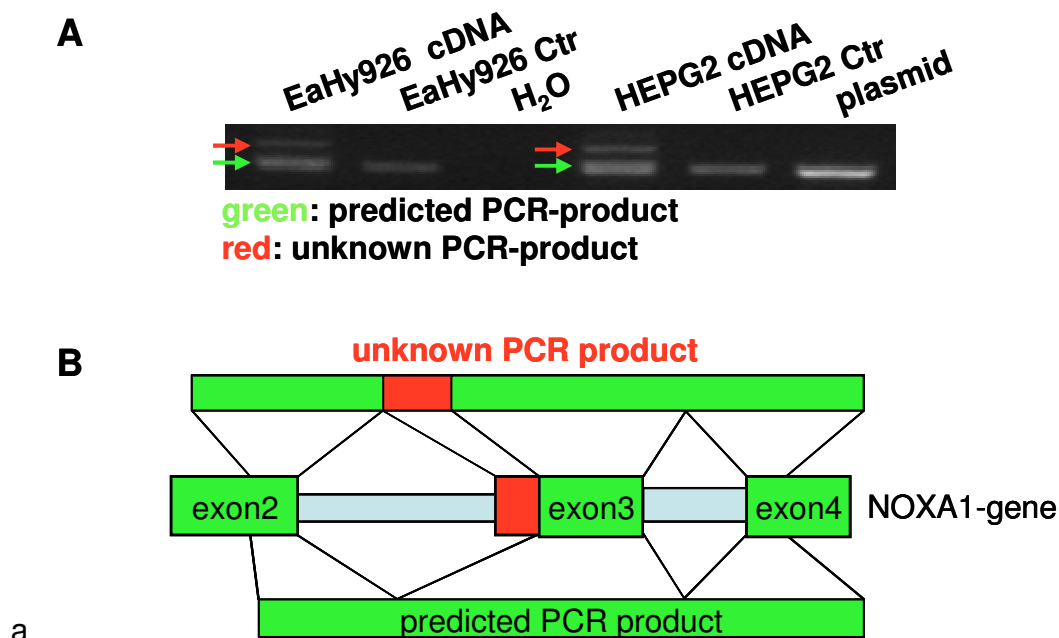


**Fig. 18 NOXA1 mRNA is expressed in endothelial cells and HEPG2 cells.**

A. RT-PCR was carried out with cDNA reverse transcribed from mRNA derived from Ea.Hy926 and HEPG2 cells using specific primers for NOXA1. Arrows indicating the predicted and and additional PCR product. B. Schematic figure of the novel PCR product. The additional band is a product of a novel conical splice site upstream of exon 3 of the NOXA1 gene, which leads to the insertion of several nucleotides in the transcript.

result of an incomplete splicing or of an alternative splicing. Under the assumption that there are no further differences between the novel cDNA and the published ones, the inclusion of intron 3 would predict an early STOP codon at 328 bp resulting in a protein of 109 amino acids instead of 369 amino acids of the full length NOXO1.

### 3.1.4 Localization of NOX2, NOX4, NOX5, but not of NOX1 in the endoplasmic reticulum of endothelial cells

In the next step we investigated the intracellular localization of the NADPH oxidase homologues. First, coimmunofluorescence studies for NOX2 and NOX4 were performed, which revealed that both NOX2 and NOX4 colocalize in an intracellular compartment in the same cell (Fig. 20A). Although NOX2 was suggested to be localized in the plasma membrane [21], only a faint peripheral staining for NOX2 (Fig. 20A, arrow), but not for NOX4, could be detected. However, a strong perinuclear staining for both NOX2 and NOX4 was found. Further coimmunofluorescence studies

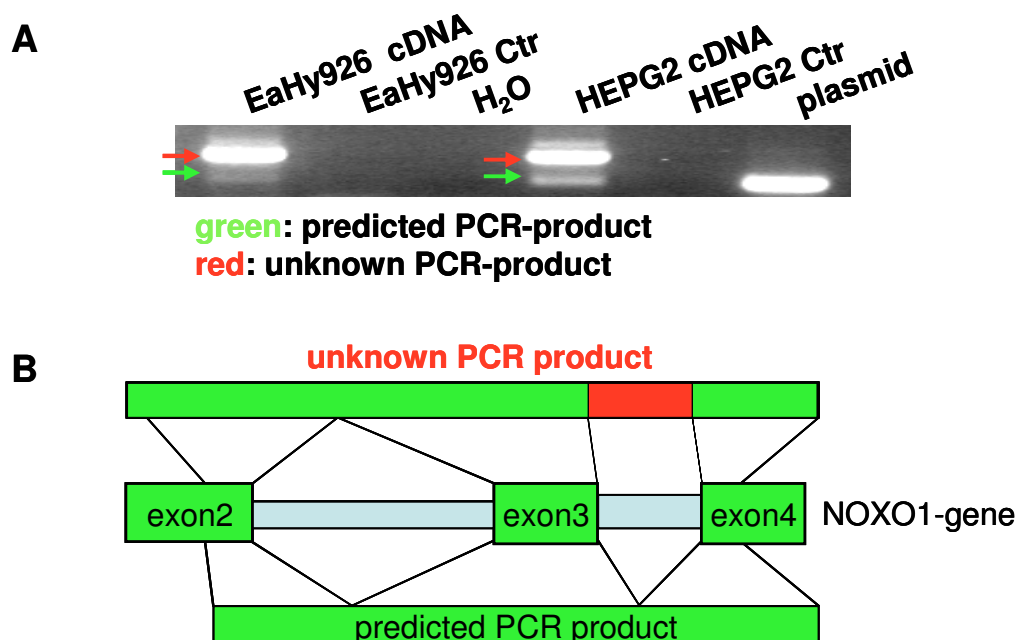


**Fig. 19** NOXO1 mRNA is expressed in endothelial cells and HEPG2 cells.

A. RT-PCR was carried out with mRNA derived from Ea.Hy926 cells and HEPG2 cells using specific primers for NOXO1. Arrows indicating the predicted and and additional PCR product. B. Schematic figure of the novel PCR-product, which includes the intron between exon 3 and exon 4.

using an Alexa Fluor488-coupled phalloidin against f-actin revealed that NOX2 shows a faint colocalization with actin at the plasma membrane whereas NOX4 did not exhibit this pattern (Fig. 20B). As the perinuclear localization of NOX2 and NOX4 resembled the ER, further co-immunofluorescence studies were performed for NOX1, NOX2 and NOX4 together with calreticulin, a marker protein for the ER (Fig. 21). NOX2 and NOX4 showed an intracellular perinuclear localization at least partially colocalising with calreticulin. NOX1 showed also an intracellular, perinuclear localization, however there was no colocalization with calreticulin (Fig. 21). For confirmation of the ER localization of p22phox, NOX2 and NOX4, Ea.Hy926 cells were cotransfected with an YFP-tagged p22phox (YFPp22phox), a CFP-tagged NOX2 (CFPNOX2) and an YFP-tagged NOX4 (YFPNOX4) together with an ER localized CFP or YFP (Fig. 22A, B, C). Furthermore, Western blot analysis demonstrated the presence of p22phox, NOX1, NOX2 and NOX4 as well as of the ER protein calnexin in microsomal fractions of Ea.Hy926 cells (Fig. 22D). In contrast, the transcription factor ARNT and the cytoplasmically located p38 MAP kinase were not present in this fraction as expected (Fig. 22D). To determine whether the expression pattern observed for p22phox, NOX2 and NOX4 were specific for endothelial cells, the intracellular localization in cervix carcinoma cells (HeLa) was investigated. HeLa cells were transfected with YFPp22phox, CFPNOX2, YFPNOX4, together with an ER-localized fluorescent protein (ERYFP or ERCFP). In contrast to the situation in endothelial cells, only p22phox showed a colocalization with the ER-marker, whereas NOX2 and NOX4 showed a more peripheral membrane staining (Fig. 23). To investigate the intracellular localization of NOX5S and calcium binding NOX5 variants, Ea.Hy926 cells were transfected with plasmids encoding for GFP-fusion proteins of NOX5S (GFPNOX5S) and NOX5 $\beta$  (GFPNOX5 $\beta$ ) as a representative member of the EF-hands containing NOX5 variants (Fig. 24A). Both

constructs showed an ER-like localization. We also investigated their intracellular localization in HMEC-1 cells. For this, cells were transfected with either GFPNOX5S or GFPNOX5 $\beta$  and coimmunofluorescence studies together with calreticulin were performed using an anti-GFP- and an anti-calreticulin antibody. Both NOX5 variants colocalized with calreticulin (Fig. 24B). Similarly, in Hela cells cotransfected with GFPNOX5S together with an ER-localized fluorescent protein (DsRed) showed a colocalization of NOX5S with the ER-marker (Fig. 24C). Immunofluorescence studies of endogenous NOX5 in HMEC-1 cells, using antibodies against NOX5 and calreticulin showed a colocalization of NOX5 with the ER-marker (Fig. 24D).

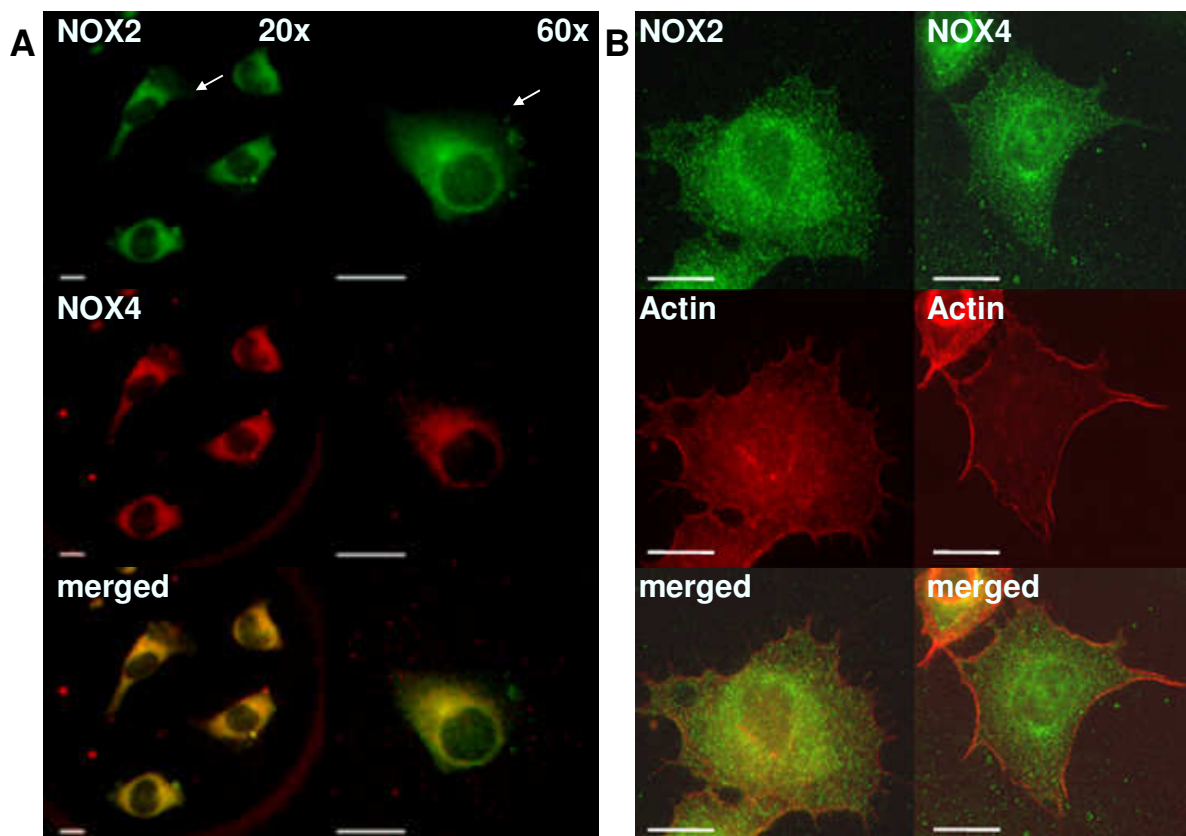


**Fig. 20** NOX2 and NOX4 colocalize in an intracellular compartment in endothelial cells, but only NOX2 colocalizes with f-actin.

A. Immunofluorescence was performed on Ea.Hy926 cells using antibodies against NOX2 (green) and NOX4 (red). Fluorescence images were taken at a 20x magnification (left column) and 60x magnification of a representative cell (right column). B. Immunofluorescence was performed on Ea.Hy926 cells using antibodies against NOX2 (left column, green) or NOX4 (right column, green) together with staining for f-actin (red). All scale bars are 20  $\mu$ m.

## 3.2 Interaction of NOX2, NOX4, NOX5S and NOX5 $\beta$ with p22phox and contribution to basal endothelial ROS generation

### 3.2.1 Interaction of NOX2, NOX4, NOXS and NOX5 $\beta$ with p22phox

In the phagocytic NADPH oxidase, dimerization of NOX2 with p22phox is required for functional activity of the enzyme. As NOX4 and the two NOX5 variants NOX5S and NOX5 $\beta$  show a homologous domain structure, we tested the interaction between NOX2, NOX4, NOX5S and NOX5 $\beta$  with p22phox in HeLa cells using bimolecular fluorescence complementation (BiFC). The BiFC approach is based on the complementation of two non-fluorescent fragments of a fluorescent protein due to

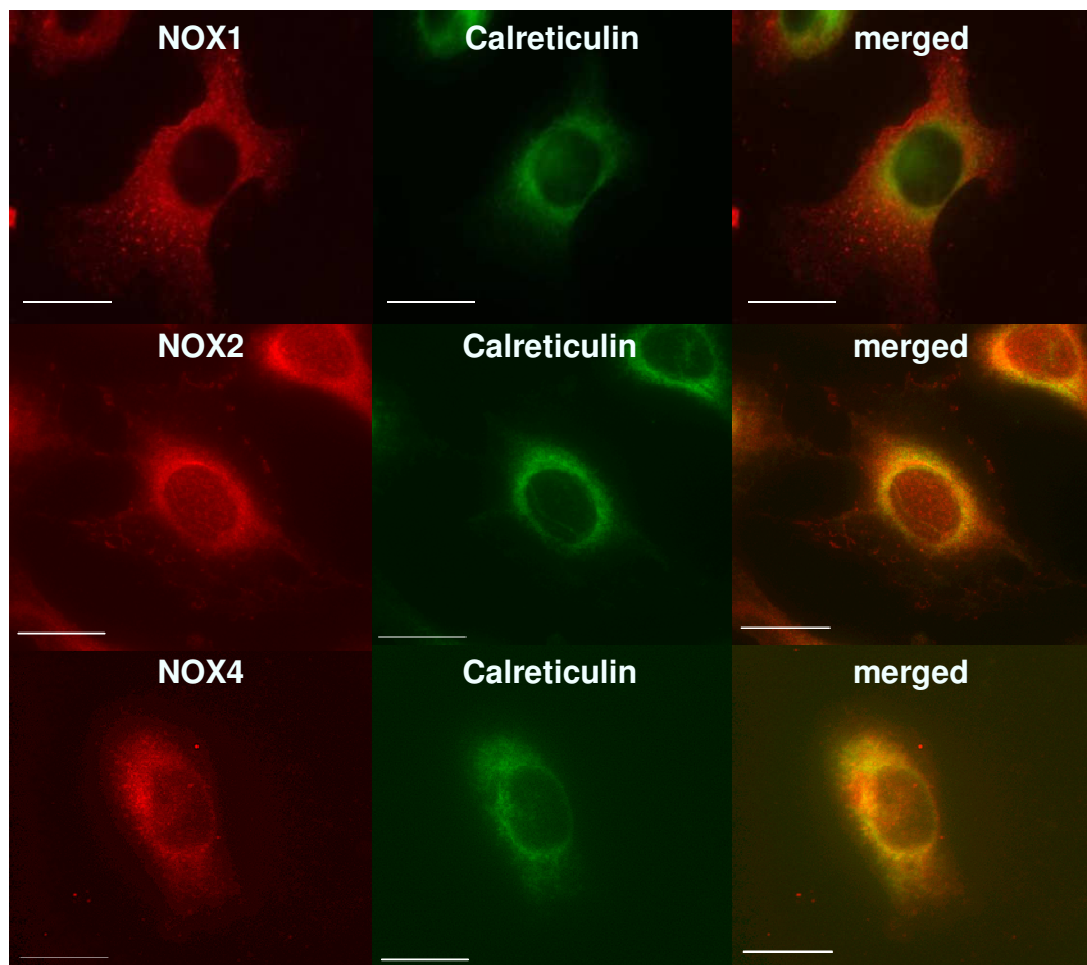


**Fig. 21** NOX2, NOX4 but not NOX1 are intracellularly localized in endothelial cells.

Ea.Hy926 cells were stained with antibodies against NOX1, NOX2 and NOX4 together with an antibody against calreticulin, a marker for the ER. Merged images show overlay of NOX2, and NOX4 but not NOX1 with calreticulin. All scale bars are 20  $\mu$ m.

protein-protein interaction of potential interacting proteins fused to these fragments (Fig. 25A) [76, 77]. Complementary fragments of YFP (YN and YC) were fused to the 3'-ends of the different NOX proteins and p22phox. Specifically, NOX2, NOX4, NOX5S and NOX5 $\beta$  were fused to the YC-fragment (NOX2YC, NOX4YC, NOX5SYC, and NOX5 $\beta$ YC) and p22phox was fused to the YN-fragment (p22phoxYN). Upon interaction of the proteins of interest, the fluorescent chromophore YFP is restored and can be detected by fluorescence microscopy. HeLa cells were transfected with the plasmid encoding p22phoxYN with either

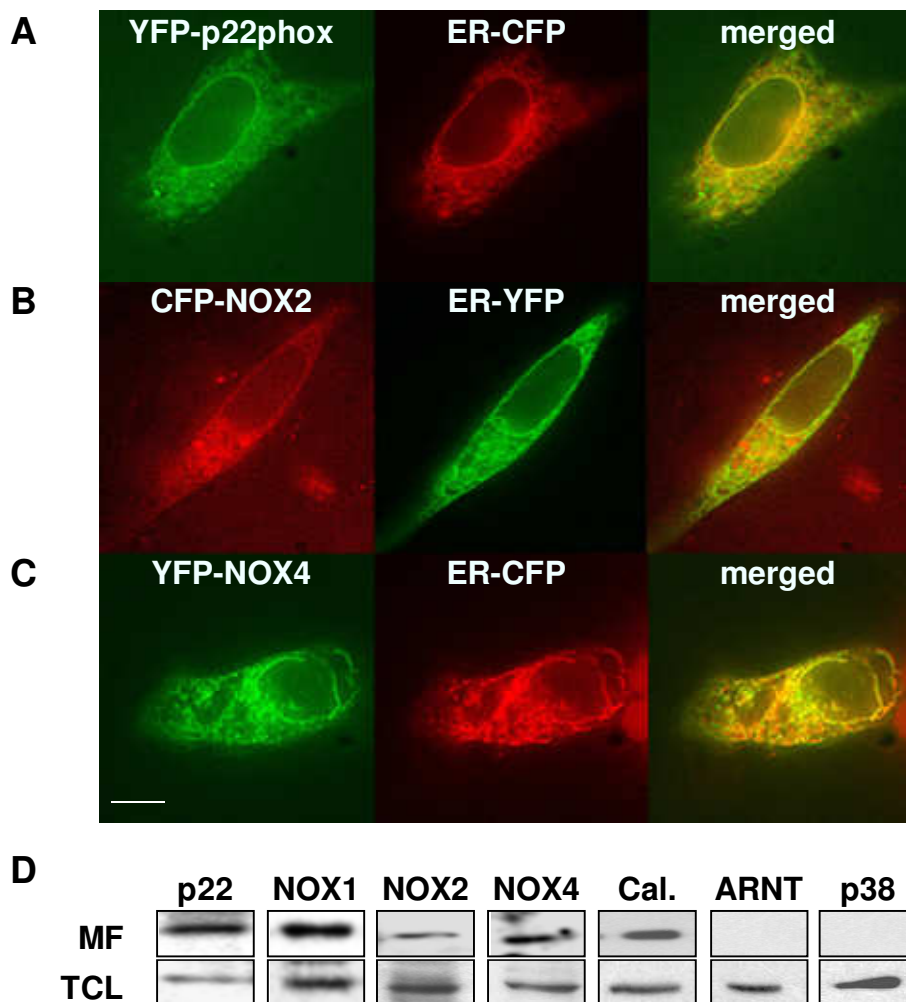


**Fig. 22** p22phox, NOX2 and NOX4 are expressed in the endoplasmic reticulum of endothelial cells.

Ea.Hy926 cells were cotransfected with YFP-p22phox (A), CFP-NOX2 (B) or YFP-NOX4 (C) and constructs where the ER localization signal was linked to either CFP or YFP. Scale bar is 20  $\mu$ m for all panels. D. Ea.Hy926 cells were fractionated and Western blot analysis was performed using the microsomal fraction (MF) or total cell lysate (TCL) and antibodies against p22phox (p22), NOX1, NOX2, NOX4, calnexin (Cal.), ARNT and p38 MAP kinase (p38).

NOX2YC or NOX4YC. YFP-fluorescence was monitored by fluorescence microscopy (Fig. 25B). Both, NOX2 and NOX4 formed complexes with p22phox in a perinuclear compartment resembling the ER. No fluorescence was detectable in cells transfected with plasmids encoding for NOX2YC or NOX4YC or p22phoxYN and YN or YC lacking a fusion, respectively (Fig. 25B). Cotransfection of NOX5 $\beta$ YC or NOX5SYC with p22phoxYN resulted in a strong perinuclear fluorescence similar to the pattern observed with NOX2 and NOX4, indicating that both NOX5 variants interact with p22phox (Fig. 25C). In contrast, transfection of NOX5 $\beta$ YC or NOX5SYC with the YN-fragment or p22phoxYN with the YC-fragment did not lead to fluorescence complementation (Fig. 25C). To confirm that p22phox interacts with both NOX2 and NOX4, coimmunoprecipitation studies of p22phox and NOX2 or NOX4 were

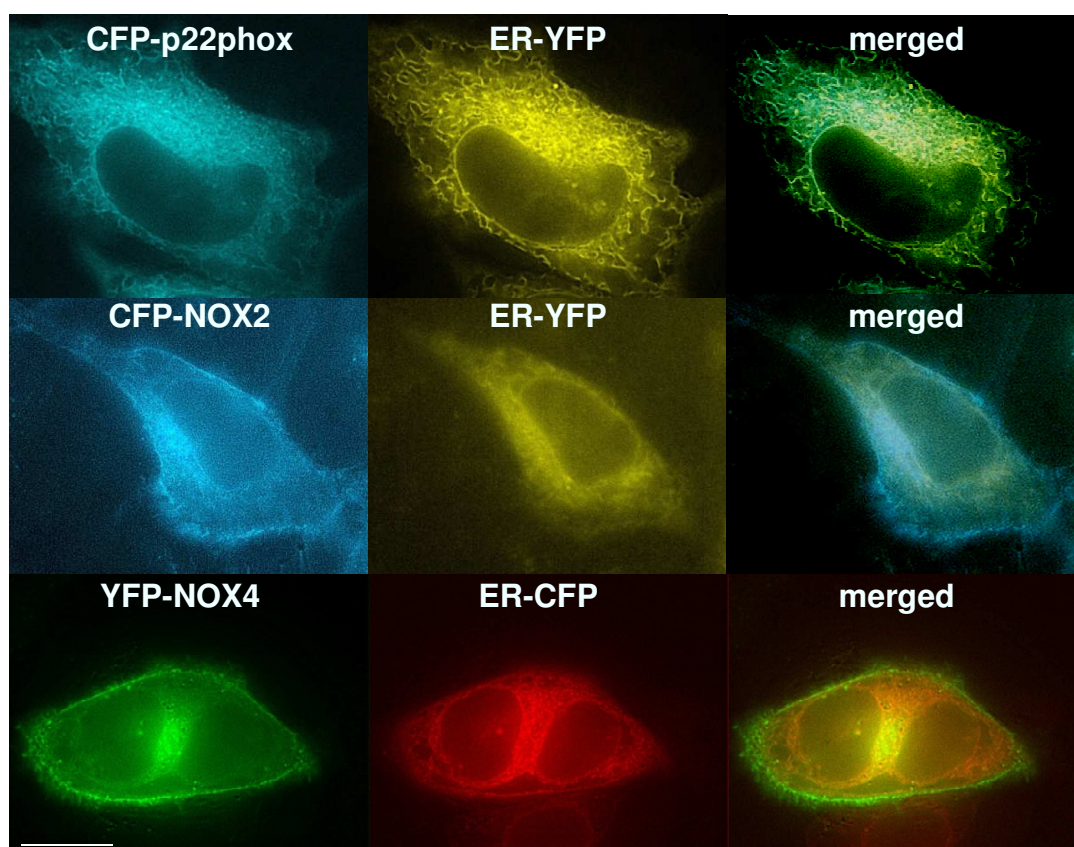


**Fig. 23** p22phox, but not NOX2 and NOX4 are localized in the endoplasmic reticulum of cervix carcinoma cells.

Cervix carcinoma cells (HeLa) were transfected either with CFP-p22phox, CFP-NOX2 and YFP-NOX4 together with constructs where the ER localization signal was linked to CFP, YFP or DsRed. Merged images show overlay of p22phox with ER-marker. Scale bar is 10  $\mu$ m for all panels.

performed (Fig. 26A). HEK293 cells were cotransfected with a plasmid encoding human p22phox and plasmids encoding NOX2 or NOX4 fused to either CFP (CFP-

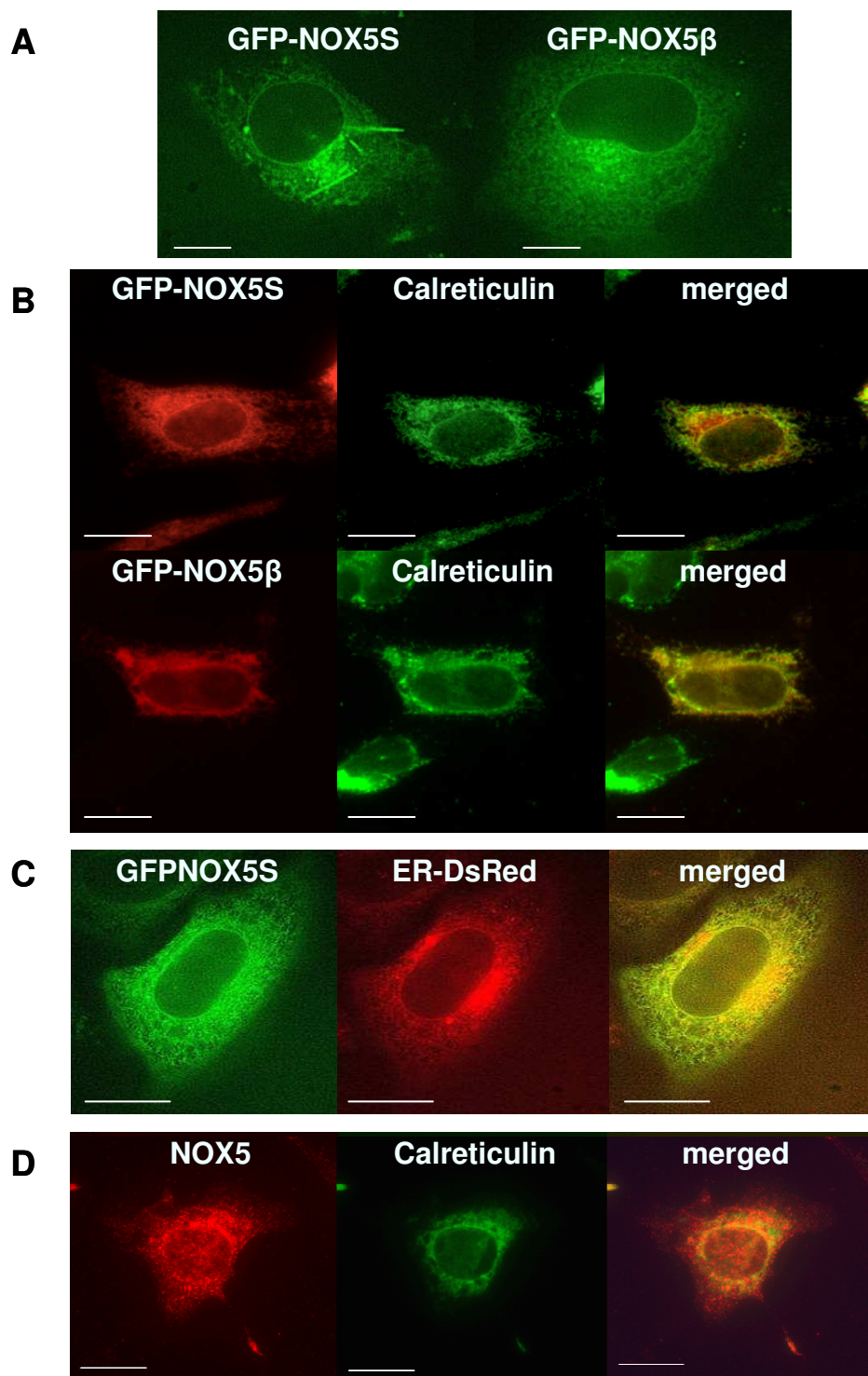


**Fig. 24** NOX5 variants are expressed in an ER like compartment in endothelial cells.

A. Ea.Hy926 cells were transfected with GFPNOX5S or GFPNOX5β and GFP-fluorescence pictures were taken. B. HMEC-1 cells were transfected with either GFPNOX5S or GFPNOX5β and stained with antibodies against GFP and calreticulin. C. HeLa cells were transfected with GFPNOX5S and ER-DsRed and GFP- and DsRed fluorescence pictures were taken. D. Endogenous NOX5 and calreticulin were stained in HMEC-1 cells using antibodies against NOX5 and calreticulin. Scale bars are 10 μm.

NOX2) or the YC- fragment (NOX4YC). Immunoprecipitation was performed with an antibody against GFP. Subsequent Western blot analysis with an antibody against

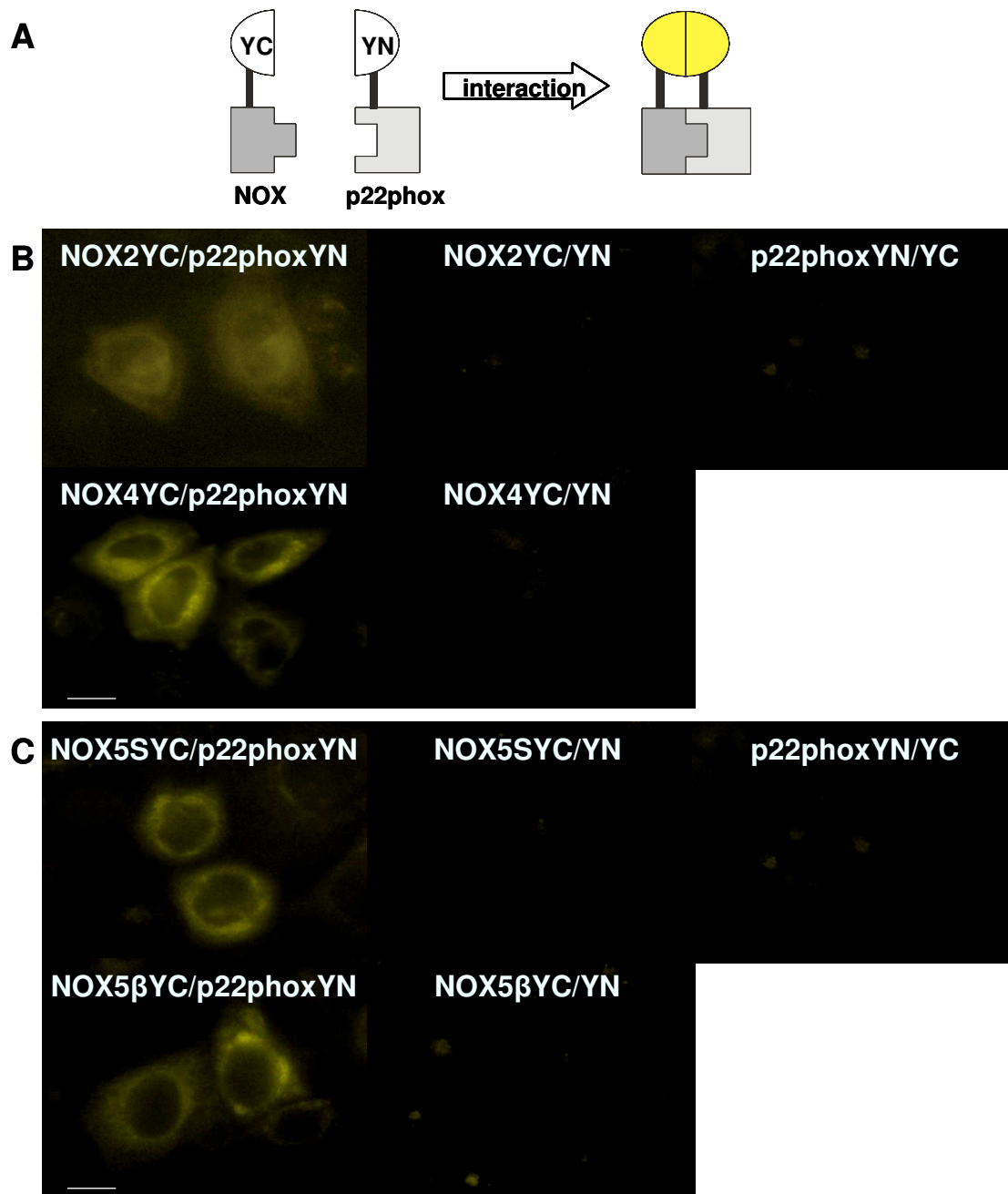


**Fig. 25** Bimolecular fluorescence studies show an interaction between NOX2, NOX4, NOX5S or NOX5 $\beta$  and p22phox.

A. Illustration of the principle of the Bimolecular Fluorescence Complementation (BiFC). After interaction, the YC and YN fragments form the fluorophore whose fluorescence light can be monitored using fluorescence microscopy. B. HeLa cells were transfected with p22phoxYN and either NOX2YC or NOX4YC and fluorescence pictures were taken showing an interaction of NOX2 and NOX4 with p22phox. C. Cells were transfected with p22phoxYN and either NOX5SYC or NOX5 $\beta$ YC and fluorescence pictures were taken showing an interaction of NOX5S and NOX5 $\beta$  with p22phox. No fluorescence was observed in negative controls (NOX2YC/YN, NOX4YC/YN, NOX5SYC/YN, NOX5 $\beta$ YC/YN and p22phoxYN/YC). Scale bar is 20 $\mu$ m for all panels.

p22phox revealed that p22phox was detectable in NOX2- and NOX4-expressing cells, but not in control cells expressing only GFP (Fig. 26A), indicating that both NOX2 and NOX4 interact with p22phox. For confirmation of the interaction between p22phox and NOX5S or NOX5 $\beta$ , coimmunoprecipitation was performed in HEK293 cells (Fig 26B). Cells were cotransfected with p22phox and GFPNOX5 $\beta$ , GFPNOX5S or GFP control vector and immunoprecipitation was carried out with a polyclonal antibody against GFP. Western blot analysis using an antibody against p22phox showed that both NOX5 $\beta$  and NOX5S can interact with p22phox whereas no specific band could be observed in cells transfected with control vector (Fig. 26B). To determine whether NOX5 proteins interact with endogenous p22phox, immunoprecipitation was performed in HEK293 cells transfected with GFPNOX5 $\beta$ , GFPNOX5S, CFPNOX2 or GFP control vector, using an antibody against GFP. As expected, Western blot analysis using the p22phox antibody revealed that NOX2 is able to interact with endogenous p22phox (Fig. 26C). In contrast, no interaction was detectable between overexpressed NOX5 proteins and endogenous p22phox under these conditions (Fig. 26C).

### **3.2.2 Contribution of p22phox, NOX2, NOX4 and NOX5 to endothelial ROS generation**

To determine the functional role of NOX2, NOX4 and NOX5 in endothelial Ea.Hy926 and HMEC-1 cells, siRNA against NOX2 (siNOX2), NOX4 (siNOX4) and p22phox (sip22phox) were designed and cloned into a vector system. Also a siRNA targeting all NOX5 variants including NOX5S was designed (siNOX5). A random sequence was used as control (siCtr). Transfection of siRNA against NOX2, NOX4, NOX5 and p22phox diminished NOX2, NOX4, NOX5 and p22phox mRNA levels (Fig. 27A) as well as protein levels (Fig. 27B), respectively. Next, we tested the contribution of

NOX2, NOX4, NOX5 and also p22phox to endothelial ROS production. Silencing of the expression of NOX2, NOX4 and NOX5 decreased ROS levels in endothelial cells to a similar extent indicating that these NOX homologues are involved in basal ROS generation in these cells (Fig. 28A). Also the silencing of p22phox decreased the

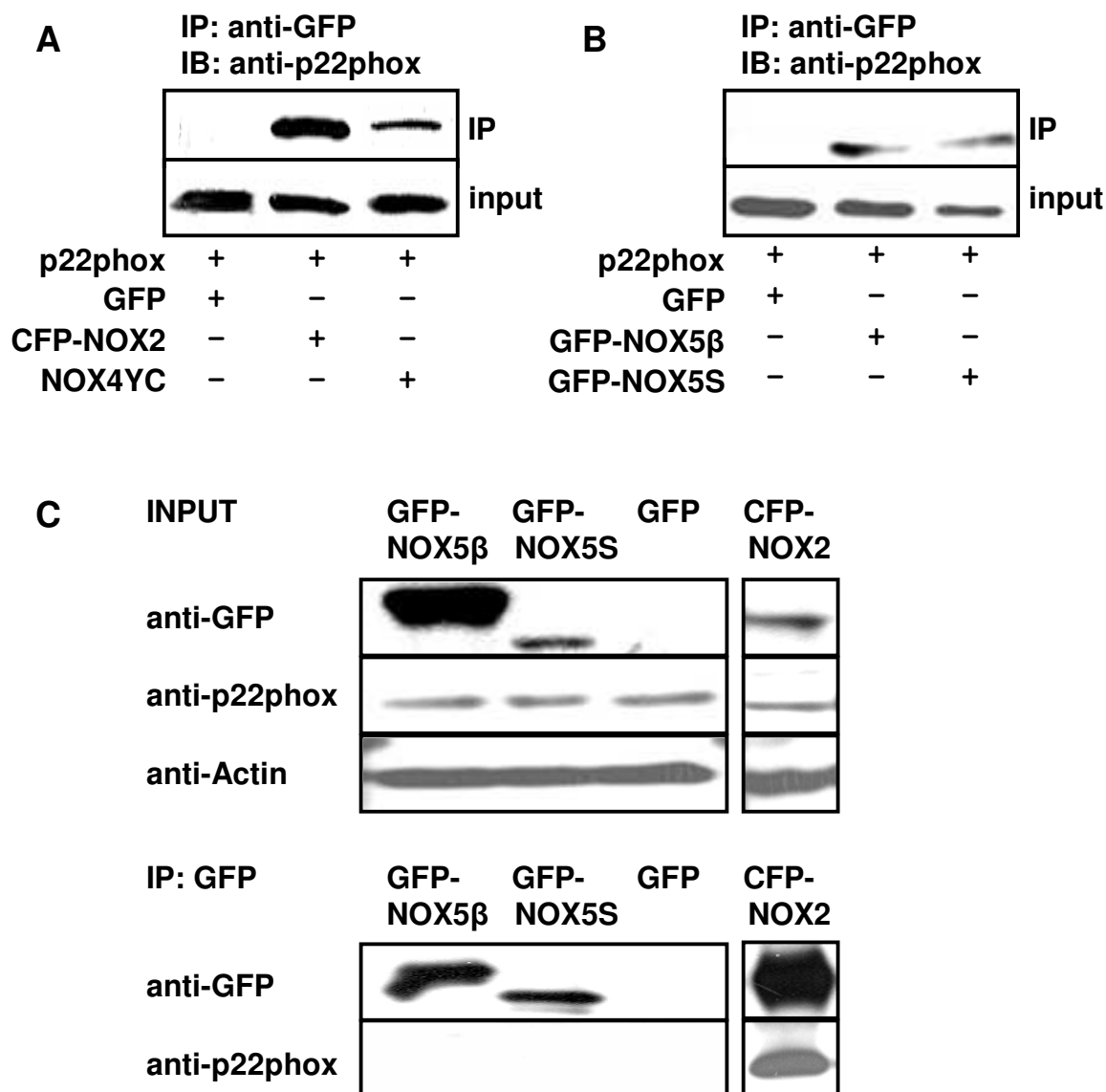


**Fig. 26** p22phox coimmunoprecipitates with NOX2, NOX4, NOX5S and NOX5β.

A./B. HEK293 cells were cotransfected with plasmids encoding for the indicated fusionproteins. CFP-NOX2 and NOX4YC (A) or GFP-NOX5S and GFP-NOX5β (B), and were precipitated with a polyclonal GFP-antibody. WB of the input showed overexpressed p22phox (input). The immunoprecipitates were subjected to Western blot analysis using an antibody against p22phox (IP). C. HEK cells were transfected only with GFP-NOX5β, GFP-NOX5S, CFP-NOX2 or GFP and immunoprecipitation was performed with a polyclonal GFP-antibody. Expression of endogenous p22phox is shown in the upper panel (INPUT) with actin staining as loading control. Lower panel shows endogenous p22phox in the immunoprecipitate.

ROS generation (Fig. 28A). Moreover, overexpression of p22phox, NOX2, NOX4, NOX5S and NOX5 $\beta$  increased ROS levels to a similar extent (Fig.28B). In order to determine whether p22phox is required for ROS production by NOX5 variants, p22phox was depleted by specific siRNA in NOX5 overexpressing HMEC-1 cells (Fig. 29A). Compared to cells cotransfected with unspecific siRNA (siCtr), no difference in ROS levels was detected in cells coexpressing sip22phox with either NOX5S or NOX5 $\beta$  (Fig. 29B). In contrast, coexpression of sip22phox significantly decreased NOX2-mediated ROS production. In addition, coexpression of p22phox with NOX5 $\beta$  or NOX5S did not significantly enhance ROS levels compared to coexpression of control vector with NOX5 variants whereas coexpression of NOX2

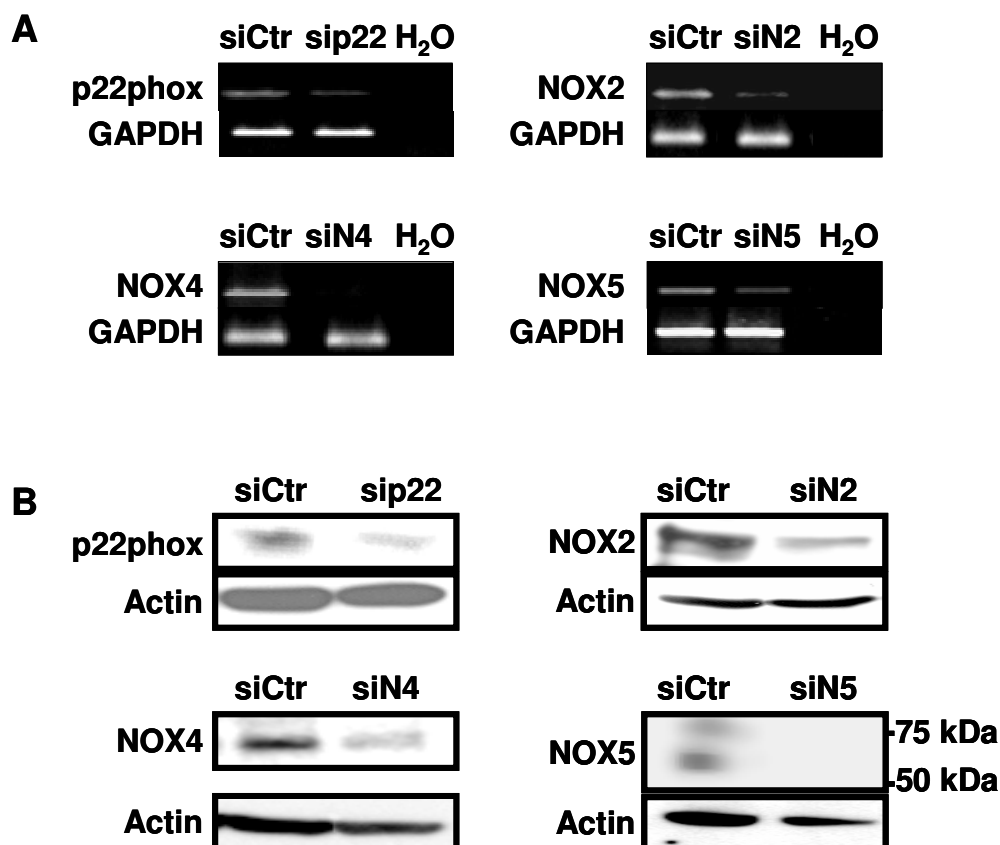


**Fig. 27** p22phox, NOX2, NOX4 and NOX5 are downregulated by specific siRNA.

Endothelial cells were transfected with constructs encoding either for a specific siRNA against p22phox (sip22), NOX2 (siNOX2), NOX4 (siNOX4), NOX5 (siNOX5) or a random sequence (siCtr). A. 24 hours after transfection mRNA levels of p22phox, NOX2, NOX4 and NOX5 were determined by RT-PCR using equal amounts of RNA for reverse transcription. B. Protein levels of p22phox, NOX2, NOX4 and NOX5 were analyzed by Western blot in comparison with actin, which was used as loading control.

with p22phox resulted in significantly elevated ROS levels compared to coexpression of a control vector (Fig. 29C). Since ROS production by NOX5 has been described to be enhanced by calcium [44, 45], HMEC-1 cells overexpressing NOX5S and NOX5 $\beta$  were treated with the calcium ionophore ionomycin and ROS levels were determined by DCF fluorescence measurements. Whereas in the absence of ionomycin NOX5S and NOX5 $\beta$  both contributed to ROS production equally, NOX5 $\beta$ - but not NOX5S-dependent ROS levels were increased in the presence of ionomycin, indicating that calcium specifically potentiates NOX5 $\beta$ -mediated ROS production (Fig. 30). In

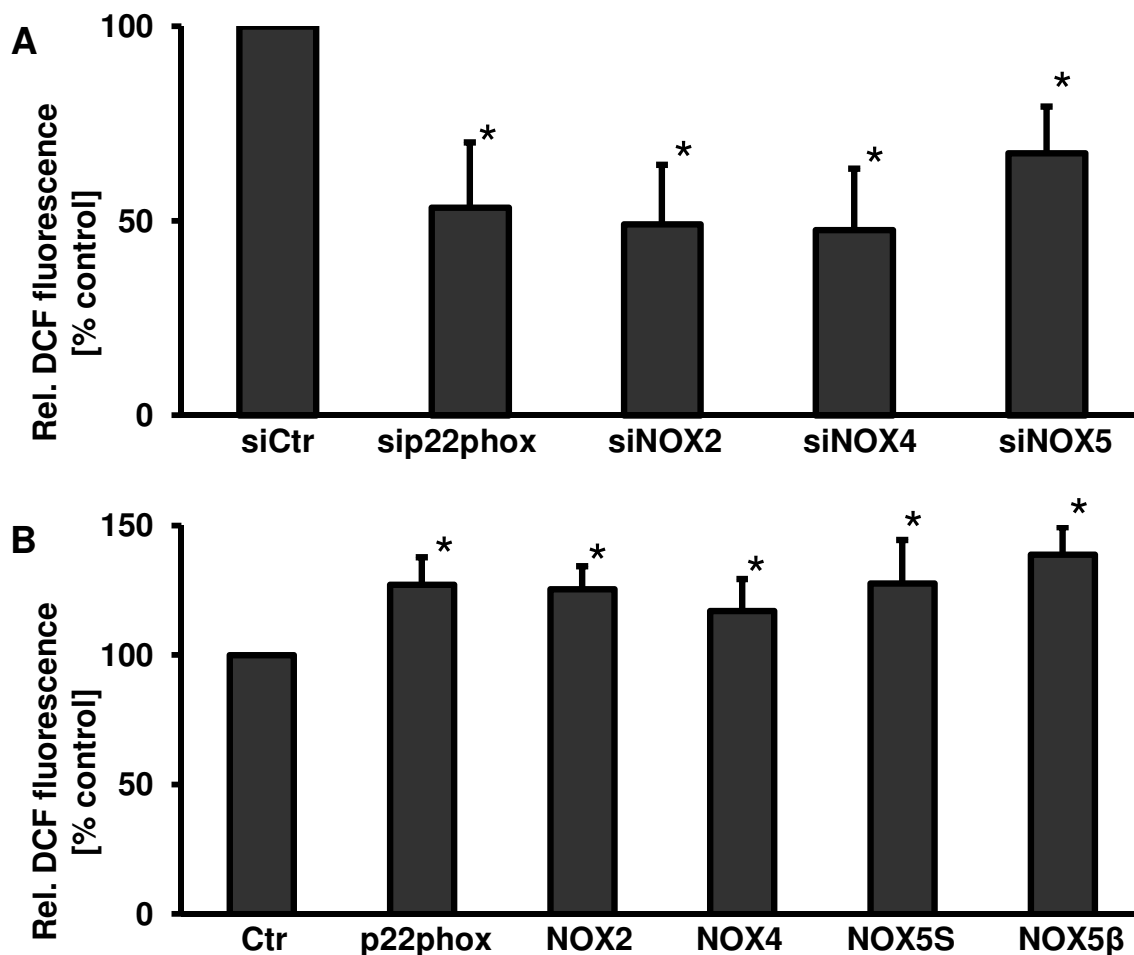


**Fig. 28** p22phox, NOX2, NOX4 and NOX5 modulate ROS generation of endothelial cells.

Ea.Hy926 cells were transfected with plasmids encoding for a siRNA against p22phox, NOX2 (siNOX2), NOX4 (siNOX4), NOX5 (siNOX5) or control siRNA (siCtr) (A) or vectors encoding for p22phox, NOX2, NOX4, NOX5S, NOX5 $\beta$  or with control vector (Ctr) (B). ROS levels were evaluated 24 hours after transfection by performing DCF fluorescence measurements. Data are presented as relative change to control (100%) (n=4-6, \*p<0.05 vs. cells transfected with control vectors [Ctr. or siCtr]).

accordance, ionomycin leads to an increase in ROS generation, which was inhibited by depletion of all NOX5 variants (Fig. 30B).

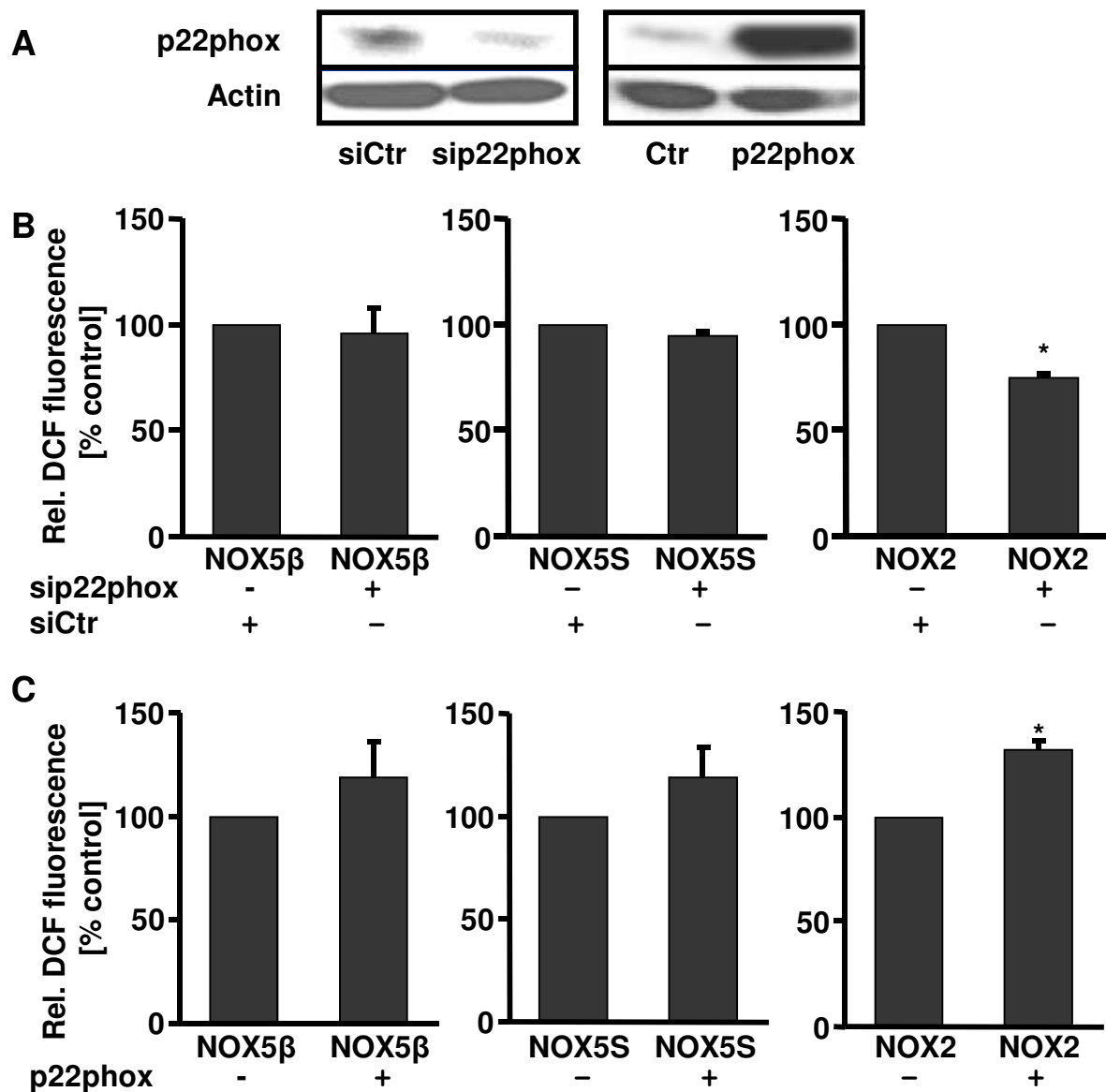


**Fig. 29** p22phox is not required for NOX5S- or NOX5 $\beta$ -mediated intracellular ROS production in endothelial cells.

A. HMEC-1 cells were transfected with control vector (Ctr) or plasmids encoding for p22phox (p22phox), a siRNA against p22phox (sip22phox), or control siRNA (siCtr), and Western blot analysis was performed with an antibody against p22phox. Reprobing with an actin antibody served as loading control. B. HMEC-1 cells were cotransfected with plasmids encoding for NOX2, NOX5S, or NOX5 $\beta$  together with plasmids encoding for siRNA against p22phox (sip22phox) or control siRNA (siCtr) and ROS levels were evaluated by performing DCF fluorescence measurement. Data are presented as relative change to control (100%) (n=3, \*p < 0.05 vs. cells cotransfected with NOX2 or siCtr). C. HMEC-1 cells were cotransfected with NOX2, NOX5S, or NOX5 $\beta$  together with a plasmid encoding for p22phox or control vector (-). ROS levels were determined by performing DCF fluorescence measurement. Data are presented as relative change to control (100%) (n=3, \*p < 0.05 vs. cells transfected with NOX2 and control vector).

### 3.2.3 Contribution of NOX2, NOX4 and NOX5 to basal endothelial proliferation

Since ROS and NADPH oxidases have been implicated in the regulation of endothelial proliferation [72], we determined the contribution of the different NOX homologues (NOX2, NOX4 and NOX5) and p22phox to the proliferative response of endothelial cells using 5'-bromo-2'-deoxyuridine (BrdU) incorporation assay. Depletion of p22phox, NOX2, NOX4 or NOX5 reduced proliferation of endothelial cells (Fig. 31A). In contrast, the proliferative activity of Ea.Hy926 cells was significantly increased when p22phox, NOX2, NOX4, NOX5S or NOX5 $\beta$  were overexpressed (Fig. 31B). Since proliferation is required for formation of capillary like structures and angiogenesis, we further performed an *in vitro* angiogenesis assay using Matrigel for determining the contributing of NOX homologues to the forming of capillary-like structures by depletion of NOX2, NOX4 and NOX5

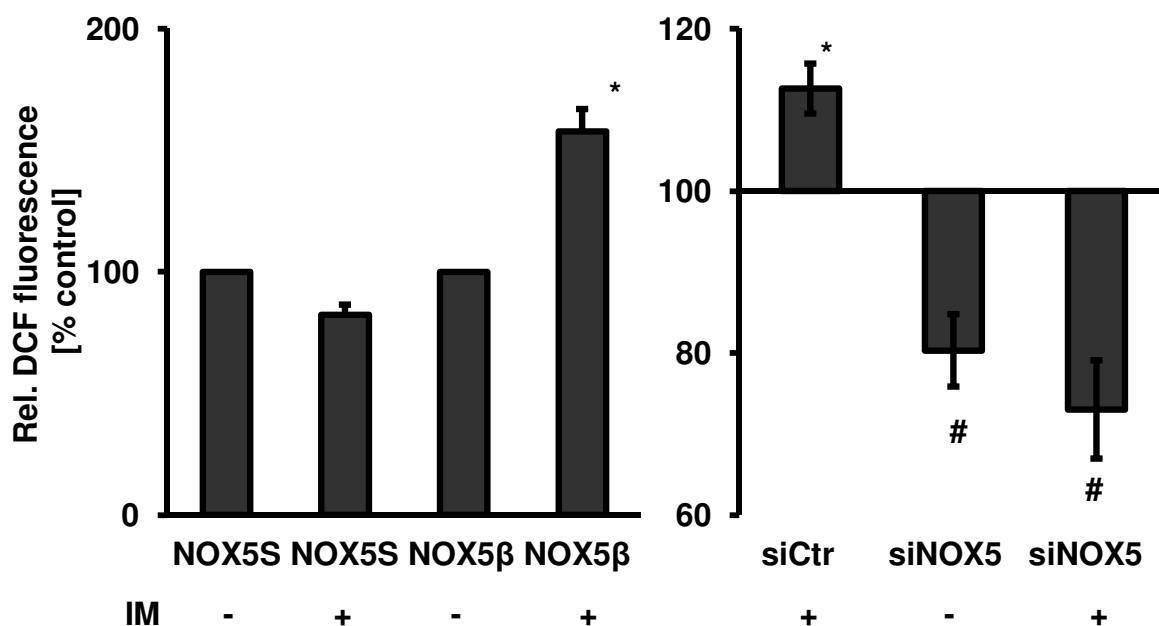


**Fig. 30 Calcium increases NOX5 dependent ROS generation in endothelial cells.**

HMEC-1 cells were transfected with plasmids encoding for NOX5S, NOX5 $\beta$ , siRNA against NOX5 (siNOX5) or control siRNA (siCtrl) and were exposed for 30 min to 3  $\mu$ M ionomycin (IM) and 1.25 mM Ca<sup>2+</sup>. ROS levels were evaluated by performing DCF fluorescence measurement. Data are presented as relative change compared to respective nontreated cells set on 100% (n=3, \*p < 0.05 vs. untreated cells transfected with NOX5 $\beta$  or untreated cells transfected with siCtrl, #p < 0.05 vs. ionomycin-treated siCtrl-transfected cells).

in HMEC-1 cells and observed an reduced capacity of HMEC-1 cells to form capillary-like structures (Fig. 31C), indicating that the NOX homologues NOX2, NOX4 and NOX5 are contributing to endothelial function.

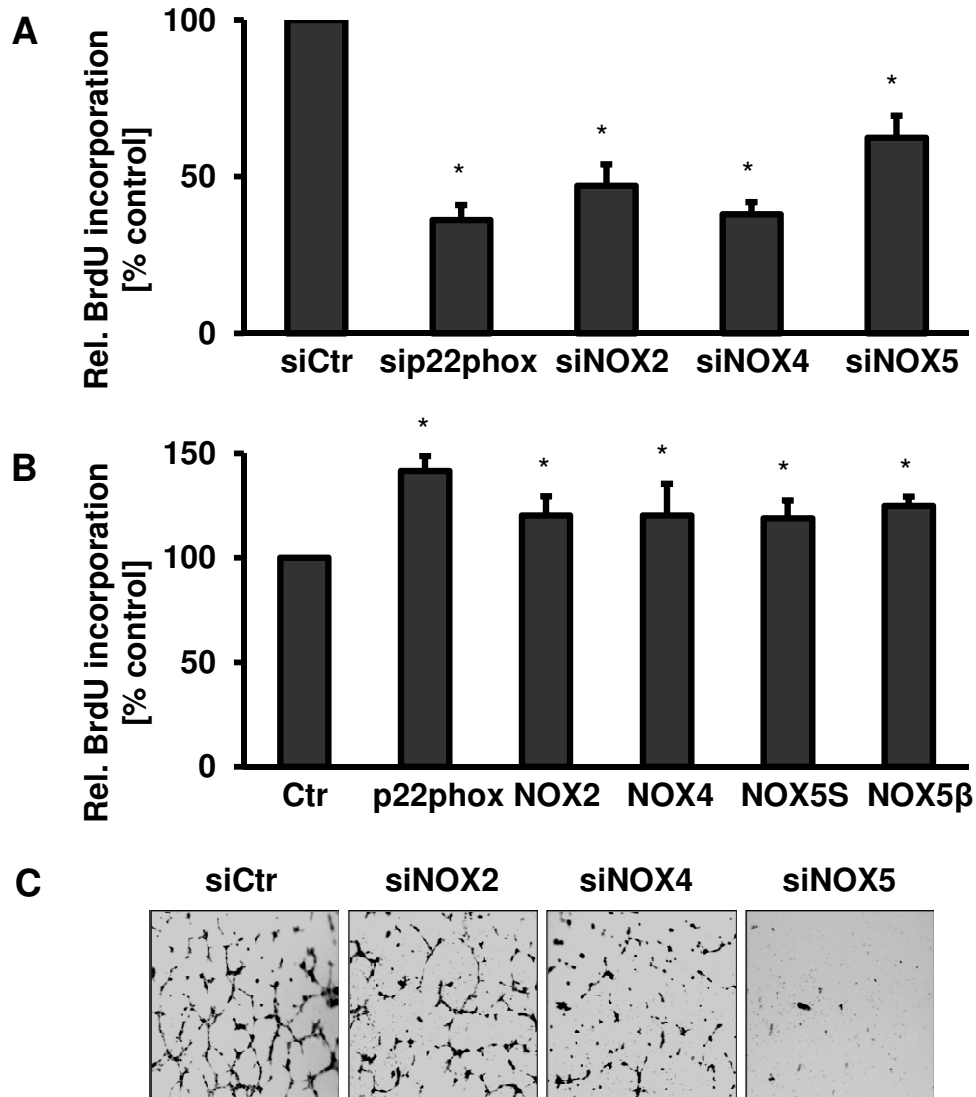


**Fig. 31 p22phox, NOX2, NOX4 and NOX5 modulate the proliferation of endothelial cells.**

A & B. Endothelial cells were transfected with plasmids encoding for siRNA against p22phox (sip22phox), NOX2 (siNOX2), NOX4 (siNOX4), NOX5 (siNOX5) or control siRNA (siCtr) (A) or plasmids encoding for p22phox, NOX2, NOX4, NOX5S, NOX5β or with control vector (Ctr) (B). Proliferation was assessed 48 h after transfection by using 5-bromo-2'-deoxyuridine (BrdU) incorporation. Data are presented as relative change to control (100%) (n=4-6, \*p<0.05 vs. cells transfected with corresponding control vectors [Ctr or siCtr]). C. HMEC-1 cells were transfected with plasmids encoding for siRNA against NOX2 (siNOX2), NOX4 (siNOX4), NOX5 (siNOX5) or control siRNA (siCtr). Cells were plated on growth factor reduced matrigel and formation of capillary-like structures was allowed for 4 h at 37°C. Pictures were taken by light microscopy using Improvision software. Representative images are shown.

### 3.2.4 The p38 MAP kinase contributes to the proliferative response mediated by NOX2 and NOX4

Since we previously showed that p38 MAP kinase is involved in endothelial proliferation dependent on p22phox [72], we determined the involvement of this kinase in the proliferative response mediated by NOX2 and NOX4. NOX2 and NOX4 were expressed in Ea.Hy926 cells. Western blot analysis showed that p38 MAP kinase was phosphorylated in the presence of either NOX2 or NOX4 (Fig. 32). Treatment with the p38 MAP kinase inhibitor SB202190 decreased both NOX2- and NOX4-mediated proliferation (Fig. 32) indicating that p38 MAP kinase contributes to the proliferative response initiated by NOX2 or NOX4.

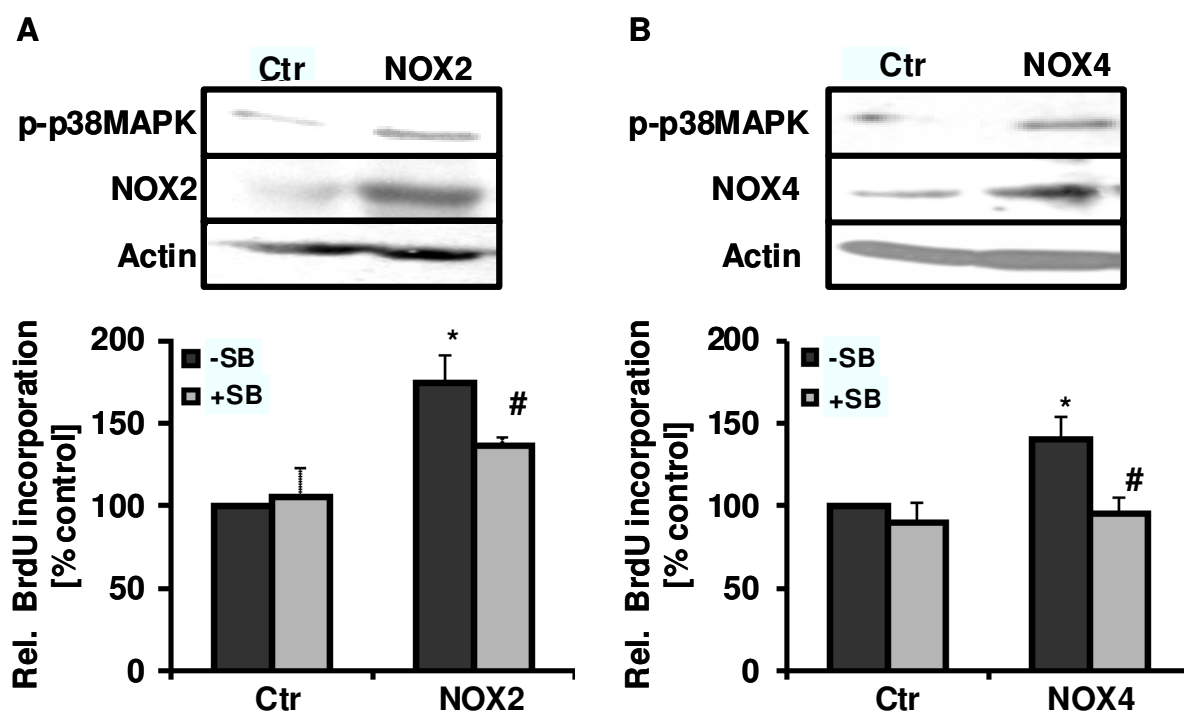


**Fig. 32** The p38 MAP kinase contributes to the proliferative response mediated by NOX2 and NOX4.

Ea.Hy926 cells were transfected either with plasmids encoding for NOX2 (A) or NOX4 (B) or with control vector (Ctr). Expression of NOX2 and NOX4 and the presence of phosphorylated p38 MAP kinase were determined by Western blot analysis. Reprobing with actin served as loading control. Cells were treated either with solvent (-SB) or with 20 μM SB202190 (+SB) and proliferation was assessed after 12 h by using a BrdU incorporation assay. Data are presented as relative change to control without SB202190 (100%; n=3, \*p < 0.05 vs. cells transfected with control vector; #p < 0.05 vs. untreated cells).

### 3.2.5 Influence on ROS generation and proliferation by NOX1 is limited in endothelial cells under basal conditions

To analyze the involvement of NOX1 in ROS generation of Ea.Hy926 cells, a specific siRNA against NOX1 (siNOX1) was designed which downregulated NOX1 protein (Fig. 33A). However, in contrast to the other investigated NOX proteins, depletion of NOX1 did not significantly alter ROS levels in Ea.Hy926 cells and was also unable to significantly downregulate endothelial proliferation (Fig. 33B, C). This indicates that NOX1 plays only a minor role in basal endothelial function in contrast to NOX2, NOX4 and NOX5.

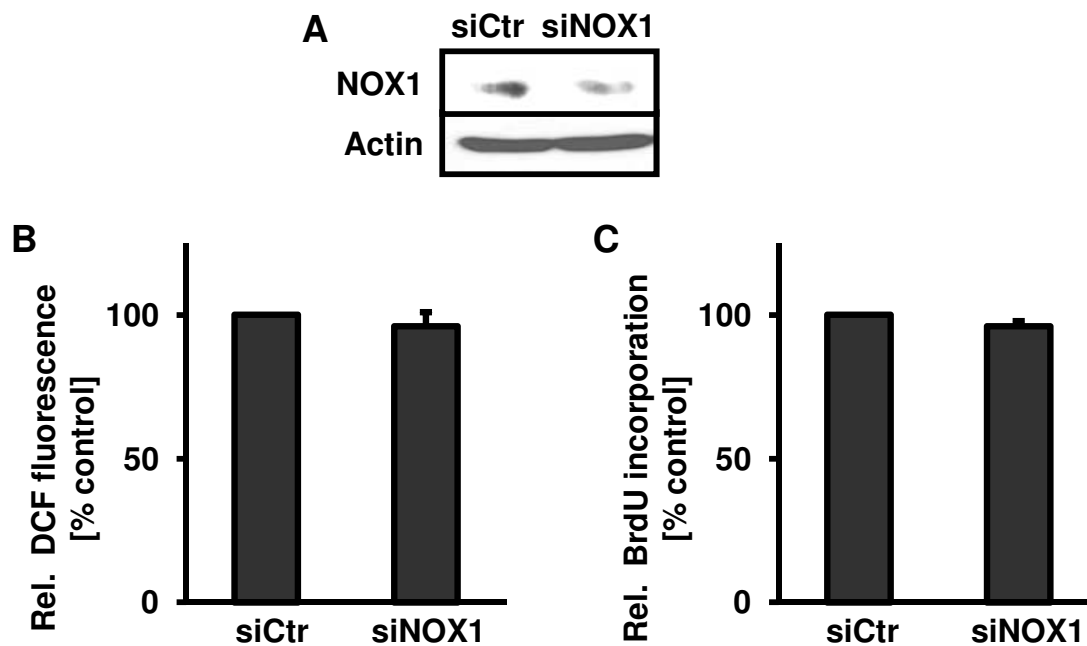


**Fig. 33** NOX1 does not contribute to basal ROS generation and proliferation of endothelial cells.

Ea.Hy926 cells were transfected with plasmids encoding for siRNA against NOX1 (siNOX1) or control siRNA (siCtr). A. Western blot analysis was performed using an antibody against NOX1. Reprobing with an actin antibody served as loading control. B. ROS levels were evaluated 24 hours post-transfection by performing DCF fluorescence measurement. Data are presented as relative change to control (100%; n=3). C. Proliferation was assessed 48 hours post-transfection using a BrdU incorporation assay. Data are presented as relative change to control (100%; n=3).

### **3.3 Function and regulation of NADPH oxidases in thrombin and endoplasmic reticulum stress activated endothelial cells**

#### **3.3.1 Contribution of NOX2 and NOX5 to thrombin-induced endothelial ROS generation and cell proliferation**

It is known that thrombin is an activator of the endothelium and we have previously shown that thrombin can induce and activate the NADPH oxidase subunits p22phox and NOX4 in the endothelial cell line Ea.Hy926 and in smooth muscle cells [33, 72, 78]. Therefore, we investigated whether NOX2 and NOX5 are also regulated by thrombin and whether they play a role in the thrombin-induced ROS generation and proliferation. Cells were stimulated with thrombin (3 U/ml) for 3 hours. Western blot analysis using an antibody against NOX5 revealed that thrombin upregulates NOX5 protein levels including NOX5S (Fig. 34A). This upregulation could be inhibited by transfecting siRNA against NOX5 (Fig. 34A), whereas upregulation of NOX5 in cells transfected with control siRNA was not affected indicating a de-novo transcription of NOX5 upon thrombin stimulation. Also the level of NOX2 protein was increased after thrombin stimulation and this upregulation was not decreased by depletion of NOX5, excluding cross-reactivity of the NOX5 siRNA and thus indicating a NOX5-independent mechanism (Fig. 34B). Then we investigated the contribution of NOX2 and NOX5 to thrombin-induced ROS generation. Thrombin-induced ROS generation was significantly reduced in NOX5-depleted cells and also depletion of NOX2 resulted in a similar reduction of ROS levels (Fig. 35) indicating an involvement of both NOX2 and NOX5 containing NADPH oxidase to thrombin-induced ROS generation. Furthermore, stimulation with thrombin increased endothelial cell proliferation. Depletion of both NOX2 and NOX5 decreased the proliferative response to thrombin (Fig. 36A). Thrombin also induced the formation of

capillary-like structures of HMEC-1 in an *in vitro* angiogenesis assay using Matrigel for simulation of the extracellular matrix. Depletion of NOX2 and NOX5 completely abolished the capillary formation under thrombin stimulation (Fig. 36B), confirming a role for NOX2 and NOX5 in this response.

### 3.3.2 Regulation of NADPH oxidase subunits by endoplasmic reticulum stress

A redox dysbalance, like an in- or decrease in ROS generation in the ER often results in a so called endoplasmic reticulum stress (ER-stress) and subsequently an accumulation of unfolded proteins triggering the unfolded protein response (UPR). We could demonstrate that the endothelial NADPH oxidase is mainly localized in the ER (Fig. 5). We therefore formulated the hypothesis of an involvement of the NADPH oxidase in the UPR. First, we investigated whether NADPH oxidase subunits are able to colocalize with protein disulfide isomerase (PDI),

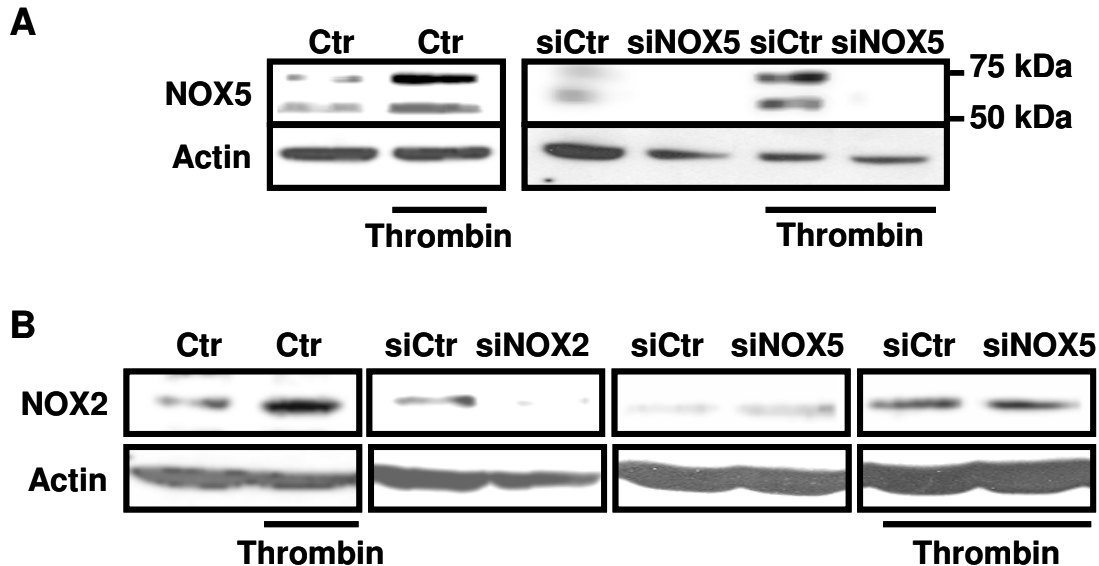


**Fig. 34** NOX2 and NOX5 are regulated by thrombin in endothelial cells.

A. HMEC-1 cells remained untransfected or were transfected with plasmids encoding for siRNA against NOX5 (siNOX5) or control siRNA (siRNA) and Western blot analysis was performed under control conditions (Ctr) or after stimulation with thrombin (3 U/ml) for 3 hours using a NOX5 antibody. Reprobing with actin was performed as loading control. B. HMEC-1 cells were stimulated with thrombin (3 U/ml) for 3 hours or transfected either with plasmids encoding for siRNA against NOX2 (siNOX2), NOX5 (siNOX5) or control siRNA (siCtrl) and Western blot analysis was performed using a NOX2 antibody. Reprobing with actin was used as loading control.

which is highly involved in the cellular answer to ER-stress. For this, coimmunofluorescence studies with antibodies against NOX1, NOX4 and PDI were performed. PDI colocalized mainly with NOX4 and only weakly with NOX1 (Fig. 37A). Interestingly, overexpression of wild-type PDI increased endothelial ROS generation whereas overexpression of a nonfunctional PDI-mutant was not able to increase ROS generation (Fig. 37B). As PDI is a target gene and mediator of the UPR in the ER-stress response, we investigated whether ER-stress itself can induce ROS generation. Two common substances which induce ER-stress are tunicamycin (Tm) and thapsigargin (Tp). Tunicamycin inhibits N-glycosylation whereas thapsigargin inhibits the Ca<sup>2+</sup>-ATPase of the ER which leads to inhibition of calcium-dependent chaperones. First, we evaluated the effects of tunicamycin and thapsigargin on ROS generation in endothelial cells. Ea.Hy 926 cells were stimulated with tunicamycin (2 µg/ml) or thapsigargin (2.5 nM) and ROS generation was measured by DCF fluorescence in a microplate reader. Exposure to tunicamycin or thapsigargin resulted in significantly increased ROS generation with a peak at

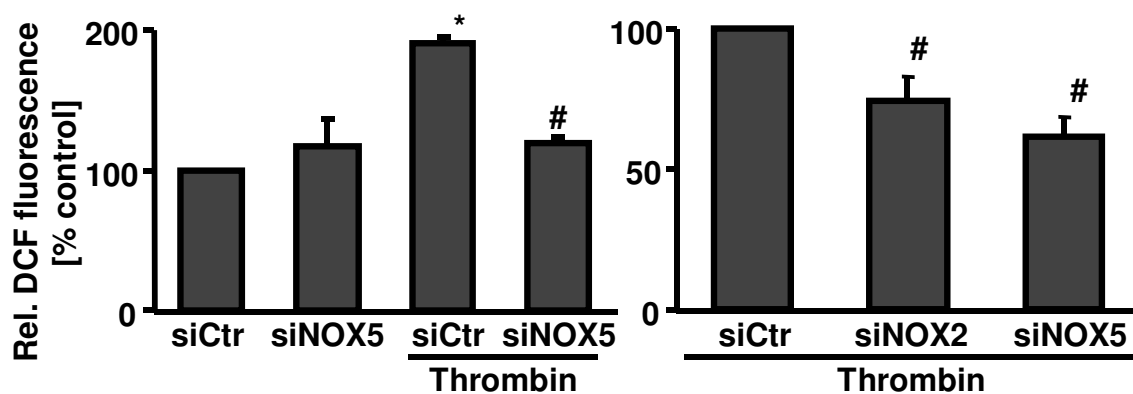


**Fig. 35** NOX2 and NOX5 mediates thrombin-induced ROS generation in endothelial cells.

HMEC-1 cells were transfected with plasmids encoding for siRNA against NOX5 (siNOX5), NOX2 (siNOX2) or control siRNA (siCtrl). Cells were stimulated with thrombin (3 U/ml) for 3 hours. ROS levels were determined by performing DCF fluorescence measurements. Data are presented as relative change to control (100%) (n=3, \*p<0.05 vs. unstimulated cells transfected with siCtrl, #p<0.05 vs. thrombin-stimulated cells transfected with siCtrl).

one hour after thapsigargin or tunicamycin stimulation (Fig. 38A). Since NADPH oxidases have been shown to contribute to endothelial ROS production, it

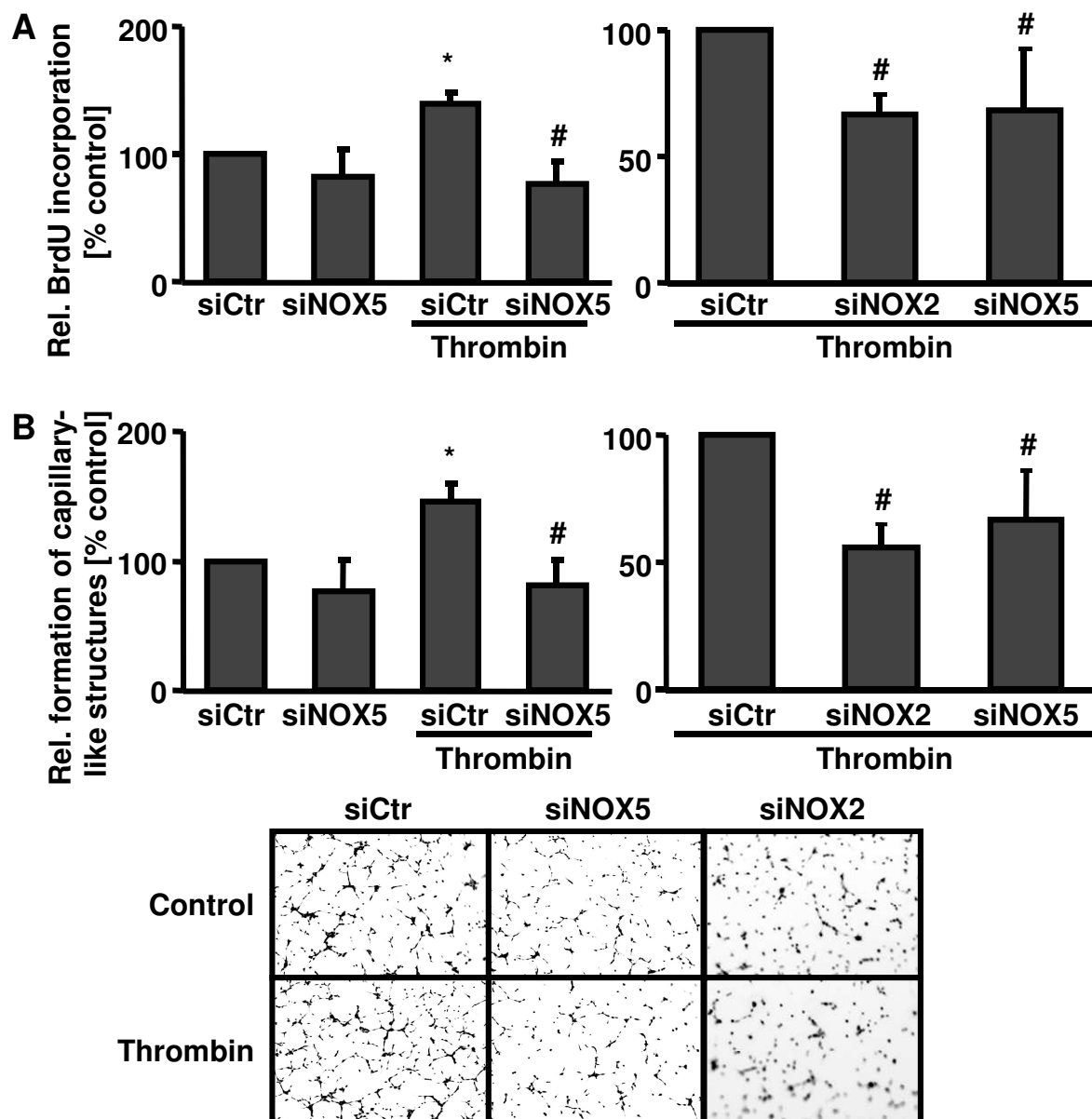


**Fig. 36** NOX2 and NOX5 mediates thrombin induced proliferation and tube formation in endothelial cells.

HMEC-1 cells were transfected with plasmids encoding for siRNA against NOX5 (siNOX5), NOX2 (siNOX2) or control siRNA (siCtr) and stimulated with 3 U/ml thrombin for 24 hours. A. Proliferation was assessed by performing BrdU incorporation. Data are presented as relative change to control (100%) (n=3, \*p<0.05 vs. unstimulated cells transfected with siCtr, #p<0.05 vs. thrombin-stimulated cells transfected with siCtr). B. Cells were plated on growth factor reduced matrigel and formation of capillary-like structures was allowed for 4 h at 37°C. Pictures were taken by light microscopy using Improvision software. Representative images are shown. The relative formation of capillary-like structures as a measure for angiogenic capacity was quantified by Image J software. Data are presented as relative change to control (100%) (n=4, \*p<0.05 vs. unstimulated cells transfected with siCtr, #p<0.05 vs. thrombin stimulated cells transfected with siCtr).

was determined whether elevated ROS production in response to prolonged ER-stress would be NADPH oxidase-dependent. For this, Ea.Hy926 cells were transfected with a plasmid encoding for a specific siRNA against p22phox (sip22phox) 48 hours prior to stimulation with tunicamycin for 0.5, 1 and 2 hours and subsequent ROS measurements (Fig. 38B). Depletion of p22phox decreased ROS generation and the response to tunicamycin was completely abolished, indicating an involvement of p22phox in tunicamycin-induced ROS generation. Next, it was analyzed whether elevated ROS generation in response to prolonged ER-stress would be associated with increased expression of the NADPH oxidase subunit p22phox. Ea.Hy926 cells were stimulated with thapsigargin for increasing time periods and mRNA and protein levels of p22phox were analyzed by Northern or Western blot, respectively. Levels of mRNA for p22phox were increased after one hour of ER-stress reaching a plateau phase at two hours up to eight hours ER-stress (Fig. 39A) and also p22phox protein was increased by ER-

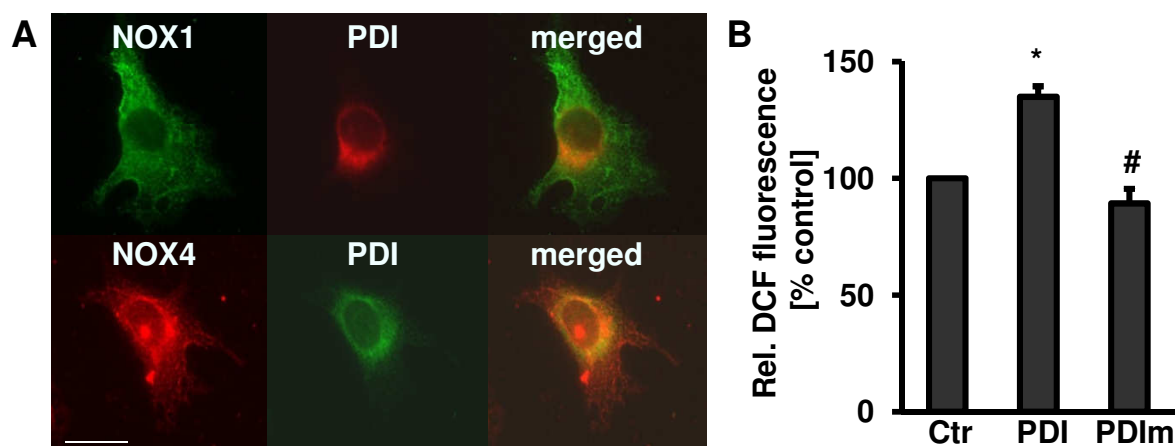


**Fig. 37 Protein disulfide isomerase is associated with NOX4 and increased ROS generation in endothelial cells.**

A. Ea.Hy926 cells were stained with antibodies against NOX1 or NOX4 together with an antibody against PDI. Merged images show overlay of NOX4 with PDI. Scale bar is 20  $\mu$ m for all panels. B. Ea.Hy926 cells were transfected with plasmids encoding either for wild-type PDI (PDI), a mutated nonfunctional PDI (PDIm) or control vector (Ctr). 24 hours post-transfection, ROS levels were measured by performing DCF fluorescence measurement. Data are presented as relative change to control cells (100%) ( $n=3$ , \* $p<0.05$  vs. cells transfected with control vector (Ctr); # $p<0.05$  vs. cells transfected with wild-type PDI).

stress (Fig. 39B). Since ER-stress and UPR increase phosphorylation of eIF2 $\alpha$ , Western blot analysis of phosphorylated eIF2 $\alpha$  was performed to confirm the presence of ER-stress or UPR (Fig. 39B). Increased phosphorylation of eIF2 $\alpha$  was observed up from 0.5 hours. To investigate whether the increase of p22phox mRNA is a transcriptional process, Ea.Hy926 cells were pretreated with

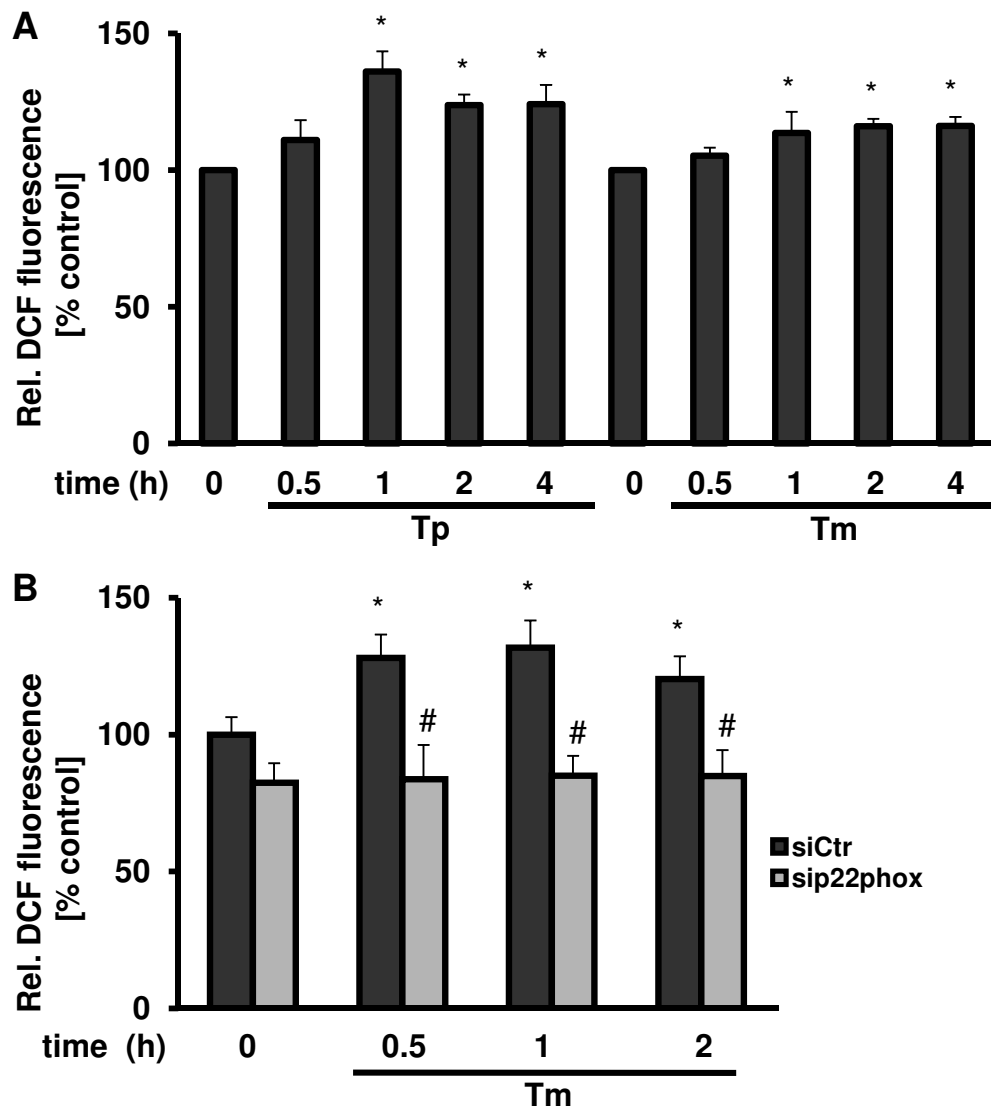


**Fig. 38 ER-stress induces ROS generation via p22phox in endothelial cells.**

A. Ea.Hy 926 cells were stimulated with either 2.5nM thapsigargin (Tp) or 2  $\mu$ g/ml tunicamycin (Tm) for indicated time points and ROS generation was analyzed using DCF fluorescence. Data are presented as relative change to control (100%) (n=3, \*p<0.05 vs. unstimulated cells). B. Ea.Hy926 cells were transfected with a plasmid encoding for a siRNA against p22phox (sip22phox) or control siRNA (siCtr) and ROS generation was analyzed using DCF fluorescence after tunicamycin (2  $\mu$ g/ml) for 0.5, 1 and 2 hours. Data are presented as relative change to control (100%) (n=3, \*p<0.05 vs. unstimulated cells; #p<0.05 sip22phox vs. siCtr).

actinomycin D (5  $\mu\text{g/ml}$ ) 30 minutes prior to stimulation with thapsigargin for 2 and 4 hours. Northern blot analysis showed that pretreatment with actinomycin D abolished thapsigargin-induced increase of p22phox mRNA levels (Fig. 39C), indicating that p22phox is indeed upregulated by a transcriptional mechanism. A bioinformatic analysis of the potential promoter region of p22phox (MatInspector™ software, Genomatix, München) was performed to search for mediators of the UPR. Two important transcription factors in the UPR are XBP1 and ATF4. Indeed, several potential binding sites for ATF4 and XBP1 were found in the upstream region of the p22phox gene (Fig. 40A). In the 6k upstream sequence of p22phox, four distal, but closely related XBP1 binding sites were found

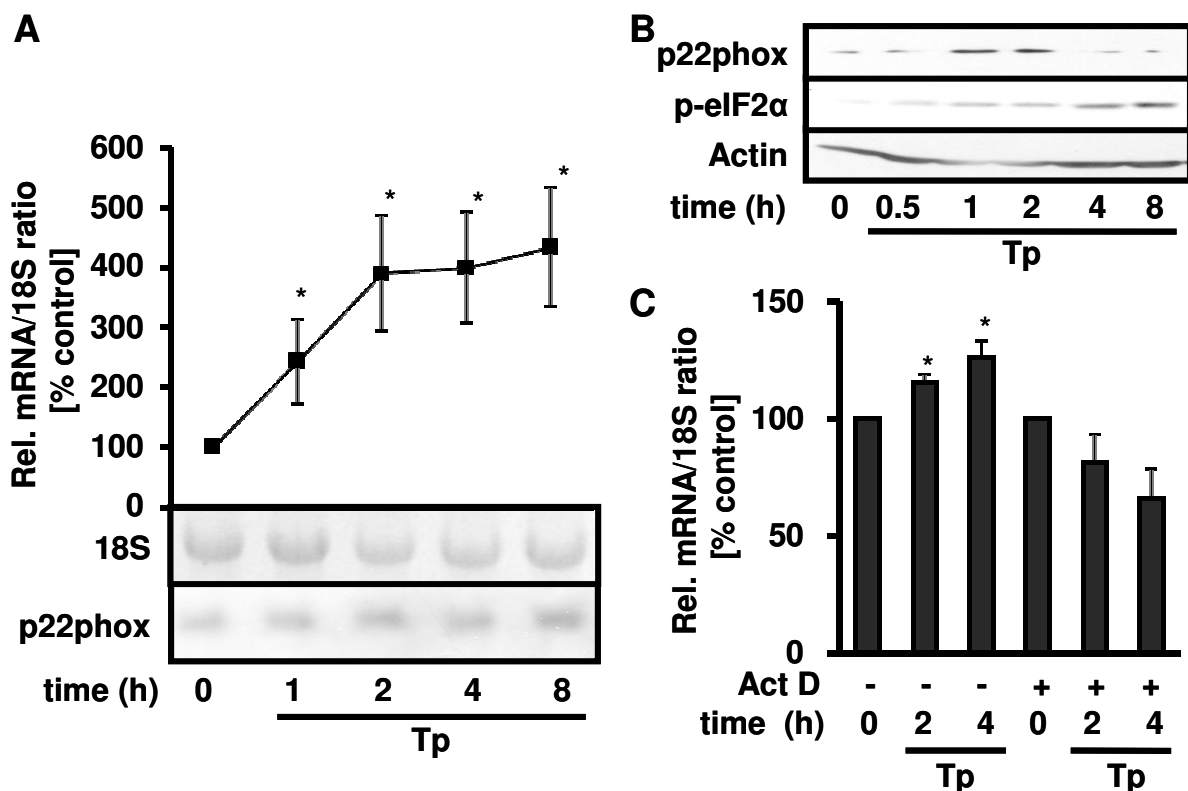


**Fig. 39 ER-stress increases p22phox mRNA and protein levels in endothelial cells.**

A. Ea.Hy926 cells were stimulated with thapsigargin (2.5 nM) for 1, 2, 4 or 8 hours and mRNA levels of p22phox were analyzed using Northern blot ( $n=3$  \* $p<0.05$  thapsigargin vs. unstimulated control). B. Cells were stimulated with thapsigargin (2.5 nM) for 0.5, 1, 2, 4 or 8 hours. Western blot analysis was performed with antibodies against p22phox, phosphorylated eIF2 $\alpha$  (p-eIF2 $\alpha$ ) and actin as loading control. C. Ea.Hy926 cells were preincubated with actinomycin D (Act D; 5  $\mu\text{g/ml}$ ) for 30 minutes prior to thapsigargin stimulation (2.5 nM) for 2 or 4 hours. mRNA level for p22phox was analyzed by Northern blot analysis ( $n=3$ ; \* $p<0.05$  thapsigargin vs. unstimulated control).

(-3967 bp, -3838 bp, -3689 bp, -3511 bp). In addition several ATF4 sites (-5847 bp, -4190 bp, -3786 bp, -2788 bp, -2568 bp, -2531 bp, -2507 bp, -587 bp) were found by bioinformatics analysis. Therefore we investigated whether ATF4 or XBP1 can induce ROS generation and p22phox expression. We investigated the role of ATF4 and XBP1 in thapsigargin-induced ROS generation and as a first step we investigated the activation of ATF4 and XBP1 by thapsigargin. XBP1 activation is characterized by splicing by IRE1. We performed RT-PCR studies for XBP1 mRNA using primers by which both splice variants were amplified and could be distinguished by their size. Indeed we could detect the smaller spliced XBP1 form after one hour of thapsigargin stimulation (Fig. 40B). ATF4 activation is characterized by increased protein expression and we could detect increased ATF4 protein levels starting from 30 minutes stimulation with thapsigargin (Fig. 40C). Next, we investigated the role of ATF4 and XBP1 on ROS generation in endothelial cells. For this, specific siRNA against ATF4 and XBP1 were designed (siATF4 and siXBP1) and Ea.Hy926 cells were transfected with these siRNAs 48 hours prior to thapsigargin stimulation for half, one and two hours and ROS generation was measured.

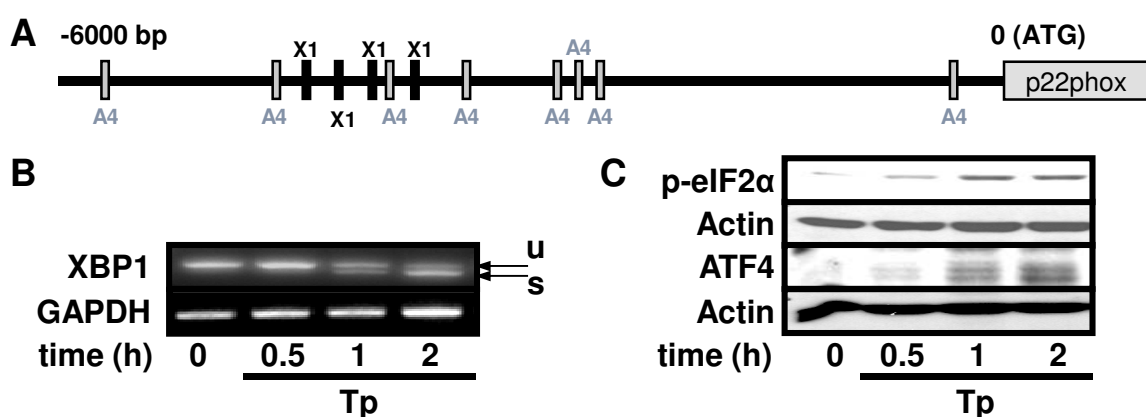


**Fig. 40 Thapsigargin induces XBP1 and ATF4 activation in endothelial cells.**

A. Schematic of the p22phox promoter with potential binding sites for ATF4 (A4, grey) and XBP1 (X1, black). B & C. Ea.Hy926 cells were stimulated with thapsigargin (2.5nM) for 0.5, 1 and 2 hours. B. RNA was extracted and splicing of XBP1 was analyzed with RT-PCR using primers spanning the splice site resulting in unspliced (u) or spliced (s) PCR-product. C. Western blot analysis was performed using antibodies against p-eIF2 $\alpha$ , ATF4 and actin as loading control.

Depletion of ATF4 and XBP1 abolished ROS generation after thapsigargin stimulation (Fig. 41A). Accordingly, overexpression of ATF4 or XBP1 increased ROS generation in Ea.Hy926 cells (Fig. 41B). Next the effect of ATF4 or XBP1 on the expression of p22phox was analyzed. Overexpression of ATF4 or XBP1 in Ea.Hy926 cells caused an increase in p22phox mRNA and protein levels (Fig. 42A, B) and silencing of XBP1 abolished the upregulation of p22phox protein levels after thapsigargin stimulation (Fig. 42C).

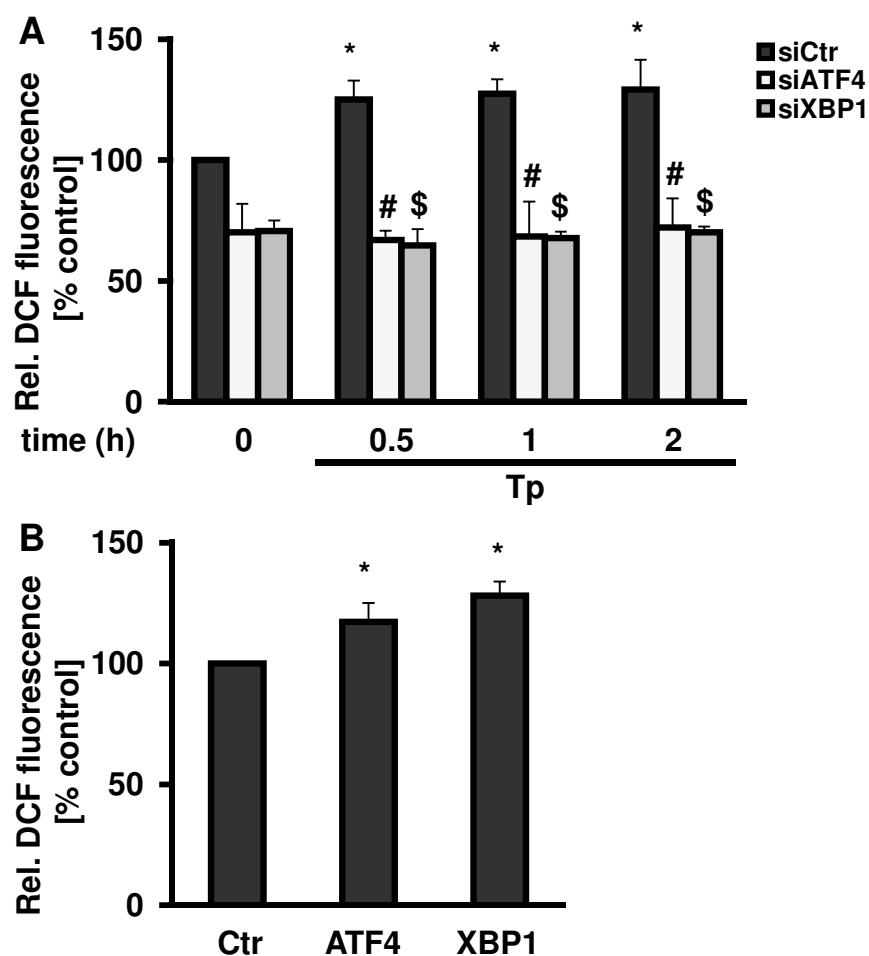


**Fig. 41** ATF4 and XBP1 mediates ROS generation under thapsigargin stimulation in endothelial cells.

A. Ea.Hy926 cells were transfected with plasmids encoding for siRNA against ATF4 (siATF4), XBP1 (siXBP1) or control siRNA (siCtrl) followed by thapsigargin (2.5 nM) stimulation for indicated time points. ROS levels were analyzed by DCF fluorescence (n=3, \*p<0.05 vs. unstimulated control cells, #p<0.05 siATF4 transfected cells vs. control transfected cells, \$p<0.05 siXBP1 transfected cells vs. control transfected cells). B. Cells were transfected with plasmids encoding for ATF4, XBP1 or control vector (Ctr) and 24 hours post-transfection, ROS levels were analyzed by DCF fluorescence (n=3, \*p<0.05 vs. cells transfected with control vector).

### 3.3.3 Regulation of p22phox upstream enhancer element activity by ATF4, XBP1 and ER-stress in endothelial cells

Since the bioinformatic analysis revealed a potential ATF4 binding site in the proximal promoter region and a potential enhancer region with four XBP1 and one ATF4 binding site, two reporter constructs were used which were already present in the lab. One construct was based on the pGL3-Basic and contained 1179 bp of the upstream promoter region including 35 bp of the 5' untranslated region of the p22phox gene creating the pGL3B-p22phox1.2Kluc plasmid (p22phox-1.2K). The other construct contained a 520 bp large fragment from -4104 bp and -3584 bp upstream of the p22phox coding sequence with three potential XBP1 and one

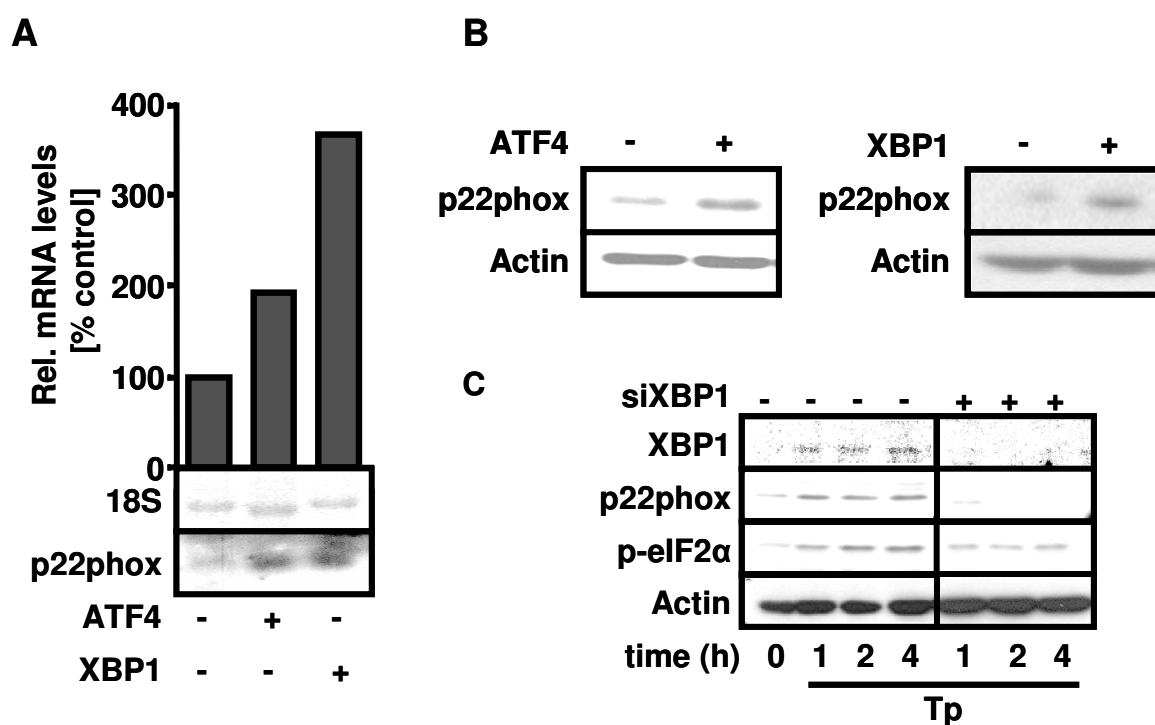


**Fig. 42** ATF4 and XBP1 mediate p22phox expression under thapsigargin stimulation in endothelial cells.

A. Ea.Hy926 cells were transfected with plasmids encoding for ATF4 (ATF4), XBP1 (XBP1) or control vector. After RNA preparation, Northern blot analysis for p22phox was performed, 18S RNA served as loading control. Graph represents the relative ratio of p22phox mRNA to 18S RNA. B. Ea.Hy926 cells were transfected with either ATF4, XBP1 or control vector and Western blot analysis for p22phox was performed. Reprobing with actin served as loading control. C. Ea.Hy926 cells were transfected with a plasmid encoding for a siRNA against XBP1 (+) or control siRNA (-). 24 hours post-transfection cells were stimulated with thapsigargin (2.5 nM) for the indicated time points and Western blot analyzes for XBP1, p22phox, p-eIF2α were performed. Reprobing with actin served as loading control.

potential ATF4 sites and was cloned as enhancer construct into the pGL3-Promoter in front of the SV40 promoter creating pGL3E-p22phox-XBPluc (p22phox-XBPluc). To test the influence of ER-stress on the function of the p22phox promoter, Ea.Hy926 cells were transfected with the p22phox-1.2K reporter construct and cells were stimulated with thapsigargin for eight hours. Indeed, an increased luciferase activity was detected upon stimulation (Fig. 43A). As this construct contains a potential ATF4 binding site, cotransfection of this construct together with ATF4 showed an increased luciferase activity (Fig. 43B) indicating a modulation function of ATF4 on the p22phox promoter. To evaluate whether the distal enhancer region can also be modulated by ER-stress, Ea.Hy926 cells were transfected with the p22phox-XBP luciferase construct and also stimulated with thapsigargin for eight hours and again an increased luciferase activity was detected upon stimulation (Fig. 44A). Also

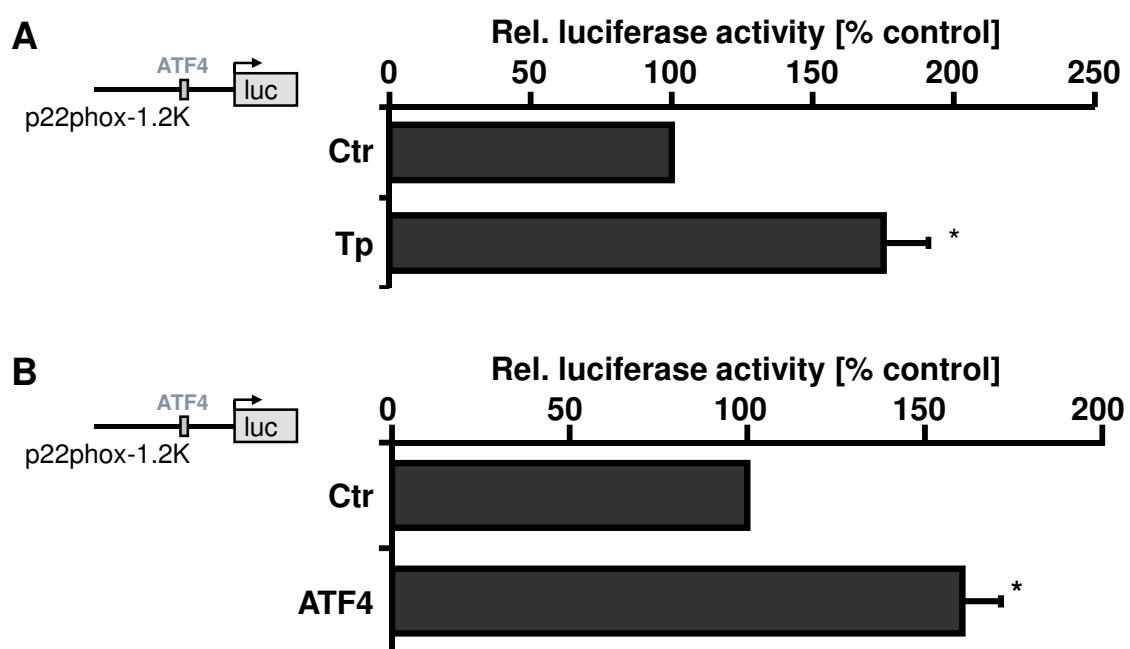


**Fig. 43 ER-stress and ATF4 activates p22phox promoter in endothelial cells.**

A. Ea.Hy926 cells were transfected with p22phox-1.2K promoter construct and stimulated with thapsigargin (Tp, 2.5 nM) for 8 hours or remained unstimulated (Ctr) and were subjected to luciferase assay. Data represented as change to nontreated cells (100%; n=3, \*p<0.05 vs. unstimulated control cells). B. Cells were transfected with p22phox-1.2K promoter construct together with a plasmid encoding either for ATF4 or empty control vector (Ctr). 24 hours post-transfection cells were subjected to luciferase assay. Data are represented as change to cells transfected with control vector (100%, n=3, \*p<0.05 vs. cells transfected with control).

coexpression of ATF4 or XBP1 with this construct resulted in an increased luciferase activity (Fig. 44B). Finally, depletion of ATF4 or XBP1 in Ea.Hy926 cells abolished the induction of luciferase activity of the p22phox-XBP1 reporter by thapsigargin (Fig. 43C). These results indicated that ATF4 and XBP1 could play a role in the activation of the p22phox-XBP1 enhancer element, the p22phox promoter and subsequently p22phox induction on mRNA as well as protein level.

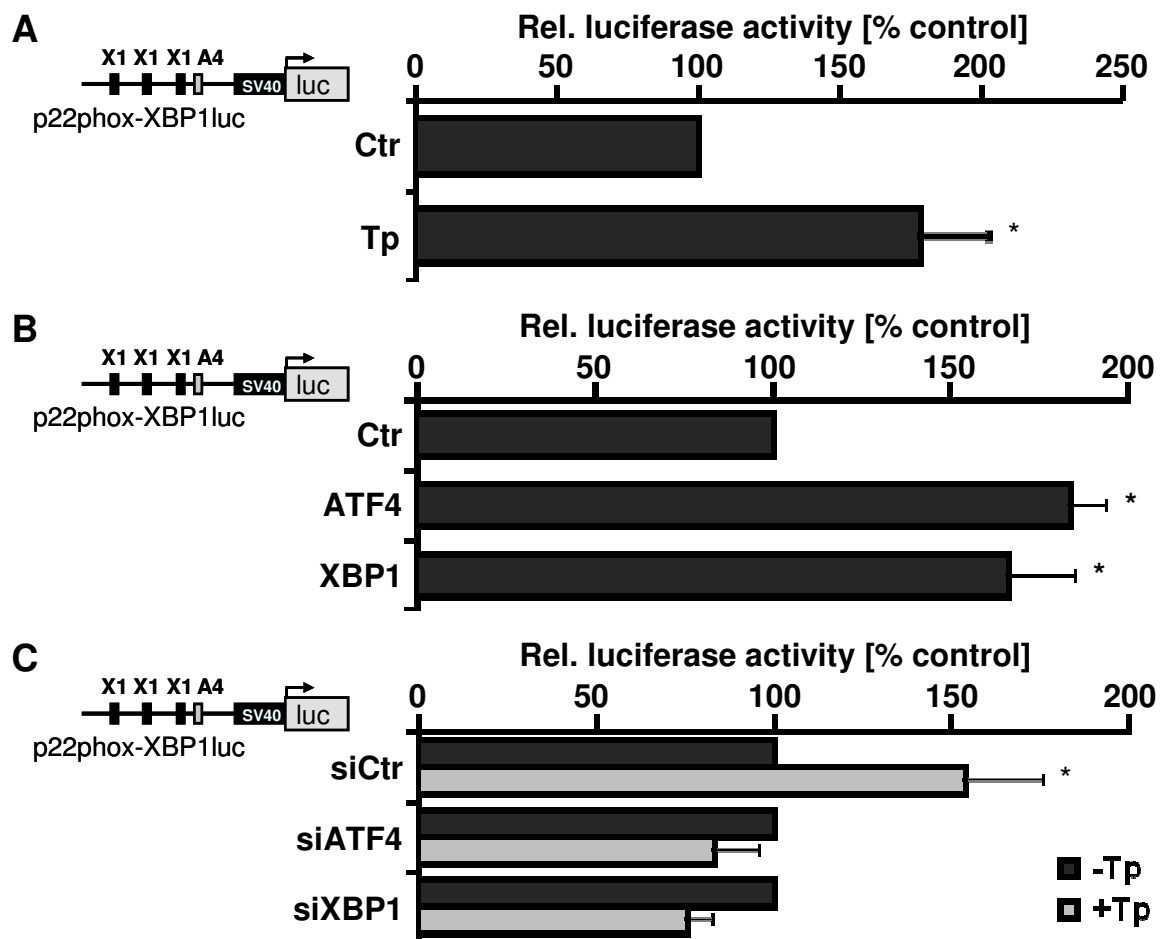


**Fig. 44 ER-stress activates a p22phox enhancer element via ATF4 and XBP1 in endothelial cells**

A. Ea.Hy926 cells were transfected with p22phox-XBP1 enhancer construct containing XBP1 (X1, black) and ATF4 (A4, grey) sites and stimulated with thapsigargin (2.5nM) for 8 hours or remained unstimulated (Ctr) and were subjected to luciferase assay. Data are represented as change to nontreated cells (100%; n=3, \*p<0.05 vs. unstimulated control cells). B. Cells were transfected with p22phox-XBP1 enhancer construct together with a plasmid encoding either for ATF4, XBP1 or empty control vector (Ctr). 24 hours post-transfection cells were subjected to luciferase assay. Data represented as change to cells transfected with control vector (100%, n=3, \*p<0.05 vs. cells transfected with control). C. Cells were transfected with p22phox-XBP1 enhancer construct together with a plasmid encoding for a siRNA against ATF4 (siATF4), against XBP1 (siXBP1) or control siRNA (siCtr). 24 hours post-transfection cells were stimulated with thapsigargin (2.5nM; +Tp) for 8 hours or were stimulated with solvent (-Tp) and subjected to luciferase assay. Data are represented as change to respective nontreated cells (100%; n=3, \*p<0.05 vs. unstimulated cells).

## 4 Discussion

### 4.1 Expression of NOX2, NOX4, NOX5, p22phox in endothelial cells

The NOX2 containing NADPH oxidase known from phagocytic cells was the first NADPH oxidase discovered in endothelial cells [79]. In the following years several homologues of NOX2 were discovered, NOX1, NOX3, NOX4 and NOX5. Whereas the expression of NOX3 seems to be limited to the inner ear and fetal tissues, all other NOX homologues were found to be expressed in several adult tissues and cell types including vascular cells. From NOX5 several splice variants are predicted, but so far little is known about their contribution and function in endothelial cells.

Therefore, as a first aim, we investigated the expression of different novel NOX proteins namely NOX1, NOX2, NOX4 and NOX5 including the EF-lacking variant NOX5S in the endothelial cell types Ea.Hy926 and HMEC-1. Briefly, the results show that

- (A) Ea.Hy926 cells and HMEC-1 express both NOX2 and NOX4 at mRNA and protein levels.
- (B) HMEC-1 cells express mRNA for NOX5 $\beta$  and NOX5 $\delta$  variants as determined by RT-PCR.
- (C) HMEC-1 cells contain NOX5 protein as well as the NOX5S variant which lacks the N-terminal calcium-binding domains.
- (D) NOX5 proteins are also present in endothelial and smooth muscle cells in the vascular wall of spleen and lung tissue.

In this study we showed that endothelial Ea.Hy926 cells as well as HMEC-1 cells express both NOX2 and NOX4, at the mRNA and protein level. In addition to the NADPH oxidase subunit NOX2 (gp91phox) which has been shown to be expressed

and functionally active in endothelial cells [32, 79], NOX4 has been recently shown to be expressed in endothelial cells suggesting that a NOX4-containing NADPH oxidase may play a functional role in these cells [40, 54]. In endothelial cells, we could earlier show that NOX2 is involved in the thrombin-induced ROS generation, proliferation and angiogenesis [80]. It was also shown that NOX2 is involved in the migrating response of endothelial cells [81]. Furthermore, in porcine cerebral microvascular endothelial cells, TNF $\alpha$  induced oxidative stress and subsequently apoptosis by NOX4 [82] and also in human coronary arterial endothelial cells, NOX4 was involved in the TNF $\alpha$  induced ROS generation [83]. Interestingly, NOX2 mediated anti-inflammatory effects induced by atrial natriuretic peptide in endothelial cells activated by TNF $\alpha$  [84], although TNF $\alpha$  is known to mediate the proinflammatory response in neutrophils in a NOX2-dependent manner [85].

We could also demonstrate that vascular cells express NOX5 transcripts, HMEC-1 cells expressed the EF-hand containing NOX5 variants NOX5 $\beta$  and NOX5 $\delta$ , whereas PASMCs expressed in addition NOX5 $\alpha$  and NOX5 $\gamma$ . Previously, the expression of NOX5 $\alpha$  has been described in the spleen and the expression of NOX5 $\beta$  in testis [45], whereas NOX5 $\delta$  and NOX5 $\gamma$  expression has not been described so far. Other findings indicate that NOX5 variants are cell type specifically expressed [37]. In addition to the EF-hand containing NOX5 variants, a shorter variant which we now termed NOX5S lacking the EF-hands and thus resembling other NOX homologues such as NOX1, NOX2 or NOX4, was detected in vascular cells. Initially, a NOX5 transcript identical to NOX5S has been described to be primarily present in fetal tissue and some cancer cell lines including CaCo2 [75]. NOX5 transcripts have been subsequently identified in vascular smooth muscle, uterus and bone marrow [45], in prostate carcinoma cells [48] and human cardiac fibroblasts [51]. Recently, NOX5 transcripts have also been detected in the stomach [50]. However, these studies

used PCR primers which amplified fragments from the “core region” of NOX5, which is common to all NOX5 variants including NOX5S making the discrimination of NOX5 and NOX5S impossible. To verify the presence of NOX5 variants at the protein level, Western blot analysis with an antibody targeted against an epitope within the core region of NOX5 was performed. This antibody recognized two proteins of 75 kDa and 60 kDa with a prevalence of the larger protein which was not present upon addition of the immunogenic peptide or after transfection of siRNA targeting NOX5. Furthermore, overexpression of NOX5 $\beta$  or NOX5S confirmed that the antibody recognizes NOX5S as well as EF-hand containing NOX5 variants indicating that NOX5 and NOX5S proteins are present in endothelial cells. Similarly, expression of NOX5 has been described in Du145 prostate carcinoma cells and in hairy cell leukemic B-cells but not in circulating B-cells [48, 49]. NOX5S was also reported to be highly expressed in Barrett esophageal adenocarcinoma cells involved in tumor progression [86-88].

In addition to the presence of NOX5 variants in cultivated endothelial cells, we could clearly demonstrate that NOX5 protein was also present in small vessels of the spleen in the endothelial as well as in the smooth muscle cell layer [53]. Although NOX5 protein has not been detected in human tissues to date, NOX5 mRNA has been found in testis, spleen, and lymph nodes by in situ hybridization and has been localized to areas rich in either spermatocytes, or immature B-lymphocytes or T-lymphocytes, respectively [45].

Consistently with these results, we found NOX5 staining for lymphocytes throughout the spleen. Although NOX5 protein could also be detected in vessels and in tissue from other highly vascularized lymphoid organs such as the tonsil [53], the presence of this protein was not restricted to lymphoid tissues since NOX5 was also found in

pulmonary vessels. These data suggest that NOX5 protein is expressed in cells of the vascular wall.

## **4.2 Expression of NOX1, NOXA1 and NOXO1 in endothelial cells**

In addition to NOX2 and NOX4, NOX1 has also been suggested to play a functional role in rat basilar and sinusoidal as well as in mouse aortic endothelial cells [41, 42, 89], although NOX1 mRNA could not be detected in HUVEC [54, 84]. Therefore it was also an aim of this study to investigate whether endothelial cells express NOX1 and its cytosolic factors NOXA1 and NOXO1. Furthermore the contribution of NOX1 to endothelial ROS generation was investigated. We could demonstrate that

- (A) NOX1 is detectable at mRNA and protein level in Ea.Hy926 cells and HMEC-1 cells.
- (B) NOX1 is present in a perinuclear compartment and is present in the microsomal fraction.
- (C) Ea.Hy926 cells and HepG2 cells express NOXA1 and NOXO1 mRNA.

Although we could confirm by RT-PCR and Western blot analyzes the presence of NOX1 in endothelial cells, detection by RT-PCR required an increased cycle number, indicating that only small amounts of NOX1 mRNA are present in endothelial cells. However, there is a report showing that a NOX1 short variant termed NOH1-S is the result of a template switching during cDNA synthesis [8] indicating that the NOX1 mRNA and subsequently cDNA is forming secondary structures inhibiting an efficient RT-PCR.

Immunofluorescence analysis further showed that NOX1 was located in a perinuclear compartment resembling the ER and NOX1 protein was also present in the microsomal fraction, although no colocalization with the ER-marker calreticulin was detected. Interestingly, NOX1 also colocalized with NOX2 within one cell (data not

shown), indicating that NOX1, NOX2 and NOX4 are co-expressed in endothelial cells. However, depletion of NOX1 by different siRNAs did not significantly reduce basal ROS levels or proliferation in endothelial cells, indicating that NOX2 and NOX4 play a major role in basal endothelial ROS production.

Since NOX1 requires preferentially the p47phox homologue NOXO1 and the p67phox homologue NOXA1 for ROS generation [47, 90], we also performed RT-PCR analysis to identify the expression of NOXO1 and NOXA1 in endothelial cells. Indeed, both NOXA1 and NOXO1 mRNA could be detected in endothelial Ea.Hy926 cells as well as in the hepatoma cell line HepG2, as the expression of NOXA1 and NOXO1 was described in the liver [90]. However, additional PCR products could be detected in our study. Sequencing and comparison of the two PCR products for NOXA1 show the insertion of several nucleotides from the intron upstream of the 5' end of exon 3. The transition of this "extended" exon 3 and exon 2 corresponded to the traditional splicing rule, GT at the 5' end and AG at the 3' end of the splice site [91], therefore indicating an alternative splicing. In the case of NOXO1, the sequencing analysis of the PCR product revealed that the complete short intron between exon 3 and exon 4 was amplified leading to a longer PCR product than expected. If these observations are the only differences between the newly discovered alternative PCR products and the known mRNA of NOXA1 and NOXO1, these nucleotide insertions would lead to a premature STOP codon and a very short protein.

For NOXO1, alternative splicing in the region of exon 2, 3 and 4 is reported, but the incorporation of the complete intron between exon 3 and 4 has not been previously observed [92, 93]. Also for NOXA1 alternative splicing was reported, but at different exons than found in our study [94]. Further experimental analyses of our

observations are necessary to confirm whether our observed larger PCR products are indeed results of an alternative splicing.

### **4.3 NOX1, NOX2, NOX4 and NOX5 localization and interaction with p22phox**

As we demonstrated that endothelial cells express the NOX homologues NOX1, NOX2, NOX4 and NOX5. We further investigated and compared the subcellular localization of NOX1, NOX2, NOX4, NOX5 and the EF-hand lacking variant NOX5S as well as the localization of p22phox. Furthermore we analyzed whether these NOX homologues, similar to the situation in the phagocytic NADPH oxidase, were able to interact with p22phox. The following results were achieved:

- (A) NOX2 and NOX4 are simultaneously expressed within the same endothelial cell.
- (B) NOX2, NOX4, NOX5, but not NOX1 are localized in the ER of endothelial cells colocalising with the ER-marker calreticulin.
- (C) NOX2 but not NOX4 is also present at the plasma membrane.
- (D) GFP-tagged p22phox, NOX2, NOX4, NOX5S and NOX5 $\beta$  are localized in the ER of endothelial cells.
- (E) GFP-tagged p22phox and NOX5 are localized in the ER of HeLa cells, whereas GFP-tagged NOX2 and NOX4 are mainly localized in the plasma membrane of these cells.
- (F) NOX2 and NOX4 are able to interact with p22phox.
- (G) both NOX5S and NOX5 $\beta$  interact with overexpressed p22phox, although p22phox was not essentially required for ROS production by either variant.

We showed that NOX2 and NOX4 are both present simultaneously within the same endothelial cells and that expression of each subunit is not limited to a subpopulation

of cells. Although the functional relevance of this observation is not clear to date, previous studies suggested that NOX homologues may be present in different cellular compartments and may thus have different functions [95]. NOX2 and NOX4 were both present in an intracellular, perinuclear compartment and colocalized with calreticulin. In addition, GFP-tagged NOX2 and NOX4 as well as p22phox were expressed and colocalized with coexpressed ER-localized fluorescent proteins, suggesting that NOX2 and NOX4 as well as p22phox, are localized in the ER. Interestingly, the intracellular localization of GFP-tagged NOX2 and NOX4 in cervix carcinoma cells (HeLa) differs from the localization observed in Ea.Hy926 cells, indicating a different localization of NOX2 and NOX4 in different cell lines. Although several publications showed a localization of NOX4 in the ER of endothelial cells and other cells [54, 96, 97], localization at the focal adhesion together with vinculin in rat vascular smooth muscle cells [95] and in the nucleus of human umbilical vein endothelial cells, stem cells and cells isolated from rat renal cortex [98-100] were also reported. We could not find a difference in the localization of p22phox and NOX5 between HeLa and endothelial cells. Similarly, GFP-tagged NOX2 and NOX4 showed an ER-like expression pattern in HUVEC [54]. Furthermore, in cell fractionation experiments we could confirm that NOX2 and NOX4 are present in the microsomal fraction. However, preliminary studies did not provide evidence that both proteins would interact with each other under the experimental conditions applied. Although NOX2 was considered to be mainly localized in leukocytes at the plasma membrane, earlier studies showed that NOX2 is also present in intracellular vesicular structures in “dormant”, non-activated leukocytes [101]. Consistently, immunofluorescence demonstrated that NOX2 and p22phox were expressed in an intracellular, perinuclear compartment in an ER-like manner in porcine iliac artery and bovine aortic endothelial cells [32]. Similarly, NOX4 has been found in the ER in human aortic

smooth muscle cells [55] and fluorescent protein-tagged NOX4 interacted with the ER-marker protein-disulfid-isomerase in rabbit vascular smooth muscle cells [56]. In contrast, NOX4 protein was found to colocalize with focal adhesions in rat vascular smooth muscle cells [95]. Although the reasons for these divergent findings are not resolved to date, the functional importance of our observations was further underlined by our findings that p22phox was also present in the ER and, more importantly, that p22phox interacted with NOX2 and NOX4 in this intracellular compartment as determined by BiFC [76, 77]. Importantly, although BiFC was performed in HeLa cells, the fluorescent complexes in these cells showed a similar distribution as the fusion proteins or the “native” proteins in Ea.Hy926 cells indicating that these studies are representative for the situation in intact Ea.Hy926 cells. In contrast to GFP-NOX2 alone, no clear membrane staining was observed in HeLa cells, indicating that the complex of p22phox and NOX2 has a different localization than NOX2 alone. Similarly, using FRET, a technique which allows the visualization of proteins located in a very close vicinity, the association of transfected rat p22phox with transfected NOX2 and NOX4 was demonstrated in HEK293 cells [96]. We could demonstrate the presence of smaller amounts of NOX2, but not NOX4 protein at the plasma membrane and its colocalization with F-actin whereby actin was found at the inner layer and NOX2 at the outer layer of the membrane. Intracellular colocalization of NOX2 with parts of the cytoskeleton has been previously described in endothelial cells [32, 54]. In addition, a recent study showed that NOX2 can be found at the leading edge of migrating HUVEC where it colocalized with actin [81].

Our immunofluorescence studies revealed that under basal conditions NOX5S and NOX5 $\beta$  were localized intracellularly in a perinuclear compartment in both Ea.Hy926 and HMEC-1 cells and colocalized with calreticulin indicating that they are present in the ER. Similarly, we could show that endogenous NOX5 was present in the same

compartment. These findings are supported by a previous report where NOX5 was shown to be expressed in a perinuclear compartment in prostate carcinoma cells [48].

Interestingly, although NOX5S and NOX5 $\beta$  were able to interact with overexpressed p22phox as we could demonstrate by BiFC and co-immunoprecipitation, only NOX2 was able to interact with endogenous p22phox under these conditions.

These findings suggest that, in contrast to NOX2, the affinity of NOX5 proteins and p22phox may be too low to detect their interaction under the applied conditions. Consistently, we found that depletion of endogenous p22phox by siRNA did not significantly reduce ROS levels induced by NOX5S or NOX5 $\beta$ , although it diminished NOX2 mediated ROS production in HMEC-1 cells. Supporting, depletion of p22phox by siRNA did not decrease NOX5 $\beta$ -dependent ROS production in HEK293 cells [102]. Furthermore, as expected, when we overexpressed p22phox the NOX2-stimulated ROS generation was enhanced, but the increased p22phox levels had no significant effect on ROS levels in the presence of NOX5S or NOX5 $\beta$ , suggesting that, in contrast to NOX2, p22phox is not essentially required for ROS production by NOX5 proteins.

#### **4.4 Contribution of p22phox, NOX2, NOX4 and NOX5 to endothelial ROS generation and proliferation**

An intact cytoskeleton and interaction of NOX2 with the actin-binding protein IQGAP1 have been shown to be required for ROS production and migration of HUVEC [81] suggesting that in migrating and possibly also in proliferating endothelial cells, the reorganization of the actin cytoskeleton may enable NOX2 to translocate to the leading edge, assemble with the actin-binding structures and generate ROS to promote migration and proliferation. We therefore investigated the role of the NOX

homologues NOX2, NOX4, NOX5 including NOX5S on ROS generation, proliferation as well as the formation of capillary-like structures of endothelial cells. Indeed, we could demonstrate that

- (A) depletion of NOX2, NOX4 and NOX5 by siRNA reduces ROS production in Ea.Hy926 and HMEC-1 cells.
- (B) both NOX5S and NOX5 $\beta$  elevate basal ROS levels while depletion of NOX5 decrease ROS generation in HMEC-1 cells.
- (C) NOX5 $\beta$ -dependent but not NOX5S-dependent ROS production is enhanced in the presence of ionomycin in a calcium-containing buffer.
- (D) depletion of NOX2, NOX4 and NOX5 reduces endothelial proliferation and formation of capillary-like structures, indicating angiogenic activity.
- (E) overexpression of NOX2, NOX4 and NOX5 $\beta$  and NOX5S stimulates endothelial proliferation and formation of capillary-like structures.
- (F) activation of p38 MAP kinase by NOX2 or NOX4 contributes to the endothelial proliferative response.

These findings indicate that NOX2, NOX4 and NOX5 contribute to ROS generation in endothelial cells under basal conditions. A role for NADPH oxidase under stimulated conditions could be already demonstrated, although the findings were sometimes controversial. It was demonstrated that NOX4 or NOX2 antisense DNA inhibited angiotensin-II-induced ROS generation in HUVEC [103]. In addition, NOX4 antisense oligonucleotides decreased ROS levels of proliferating rat aortic endothelial cells by 50% although the contribution of NOX2 to ROS production has not been evaluated in that study [40]. On the other hand, ANP-stimulated ROS production was decreased by NOX2, but not by NOX4 antisense treatment in HUVEC [84]. Similarly, NOX2 antisense oligonucleotides reduced VEGF-stimulated ROS production in HUVEC [104]. Although the reasons for these controversial findings are not resolved to date

and may relate to the cell type used and the specific experimental conditions applied, we demonstrate that depletion of NOX2 or NOX4 also decreased ROS production in HMEC-1 cells, further emphasizing the importance of both homologues for endothelial ROS production.

Moreover, our results show that NOX2, NOX4, NOX5 $\beta$  and NOX5S overexpression enhanced ROS levels in Ea.Hy926 cells and HMEC-1 cells further indicating that these homologues contribute to endothelial ROS production, and that the amount of NOX2, NOX4 and NOX5 present in the cell is limiting the levels of ROS production. Consistently, studies in other cellular systems demonstrated that NOX4 overexpression increased ROS production with no need for concomitant expression of other subunits as long as p22phox levels were sufficient and that NOX5 $\beta$  overexpression increased ROS generation to a similar extent than NOX4 in HEK293 cells [102, 105]. In contrast, NOX2 function has been suggested to require p22phox as well as cytosolic subunits and Rac [19, 20, 53]. Thus, our findings - demonstrating that NOX2 overexpression increases ROS levels - suggest that sufficient cytosolic proteins are available in Ea.Hy926 cells or HMEC-1 cells in order to allow functional activation of a NOX2-dependent NADPH oxidase.

Moreover, consistent with previous reports [29, 30], we demonstrate that an elevation of calcium levels by the addition of ionomycin selectively enhanced NOX5 $\beta$ - but not NOX5S-mediated ROS levels. These findings indicate that increased calcium concentrations can further stimulate NOX5 $\beta$ -dependent ROS production.

We previously showed that low levels of H<sub>2</sub>O<sub>2</sub> increase the proliferative activity of Ea.Hy926 cells, and that modulation of p22phox levels affect the proliferative response of these cells [72]. Here, we demonstrate that overexpression of NOX2, NOX4, NOX5 $\beta$  and NOX5S as well as p22phox which lead to increased ROS production, also enhanced proliferative activity of Ea.Hy926 and HMEC-1 cells,

whereas depletion of NOX2, NOX4, NOX5 and p22phox decreased endothelial proliferation to a similar extent. These findings indicate that NOX2, NOX4 and NOX5-mediated ROS production contributes to endothelial proliferation.

Consistently, depletion of NOX2 decreased VEGF-induced migration and proliferation of HUVEC and depletion of NOX5 by antisense oligonucleotides decreased proliferation of prostate carcinoma cells [48, 104]. Furthermore, we showed that depletion of NOX2, NOX4 and NOX5 decreased the endothelial tube forming ability which is indicative of angiogenic activity.

Although to date the role of NOX4 in endothelial proliferation has not been fully investigated, overexpression of NOX4 has been previously shown to decrease proliferation of NIH3T3 cells [106] and depletion of NOX4 prevented the induction of apoptosis by 7-ketocholesterol in human aortic smooth muscle cells [55]. In contrast, and consistent with our study, recent studies showed that depletion of NOX4 decreased proliferation of melanoma cells [48], abrogated urotensin-II-stimulated proliferation of pulmonary artery smooth muscle cells [107] and increased apoptosis of pancreatic cancer cells [108]. Similar to our study it was also shown that NOX4 promoted proliferation and in vitro angiogenesis of HMEC-1 cells [109], indicating that NOX4 has also a pro-proliferative effect. Interestingly, we observed that both NOX2 and NOX4 activate p38 MAP kinase in Ea.Hy926 cells, and inhibition of this kinase prevents the proliferative response by these NOX proteins indicating that p38 MAP kinase contributes to the proliferative response induced by NOX2 or NOX4. Several other studies confirmed an involvement of NADPH oxidases in the activation of p38 MAP kinase [53, 72, 110]. Moreover, p38 MAP kinase was involved in NOX4-mediated proliferation of pulmonary artery smooth muscle cells in response to urotensin-II [107] and in NOX2-mediated proliferation of hepatic stellate cells by PDGF [110].

#### **4.5 Regulation of NADPH oxidase subunits NOX2 and NOX5 by thrombin**

As we could already show that a prothrombotic state induces ROS generation and the expression of p22phox, we further investigated whether NOX5 and NOX2 are involved in these processes. We could show that

(A) thrombin upregulates NOX2, NOX5 and NOX5S protein levels.

(B) depletion of NOX2 and NOX5 by siRNA diminishes ROS production, proliferation, and the formation of capillary-like structures in response to thrombin.

Interestingly, addition of thrombin, which is known to enhance ROS production of endothelial cells and of smooth muscle cells involving activation and induction of NADPH oxidases [33, 72, 78, 111], also enhanced NOX5 and NOX5S as well as NOX2 protein levels, and depletion of NOX5 or NOX2 decreased endothelial ROS production by thrombin. Similar to the situation in endothelial Ea.Hy926 cells where thrombin induced the NADPH oxidase subunit p22phox thus leading to enhanced ROS levels [72], upregulation of NOX5 proteins may also be required for NOX5-dependent ROS production upon prolonged exposure to thrombin. This hypothesis is supported by our findings that ionomycin does not enhance ROS levels in quiescent HMEC-1 cells, but effectively enhances ROS levels in response to thrombin [53]. Similar to our study, however, ionomycin did not enhance ROS levels in mouse microvascular endothelial cells under basal conditions [112], suggesting that NOX5 levels may be limiting in mediating a response to enhanced calcium levels in resting endothelial cells.

Since thrombin is known to enhance calcium levels in endothelial cells [113], it is tempting to speculate that such a pathway may contribute to ROS generation by NOX5 activation. Initial studies in our group using the calcium chelator BAPTA-AM showed a decrease in ROS levels in HMEC-1 cells in response to thrombin. However, since BAPTA-AM also reduced basal ROS levels, and thrombin also upregulated NOX5S and NOX2 which are not activated by calcium, it appears that a certain calcium level may be required for signaling processes leading to the activation of NADPH oxidase-dependent ROS production. Additional elevation of calcium may then specifically lead to the activation of calcium-binding NOX5 variants.

In contrast, depletion of NOX5 and NOX2 diminished thrombin-stimulated proliferation and in vitro angiogenesis, indicating that both proteins are involved in the control of the endothelial proliferative response to thrombin. Similarly, ROS derived from a NOX2-based NADPH oxidase have been shown to be involved in VEGF-regulated angiogenesis [48].

#### **4.6 Regulation of the NADPH oxidase subunit p22phox by ER-stress**

It has been previously shown that the NADPH oxidase subunits NOX1 and NOX4 can interact with PDI [56] and that NOX4 is involved in 7-ketocholesterol-induced ER-stress and subsequently in the apoptosis of smooth muscle cells [55]. We therefore investigated the effect of thapsigargin- and tunicamycin-induced ER-stress [50] on the endothelial ROS generation and the expression of p22phox. We could show that

- (A) PDI colocalizes with NOX4 and induces ROS generation in endothelial cells.
- (B) thapsigargin and tunicamycin induces ROS generation in endothelial Ea.Hy926 cells.

- (C) expression of p22phox is induced by ER-stress and depletion of p22phox diminishes ER-stress-induced ROS generation.
- (D) depletion of the transcription factors ATF4 and XBP1 reduces not only ER-stress-induced ROS generation, but - in the case of XBP1 - also p22phox induction by ER-stress, whereas overexpression of ATF4 and XBP1 increases p22phox expression and ROS generation.
- (E) ER-stress and overexpression of ATF4 increases the luciferase activity of a reporter construct containing the p22phox promoter.
- (F) ER-stress increases the luciferase activity of a reporter construct containing XBP1 and ATF4 binding sites cloned from a distal upstream region of the p22phox gene in a XBP1- and ATF4-dependent manner.

As we have shown, NOX2, NOX4, NOX5 as well as p22phox were localized in the ER of endothelial cells, where also PDI is localized, an ER-localized thiol oxidoreductase assisting in redox protein folding [56-58].

Similar to the situation in smooth muscle cells [56, 114], we could localize PDI together with NOX4 and to a weaker extent also with NOX1. Furthermore, we could demonstrate that PDI mediates ROS generation. These results match the observation that NOX1, NOX4 as well as p22phox interact with PDI and that PDI contributes to ROS generation in smooth muscle cells [56-58]. Interestingly, also in phagocytic cells an interaction between PDI and p22phox could be demonstrated [115]. Although we could show that a PDI mutant without chaperone function is not able to increase ROS generation in endothelial cells, in vascular smooth muscle cells the chaperone function of PDI did not seem not to be required to support the NADPH oxidase activity [56, 114], indicating a cell-type specific function of PDI.

Pro-inflammatory stimuli such as angiotensin-II, PDGF [116] or thrombin [53, 72] are known to induce NADPH oxidase expression and ROS generation. These stimuli are

involved in pathophysiological processes like atherosclerosis or pulmonary hypertension which in turn are associated with an increased ROS generation and increased expression of NADPH oxidases. On the other hand, pathophysiological processes such as atherosclerosis are associated with the accumulation of oxysterols which induce ER-stress, triggering the unfolded protein response (UPR) [16, 55, 60]. Therefore it is possible that the UPR plays also a role in the regulation of NADPH oxidase. The UPR is characterized by a general attenuation in protein synthesis with a simultaneous increase in the expression of so-called UPR genes such as specific transcription factors like XBP1 and ATF4 [61, 62].

In this study, we could demonstrate that ATF4 and XBP1 modulate ROS generation in endothelial cells. Oxidative stress is a common event upon UPR [62], as the ER has an oxidizing environment to promote protein folding [117], which is maintained by the ER oxidoreductase 1 (Ero1). It has been reported that Ero1 is upregulated upon cellular stress conditions and that Ero1 is able to transfer electrons to molecular oxygen to generate H<sub>2</sub>O<sub>2</sub> [118]. Furthermore, it has been shown in *Caenorhabditis elegans* that silencing of Ero1 inhibits tunicamycin-induced ROS generation [119]. Interestingly, a constitutively active Ero1 alone was not able to induce ROS generation when overexpressed in yeast [120], indicating that other proteins than Ero1 are important to induce ROS generation upon ER-stress. We observed a complete abolishment of ROS generation in response to thapsigargin-induced ER-stress upon depletion of p22phox in endothelial cells suggesting the involvement of NADPH oxidase in ROS production by ER-stress. In support, it has been reported that NOX4 may contribute to ER-stress induced ROS generation in smooth muscle cells [55].

This assumption was supported by our findings that ER stressors leading to UPR as well as ATF4 and XBP1 are able to enhance p22phox expression and p22phox

promoter activity. In line, we identified a proximal putative ATF4 binding site in the p22phox promoter as well as a distal cluster of potential XBP1 and ATF4 binding sites which could serve as an enhancer element. In support, ER-stress and ATF4 or XBP1 overexpression increased luciferase activity of a construct driven by this putative UPR-responsive element and depletion of ATF4 and XBP1 abolished the ER-stress induced activity of this construct. These findings suggest that the NADPH oxidase subunit p22phox which is common to most of the NADPH oxidase family members, is regulated by a transcriptional mechanism in response to ER-stress involving ATF4 and XBP1. This is further supported by our findings that inhibition of the transcription abolished p22phox induced mRNA expression upon ER-stress and that silencing of XBP1 also decreased ER-stress induced p22phox protein expression.

To date, only little is known about the regulation of the p22phox gene expression. It was shown that AP-1 and NF $\kappa$ B, two redox sensitive transcription factors, are both able to regulate p22phox gene expression [121, 122], which is consistent with our previous observation of a redox-sensitive regulation of p22phox mRNA expression upon thrombin stimulation [72]. Furthermore, both transcription factors can be induced by prolonged UPR [123-125]. However, our study demonstrated a direct involvement of the UPR genes ATF4 and XBP1 in the control of p22phox gene expression. Although we cannot completely rule out a contribution of AP-1 or NF $\kappa$ B on ER-stress-induced p22phox expression, our findings that the distal UPR responsive p22phox enhancer element seems not to contain putative binding sites for these transcription factors gives a strong hint on the involvement of UPR genes in p22phox expression.

In addition, XBP1 can also induce PDI which can increase ROS generation in response to ER-stress, and can have a regulatory function on NADPH oxidases in

smooth muscle cells [56]. In line, our preliminary results suggest that XBP1 could also modulate NOX4 expression in endothelial cells further emphasizing that UPR genes may affect NADPH oxidase expression and activity on multiple levels. Another pro-apoptotic transcription factor which is induced by XBP1 and by ATF4 is the C/EBP-homologous protein (CHOP). However, we could not find any potential CHOP binding site in the upstream region of p22phox and therefore an involvement of CHOP appeared to be unlikely in the regulation of p22phox.

One potential target for the ROS generated during ER-stress is the protein phosphatase 1 (PP1). PP1 counteracts PERK which phosphorylates eIF1 $\alpha$  during UPR by dephosphorylating eIF2 $\alpha$  thus restoring protein translation [62]. Consistently with our observation that ER-stress induces p22phox levels and subsequently increases ROS levels, it was reported that PP1 can be reversibly inhibited by H<sub>2</sub>O<sub>2</sub> [126]. Another target for increased ROS generation in the UPR is the protein tyrosine phosphatase 1B (PTP1B), localized in the ER-membrane. It was reported for endothelial cells, that NOX4 is able to interact and subsequently inactivate PTP1B [127]. Interestingly, there is evidence that this phosphatase may potentiate the IRE1-dependent signaling during the UPR as silencing of PTP1B results in reduced apoptosis [128]. Interestingly this is controversial to the reported pro-apoptotic function of NOX4 upon prolonged ER-stress in smooth muscle cells, where a phosphorylation cascade initiated by IRE1 resulted in NOX4-dependent apoptosis [55]. Again, different cell types and species could be one reason for the controversial observations. Altogether, our observations indicate that NADPH oxidase expression and function can be induced by ER-stress and UPR mediators, suggesting a possible role of NADPH oxidase-derived ROS generation in the UPR.

## 4.7 Conclusion

The importance of the various NOX homologues for vascular function is still an open question. This present study showed that endothelial cells express at least four of the five known NOX homologues as we could show that these cells express in addition to NOX2 and NOX4 also NOX1 and NOX5, and that coexpression of various NOX proteins in one single cell can take place. However, the contribution of NOX1 to endothelial basal ROS generation and proliferation seems to be limited. Still, NOX1 could be important under specific conditions of endothelial cell activation, the elucidation of which needs further investigations.

The other NOX homologues NOX2, NOX4 and NOX5 contribute equally to basal endothelial ROS generation, proliferation and angiogenesis. There are differences in the intracellular localization of the NOX homologues in endothelial cells. NOX2, NOX4 and NOX5 are mainly localized in the ER, but NOX2 is also partially localized to the plasma membrane while the precise localization of NOX1 is still unclear. Stress factors such as thrombin and ER-stress are able to induce ROS generation. Here we showed that thrombin induces NOX2 and NOX5 expression and that NOX2 and NOX5 contribute to endothelial ROS generation, proliferation and angiogenesis upon thrombin stimulation. Differences in the fine tuning of NOX2 and NOX5 activation could be relevant and the exact role of ROS generation by either NOX2 or NOX5 is still not precisely known. However, these novel findings mark NOX2, NOX5 as well as ROS in general as novel targets for antithrombotic research in the future.

Furthermore, the identification of calcium-dependent and –independent NOX5 variants in endothelial cells is a novel finding. However, activation and embedment of NOX5 in calcium-related pathways remains still unclear and constitutes a promising topic for future research.

The present study also shows for the first time that p22phox, which is required for the function of most NOX homologues except NOX5, is induced by ER-stress, and that the UPR genes ATF4 and XBP1 enhance ROS generation by upregulating p22phox. Although, little is known about the involvement of NADPH oxidases in the UPR, these findings suggest that NADPH oxidases may play a role in the this stress response.

In summary, the results of this study reveal new insights in the role of ROS and novel NADPH oxidases in endothelial cells under basal and stress conditions which can serve as new background for further research in this field.

## 5 Summary

Increased levels of reactive oxygen species (ROS) contribute to vascular diseases like pulmonary hypertension and atherosclerosis. Although a NOX2-containing NADPH oxidase similar to the neutrophil one has been described to be active in endothelial cells, the contribution of newly discovered NOX homologues (NOX1-NOX5) was still unclear. Therefore, the overall aim of this study was to better characterize the expression, regulation and function of NOX homologues in different endothelial cell models.

First, we could demonstrate the presence of NOX1, NOX2, NOX4, NOX5 including NOX5S as well as p22phox mRNA and protein levels in Ea.Hy926 or HMEC-1 cells. Furthermore, NOX5 protein was also present in endothelial and smooth muscle cells in the vascular wall of spleen and lung tissue. We found that NOX2, NOX4 and NOX5 were present in an intracellular perinuclear compartment, whereby NOX2 and NOX4 could be localized simultaneously in one cell. NOX2, NOX4, NOX5 were able to interact with p22phox and overexpression of NOX2, NOX4 and NOX5 increased ROS generation, although NOX5-dependent ROS generation did not require the presence of p22phox. NOX2, NOX4 and NOX5 also increased endothelial proliferation while depletion of NOX2, NOX4 and NOX5 decreased ROS generation, proliferation and tube forming ability indicating angiogenic activity under basal conditions. NOX2- and NOX4-induced proliferation was mediated by p38 MAP kinase.

Although NOX1 expression as well as the expression of its regulatory subunits NOXO1 and NOXA1 was detectable in endothelial cells, depletion of NOX1 did not significantly affect basal ROS generation or proliferation of endothelial cells.

Second, we could demonstrate the upregulation of NOX2, NOX5 and NOX5S after thrombin stimulation in endothelial cells and the modulation of p22phox expression in an ATF4- and XBP1-dependent manner under ER-stress conditions. Cellular stress either by thrombin or UPR also induced ROS generation of endothelial cells. In addition, thrombin induced proliferation and enhanced the tube forming ability of endothelial cells. Thrombin-induced ROS generation, proliferation and tube forming ability were diminished by silencing NOX2 or NOX5, whereas UPR induced ROS generation was inhibited by silencing p22phox as well as by silencing ATF4 or XBP1. In summary, this work provides evidence that in endothelial cells, NOX2, NOX4 and NOX5, but not NOX1, contribute to basal ROS generation, proliferation and angiogenesis and that the NOX proteins NOX2 and NOX5 as well as p22phox play an important role in the response to thrombin and ER-stress providing new insights in endothelial function and redox signaling.

## 6 References

1. Stocker, R. and J.F. Keane, Jr., *Role of oxidative modifications in atherosclerosis*. *Physiol Rev*, 2004. **84**(4): p. 1381-478.
2. Farber, H.W. and J. Loscalzo, *Pulmonary arterial hypertension*. *N Engl J Med*, 2004. **351**(16): p. 1655-65.
3. Humbert, M., et al., *Cellular and molecular pathobiology of pulmonary arterial hypertension*. *J Am Coll Cardiol*, 2004. **43**(12 Suppl S): p. 13S-24S.
4. Paravicini, T.M. and R.M. Touyz, *NADPH oxidases, reactive oxygen species, and hypertension: clinical implications and therapeutic possibilities*. *Diabetes Care*, 2008. **31 Suppl 2**: p. S170-80.
5. Veyssier-Belot, C. and P. Cacoub, *Role of endothelial and smooth muscle cells in the pathophysiology and treatment management of pulmonary hypertension*. *Cardiovasc Res*, 1999. **44**(2): p. 274-82.
6. Willeit, J. and S. Kiechl, *Biology of arterial atheroma*. *Cerebrovasc Dis*, 2000. **10 Suppl 5**: p. 1-8.
7. Siegel-Axel, D., et al., *Platelet lipoprotein interplay: trigger of foam cell formation and driver of atherosclerosis*. *Cardiovasc Res*, 2008. **78**(1): p. 8-17.
8. Geiszt, M. and T.L. Leto, *The Nox family of NAD(P)H oxidases: host defense and beyond*. *J Biol Chem*, 2004. **279**(50): p. 51715-8.
9. Segal, A.W., *How neutrophils kill microbes*. *Annu Rev Immunol*, 2005. **23**: p. 197-223.
10. Nozik-Grayck, E., et al., *Bicarbonate-dependent superoxide release and pulmonary artery tone*. *Am J Physiol Heart Circ Physiol*, 2003. **285**(6): p. H2327-35.
11. Ghio, A.J., et al., *Superoxide-dependent iron uptake: a new role for anion exchange protein 2*. *Am J Respir Cell Mol Biol*, 2003. **29**(6): p. 653-60.
12. Droge, W., *Free radicals in the physiological control of cell function*. *Physiol Rev*, 2002. **82**(1): p. 47-95.
13. Cai, H., *Hydrogen peroxide regulation of endothelial function: Origins, mechanisms, and consequences*. *Cardiovasc Res*, 2005. **68**(1): p. 26-36.
14. Ushio-Fukai, M. and R.W. Alexander, *Reactive oxygen species as mediators of angiogenesis signaling: role of NAD(P)H oxidase*. *Mol Cell Biochem*, 2004. **264**(1-2): p. 85-97.
15. Herkert, O., et al., *Insights into the redox control of blood coagulation: role of vascular NADPH oxidase-derived reactive oxygen species in the thrombogenic cycle*. *Antioxid Redox Signal*, 2004. **6**(4): p. 765-76.
16. Li, J.M. and A.M. Shah, *Endothelial cell superoxide generation: regulation and relevance for cardiovascular pathophysiology*. *Am J Physiol Regul Integr Comp Physiol*, 2004. **287**(5): p. R1014-30.
17. Taniyama, Y. and K.K. Griendling, *Reactive oxygen species in the vasculature: molecular and cellular mechanisms*. *Hypertension*, 2003. **42**(6): p. 1075-81.
18. Cai, H., K.K. Griendling, and D.G. Harrison, *The vascular NAD(P)H oxidases as therapeutic targets in cardiovascular diseases*. *Trends Pharmacol Sci*, 2003. **24**(9): p. 471-8.
19. Nauseef, W.M., *Assembly of the phagocyte NADPH oxidase*. *Histochem Cell Biol*, 2004. **122**(4): p. 277-91.
20. Babior, B.M., J.D. Lambeth, and W. Nauseef, *The neutrophil NADPH oxidase*. *Arch Biochem Biophys*, 2002. **397**(2): p. 342-4.

21. El-Benna, J., et al., *Phagocyte NADPH oxidase: a multicomponent enzyme essential for host defenses*. Arch Immunol Ther Exp (Warsz), 2005. **53**(3): p. 199-206.
22. Rahman, I., S.K. Biswas, and A. Kode, *Oxidant and antioxidant balance in the airways and airway diseases*. Eur J Pharmacol, 2006. **533**(1-3): p. 222-39.
23. Dinauer, M.C., *Regulation of neutrophil function by Rac GTPases*. Curr Opin Hematol, 2003. **10**(1): p. 8-15.
24. Price, M.O., et al., *Rac activation induces NADPH oxidase activity in transgenic COSphox cells, and the level of superoxide production is exchange factor-dependent*. J Biol Chem, 2002. **277**(21): p. 19220-8.
25. Parkos, C.A., et al., *Primary structure and unique expression of the 22-kilodalton light chain of human neutrophil cytochrome b*. Proc Natl Acad Sci U S A, 1988. **85**(10): p. 3319-23.
26. Quinn, M.T., et al., *Reconstitution of defective respiratory burst activity with partially purified human neutrophil cytochrome B in two genetic forms of chronic granulomatous disease: possible role of Rap1A*. Blood, 1992. **79**(9): p. 2438-45.
27. Moreno, M.U., et al., *Preliminary characterisation of the promoter of the human p22(phox) gene: identification of a new polymorphism associated with hypertension*. FEBS Lett, 2003. **542**(1-3): p. 27-31.
28. Brennan, L.A., et al., *Increased superoxide generation is associated with pulmonary hypertension in fetal lambs: a role for NADPH oxidase*. Circ Res, 2003. **92**(6): p. 683-91.
29. Guzik, T.J., et al., *Systemic regulation of vascular NAD(P)H oxidase activity and nox isoform expression in human arteries and veins*. Arterioscler Thromb Vasc Biol, 2004. **24**(9): p. 1614-20.
30. Miller, F.J., Jr., et al., *Superoxide production in vascular smooth muscle contributes to oxidative stress and impaired relaxation in atherosclerosis*. Circ Res, 1998. **82**(12): p. 1298-305.
31. Heymes, C., et al., *Increased myocardial NADPH oxidase activity in human heart failure*. J Am Coll Cardiol, 2003. **41**(12): p. 2164-71.
32. Li, J.M. and A.M. Shah, *Intracellular localization and preassembly of the NADPH oxidase complex in cultured endothelial cells*. J Biol Chem, 2002. **277**(22): p. 19952-60.
33. Gorlach, A., et al., *Thrombin activates the hypoxia-inducible factor-1 signaling pathway in vascular smooth muscle cells: Role of the p22(phox)-containing NADPH oxidase*. Circ Res, 2001. **89**(1): p. 47-54.
34. Matsuo, J., et al., *Involvement of NADPH oxidase and protein kinase C in endothelin-1-induced superoxide production in retinal microvessels*. Exp Eye Res, 2009.
35. Galle, J., et al., *Impact of oxidized low density lipoprotein on vascular cells*. Atherosclerosis, 2006. **185**(2): p. 219-26.
36. Li, Q., et al., *Nox2 and Rac1 regulate H2O2-dependent recruitment of TRAF6 to endosomal interleukin-1 receptor complexes*. Mol Cell Biol, 2006. **26**(1): p. 140-54.
37. Brown, D.I. and K.K. Griendling, *Nox proteins in signal transduction*. Free Radic Biol Med, 2009.
38. Griendling, K.K., *Novel NAD(P)H oxidases in the cardiovascular system*. Heart, 2004. **90**(5): p. 491-3.
39. Lambeth, J.D., *NOX enzymes and the biology of reactive oxygen*. Nat Rev Immunol, 2004. **4**(3): p. 181-9.

40. Ago, T., et al., *Nox4 as the major catalytic component of an endothelial NAD(P)H oxidase*. *Circulation*, 2004. **109**(2): p. 227-33.
41. Sorescu, G.P., et al., *Bone morphogenic protein 4 produced in endothelial cells by oscillatory shear stress induces monocyte adhesion by stimulating reactive oxygen species production from a nox1-based NADPH oxidase*. *Circ Res*, 2004. **95**(8): p. 773-9.
42. Ago, T., et al., *NAD(P)H oxidases in rat basilar arterial endothelial cells*. *Stroke*, 2005. **36**(5): p. 1040-6.
43. Paffenholz, R., et al., *Vestibular defects in head-tilt mice result from mutations in Nox3, encoding an NADPH oxidase*. *Genes Dev*, 2004. **18**(5): p. 486-91.
44. Banfi, B., et al., *Mechanism of Ca<sup>2+</sup> activation of the NADPH oxidase 5 (NOX5)*. *J Biol Chem*, 2004. **279**(18): p. 18583-91.
45. Banfi, B., et al., *A Ca(2+)-activated NADPH oxidase in testis, spleen, and lymph nodes*. *J Biol Chem*, 2001. **276**(40): p. 37594-601.
46. De Deken, X., et al., *Cloning of two human thyroid cDNAs encoding new members of the NADPH oxidase family*. *J Biol Chem*, 2000. **275**(30): p. 23227-33.
47. Banfi, B., et al., *Two novel proteins activate superoxide generation by the NADPH oxidase NOX1*. *J Biol Chem*, 2003. **278**(6): p. 3510-3.
48. Brar, S.S., et al., *An NAD(P)H oxidase regulates growth and transcription in melanoma cells*. *Am J Physiol Cell Physiol*, 2002. **282**(6): p. C1212-24.
49. Kamiguti, A.S., et al., *Expression and activity of NOX5 in the circulating malignant B cells of hairy cell leukemia*. *J Immunol*, 2005. **175**(12): p. 8424-30.
50. Salles, N., et al., *Expression of mRNA for ROS-generating NADPH oxidases in the aging stomach*. *Exp Gerontol*, 2005. **40**(4): p. 353-7.
51. Cucoranu, I., et al., *NAD(P)H oxidase 4 mediates transforming growth factor-beta1-induced differentiation of cardiac fibroblasts into myofibroblasts*. *Circ Res*, 2005. **97**(9): p. 900-7.
52. Rachida S. Belaiba, T.D., Andreas Petry, Kerstin Diemer, Steve Bonello, Botond Banfi, John Hess, Alexej Pogrebniak, Christian Bickel and Agnes Görlach, *NOX5 variants are functionally active in endothelial cells*. *Free Radical Biology and Medicine*, 2006. **In Press**.
53. Belaiba, R.S., et al., *NOX5 variants are functionally active in endothelial cells*. *Free Radic Biol Med*, 2007. **42**(4): p. 446-59.
54. Van Buul, J.D., et al., *Expression and localization of NOX2 and NOX4 in primary human endothelial cells*. *Antioxid Redox Signal*, 2005. **7**(3-4): p. 308-17.
55. Pedruzzi, E., et al., *NAD(P)H oxidase Nox-4 mediates 7-ketocholesterol-induced endoplasmic reticulum stress and apoptosis in human aortic smooth muscle cells*. *Mol Cell Biol*, 2004. **24**(24): p. 10703-17.
56. Janiszewski, M., et al., *Regulation of NAD(P)H oxidase by associated protein disulfide isomerase in vascular smooth muscle cells*. *J Biol Chem*, 2005.
57. Wilkinson, B. and H.F. Gilbert, *Protein disulfide isomerase*. *Biochim Biophys Acta*, 2004. **1699**(1-2): p. 35-44.
58. Clissold, P.M. and R. Bicknell, *The thioredoxin-like fold: hidden domains in protein disulfide isomerases and other chaperone proteins*. *Bioessays*, 2003. **25**(6): p. 603-11.
59. Bedard, K. and K.H. Krause, *The NOX family of ROS-generating NADPH oxidases: physiology and pathophysiology*. *Physiol Rev*, 2007. **87**(1): p. 245-313.
60. Peng, T., X. Lu, and Q. Feng, *Pivotal role of gp91phox-containing NADH oxidase in lipopolysaccharide-induced tumor necrosis factor-alpha expression and myocardial depression*. *Circulation*, 2005. **111**(13): p. 1637-44.

61. Marciniak, S.J. and D. Ron, *Endoplasmic reticulum stress signaling in disease*. *Physiol Rev*, 2006. **86**(4): p. 1133-49.
62. Liu, C.Y. and R.J. Kaufman, *The unfolded protein response*. *J Cell Sci*, 2003. **116**(Pt 10): p. 1861-2.
63. Ron, D. and P. Walter, *Signal integration in the endoplasmic reticulum unfolded protein response*. *Nat Rev Mol Cell Biol*, 2007. **8**(7): p. 519-29.
64. Shuman, S., *Recombination mediated by vaccinia virus DNA topoisomerase I in Escherichia coli is sequence specific*. *Proc Natl Acad Sci U S A*, 1991. **88**(22): p. 10104-8.
65. Shuman, S., *Site-specific interaction of vaccinia virus topoisomerase I with duplex DNA. Minimal DNA substrate for strand cleavage in vitro*. *J Biol Chem*, 1991. **266**(30): p. 20576-7.
66. Shuman, S., *Site-specific interaction of vaccinia virus topoisomerase I with duplex DNA. Minimal DNA substrate for strand cleavage in vitro*. *J Biol Chem*, 1991. **266**(17): p. 11372-9.
67. Shuman, S., *Site-specific DNA cleavage by vaccinia virus DNA topoisomerase I. Role of nucleotide sequence and DNA secondary structure*. *J Biol Chem*, 1991. **266**(3): p. 1796-803.
68. Shuman, S., *Novel approach to molecular cloning and polynucleotide synthesis using vaccinia DNA topoisomerase*. *J Biol Chem*, 1994. **269**(51): p. 32678-84.
69. Edgell, C.J., C.C. McDonald, and J.B. Graham, *Permanent cell line expressing human factor VIII-related antigen established by hybridization*. *Proc Natl Acad Sci U S A*, 1983. **80**(12): p. 3734-7.
70. Ades, E.W., et al., *HMEC-1: establishment of an immortalized human microvascular endothelial cell line*. *J Invest Dermatol*, 1992. **99**(6): p. 683-90.
71. Sambrook, J., *Molecular Cloning: A Laboratory Manual, Third Edition*. 2001: Cold Spring Harbor Laboratory Press.
72. Djordjevic, T., et al., *The expression of the NADPH oxidase subunit p22phox is regulated by a redox-sensitive pathway in endothelial cells*. *Free Radic Biol Med*, 2005. **38**(5): p. 616-30.
73. Barry, D.M., et al., *Differential expression of voltage-gated K<sup>+</sup> channel subunits in adult rat heart. Relation to functional K<sup>+</sup> channels?* *Circ Res*, 1995. **77**(2): p. 361-9.
74. Bradford, M.M., *A rapid and sensitive method for the quantitation of microgram quantities of protein utilizing the principle of protein-dye binding*. *Anal Biochem*, 1976. **72**: p. 248-54.
75. Cheng, G., et al., *Homologs of gp91phox: cloning and tissue expression of Nox3, Nox4, and Nox5*. *Gene*, 2001. **269**(1-2): p. 131-40.
76. Hu, C.D. and T.K. Kerppola, *Simultaneous visualization of multiple protein interactions in living cells using multicolor fluorescence complementation analysis*. *Nat Biotechnol*, 2003. **21**(5): p. 539-45.
77. Hu, C.D., Y. Chinenov, and T.K. Kerppola, *Visualization of interactions among bZIP and Rel family proteins in living cells using bimolecular fluorescence complementation*. *Mol Cell*, 2002. **9**(4): p. 789-98.
78. Herkert, O., et al., *NADPH oxidase mediates tissue factor-dependent surface procoagulant activity by thrombin in human vascular smooth muscle cells*. *Circulation*, 2002. **105**(17): p. 2030-6.

79. Gorlach, A., et al., *A gp91phox containing NADPH oxidase selectively expressed in endothelial cells is a major source of oxygen radical generation in the arterial wall.* *Circ Res*, 2000. **87**(1): p. 26-32.
80. Diebold, I., et al., *Phosphodiesterase 2 mediates redox-sensitive endothelial cell proliferation and angiogenesis by thrombin via Rac1 and NADPH oxidase 2.* *Circ Res*, 2009. **104**(10): p. 1169-77.
81. Ikeda, S., et al., *IQGAP1 Regulates Reactive Oxygen Species-Dependent Endothelial Cell Migration Through Interacting With Nox2.* *Arterioscler Thromb Vasc Biol*, 2005.
82. Basuroy, S., et al., *Nox4 NADPH oxidase mediates oxidative stress and apoptosis caused by TNF-alpha in cerebral vascular endothelial cells.* *Am J Physiol Cell Physiol*, 2009. **296**(3): p. C422-32.
83. Yoshida, L.S. and S. Tsunawaki, *Expression of NADPH oxidases and enhanced H(2)O(2)-generating activity in human coronary artery endothelial cells upon induction with tumor necrosis factor-alpha.* *Int Immunopharmacol*, 2008. **8**(10): p. 1377-85.
84. Furst, R., et al., *Atrial natriuretic peptide induces mitogen-activated protein kinase phosphatase-1 in human endothelial cells via Rac1 and NAD(P)H oxidase/Nox2-activation.* *Circ Res*, 2005. **96**(1): p. 43-53.
85. Newburger, P.E., Q. Dai, and C. Whitney, *In vitro regulation of human phagocyte cytochrome b heavy and light chain gene expression by bacterial lipopolysaccharide and recombinant human cytokines.* *J Biol Chem*, 1991. **266**(24): p. 16171-7.
86. Fu, X., et al., *cAMP-response element-binding protein mediates acid-induced NADPH oxidase NOX5-S expression in Barrett esophageal adenocarcinoma cells.* *J Biol Chem*, 2006. **281**(29): p. 20368-82.
87. Si, J., et al., *NADPH oxidase NOX5-S mediates acid-induced cyclooxygenase-2 expression via activation of NF-kappaB in Barrett's esophageal adenocarcinoma cells.* *J Biol Chem*, 2007. **282**(22): p. 16244-55.
88. Si, J., et al., *STAT5 mediates PAF-induced NADPH oxidase NOX5-S expression in Barrett's esophageal adenocarcinoma cells.* *Am J Physiol Gastrointest Liver Physiol*, 2008. **294**(1): p. G174-83.
89. Kobayashi, S., et al., *Nox1 regulates apoptosis and potentially stimulates branching morphogenesis in sinusoidal endothelial cells.* *Exp Cell Res*, 2004. **300**(2): p. 455-62.
90. Takeya, R., et al., *Novel human homologues of p47phox and p67phox participate in activation of superoxide-producing NADPH oxidases.* *J Biol Chem*, 2003. **278**(27): p. 25234-46.
91. Carmel, I., et al., *Comparative analysis detects dependencies among the 5' splice-site positions.* *Rna*, 2004. **10**(5): p. 828-40.
92. Ueyama, T., et al., *Subcellular localization and function of alternatively spliced Noxo1 isoforms.* *Free Radic Biol Med*, 2007. **42**(2): p. 180-90.
93. Takeya, R., et al., *Expression and function of Noxo1gamma, an alternative splicing form of the NADPH oxidase organizer 1.* *Febs J*, 2006. **273**(16): p. 3663-77.
94. Valente, A.J., et al., *NOX1 NADPH oxidase regulation by the NOXA1 SH3 domain.* *Free Radic Biol Med*, 2007. **43**(3): p. 384-96.
95. Hilenski, L.L., et al., *Distinct subcellular localizations of Nox1 and Nox4 in vascular smooth muscle cells.* *Arterioscler Thromb Vasc Biol*, 2004. **24**(4): p. 677-83.
96. Ambasta, R.K., et al., *Direct interaction of the novel Nox proteins with p22phox is required for the formation of a functionally active NADPH oxidase.* *J Biol Chem*, 2004. **279**(44): p. 45935-41.

97. Chen, K., S.E. Craige, and J. Keane, *Downstream Targets and Intracellular Compartmentalization in Nox Signaling*. Antioxid Redox Signal, 2009.
98. Kuroda, J., et al., *The superoxide-producing NAD(P)H oxidase Nox4 in the nucleus of human vascular endothelial cells*. Genes Cells, 2005. **10**(12): p. 1139-51.
99. Pendergrass, K.D., et al., *The angiotensin II-AT1 receptor stimulates reactive oxygen species within the cell nucleus*. Biochem Biophys Res Commun, 2009. **384**(2): p. 149-54.
100. Xiao, Q., et al., *Embryonic stem cell differentiation into smooth muscle cells is mediated by Nox4-produced H<sub>2</sub>O<sub>2</sub>*. Am J Physiol Cell Physiol, 2009. **296**(4): p. C711-23.
101. Calafat, J., et al., *Evidence for small intracellular vesicles in human blood phagocytes containing cytochrome b558 and the adhesion molecule CD11b/CD18*. Blood, 1993. **81**(11): p. 3122-9.
102. Kawahara, T., et al., *Point mutations in the proline-rich region of p22phox are dominant inhibitors of Nox1- and Nox2-dependent reactive oxygen generation*. J Biol Chem, 2005. **280**(36): p. 31859-69.
103. Yamagishi, S., et al., *Pigment epithelium-derived factor (PEDF) blocks angiotensin II signaling in endothelial cells via suppression of NADPH oxidase: a novel anti-oxidative mechanism of PEDF*. Cell Tissue Res, 2005. **320**(3): p. 437-45.
104. Ushio-Fukai, M., et al., *Novel role of gp91(phox)-containing NAD(P)H oxidase in vascular endothelial growth factor-induced signaling and angiogenesis*. Circ Res, 2002. **91**(12): p. 1160-7.
105. Martyn, K.D., et al., *Functional analysis of Nox4 reveals unique characteristics compared to other NADPH oxidases*. Cell Signal, 2006. **18**(1): p. 69-82.
106. Shiose, A., et al., *A novel superoxide-producing NAD(P)H oxidase in kidney*. J Biol Chem, 2001. **276**(2): p. 1417-23.
107. Djordjevic, T., et al., *Human urotensin II is a novel activator of NADPH oxidase in human pulmonary artery smooth muscle cells*. Arterioscler Thromb Vasc Biol, 2005. **25**(3): p. 519-25.
108. Vaquero, E.C., et al., *Reactive oxygen species produced by NAD(P)H oxidase inhibit apoptosis in pancreatic cancer cells*. J Biol Chem, 2004. **279**(33): p. 34643-54.
109. Datla, S.R., et al., *Important role of Nox4 type NADPH oxidase in angiogenic responses in human microvascular endothelial cells in vitro*. Arterioscler Thromb Vasc Biol, 2007. **27**(11): p. 2319-24.
110. Adachi, T., et al., *NAD(P)H oxidase plays a crucial role in PDGF-induced proliferation of hepatic stellate cells*. Hepatology, 2005. **41**(6): p. 1272-81.
111. Holland, J.A., et al., *Thrombin stimulated reactive oxygen species production in cultured human endothelial cells*. Endothelium, 1998. **6**(2): p. 113-21.
112. Cook-Mills, J.M., et al., *Calcium mobilization and Rac1 activation are required for VCAM-1 (vascular cell adhesion molecule-1) stimulation of NADPH oxidase activity*. Biochem J, 2004. **378**(Pt 2): p. 539-47.
113. Bogatcheva, N.V., J.G. Garcia, and A.D. Verin, *Molecular mechanisms of thrombin-induced endothelial cell permeability*. Biochemistry (Mosc), 2002. **67**(1): p. 75-84.
114. Fernandes, D.C., et al., *Protein disulfide isomerase overexpression in vascular smooth muscle cells induces spontaneous preemptive NADPH oxidase activation and Nox1 mRNA expression: effects of nitrosothiol exposure*. Arch Biochem Biophys, 2009. **484**(2): p. 197-204.

115. Santos, C.X., et al., *Protein disulfide isomerase (PDI) associates with NADPH oxidase and is required for phagocytosis of Leishmania chagasi promastigotes by macrophages*. J Leukoc Biol, 2009.
116. Lassegue, B. and R.E. Clempus, *Vascular NAD(P)H oxidases: specific features, expression, and regulation*. Am J Physiol Regul Integr Comp Physiol, 2003. **285**(2): p. R277-97.
117. Sitia, R. and I. Braakman, *Quality control in the endoplasmic reticulum protein factory*. Nature, 2003. **426**(6968): p. 891-4.
118. Malhotra, J.D. and R.J. Kaufman, *Endoplasmic reticulum stress and oxidative stress: a vicious cycle or a double-edged sword?* Antioxid Redox Signal, 2007. **9**(12): p. 2277-93.
119. Harding, H.P., et al., *An integrated stress response regulates amino acid metabolism and resistance to oxidative stress*. Mol Cell, 2003. **11**(3): p. 619-33.
120. Sevier, C.S., et al., *Modulation of cellular disulfide-bond formation and the ER redox environment by feedback regulation of Ero1*. Cell, 2007. **129**(2): p. 333-44.
121. Manea, A., et al., *Regulation of NADPH oxidase subunit p22(phox) by NF-kB in human aortic smooth muscle cells*. Arch Physiol Biochem, 2007. **113**(4-5): p. 163-72.
122. Manea, A., et al., *AP-1-dependent transcriptional regulation of NADPH oxidase in human aortic smooth muscle cells: role of p22phox subunit*. Arterioscler Thromb Vasc Biol, 2008. **28**(5): p. 878-85.
123. Kim, R., et al., *Role of the unfolded protein response in cell death*. Apoptosis, 2006. **11**(1): p. 5-13.
124. Kaneko, M., Y. Niinuma, and Y. Nomura, *Activation signal of nuclear factor-kappa B in response to endoplasmic reticulum stress is transduced via IRE1 and tumor necrosis factor receptor-associated factor 2*. Biol Pharm Bull, 2003. **26**(7): p. 931-5.
125. Hu, P., et al., *Autocrine tumor necrosis factor alpha links endoplasmic reticulum stress to the membrane death receptor pathway through IRE1alpha-mediated NF-kappaB activation and down-regulation of TRAF2 expression*. Mol Cell Biol, 2006. **26**(8): p. 3071-84.
126. O'Loughlen, A., et al., *Reversible inhibition of the protein phosphatase 1 by hydrogen peroxide. Potential regulation of eIF2 alpha phosphorylation in differentiated PC12 cells*. Arch Biochem Biophys, 2003. **417**(2): p. 194-202.
127. Chen, K., et al., *Regulation of ROS signal transduction by NADPH oxidase 4 localization*. J Cell Biol, 2008. **181**(7): p. 1129-39.
128. Gu, F., et al., *Protein-tyrosine phosphatase 1B potentiates IRE1 signaling during endoplasmic reticulum stress*. J Biol Chem, 2004. **279**(48): p. 49689-93.

## 7 Appendix

### 7.1 Abbreviations

Akt	protein kinase B (PKB)
AngII	angiotensin II
ARNT	arylhydrocarbon receptor nuclear translocator
ATF4	activating transcription factor 4
ATF6	activating transcription factor 6
BAPTA	1,2-bis(o-aminophenoxy)ethane-N,N,N',N'-tetraacetic acid
BiFC	bimolecular fluorescence complementation
BiP	binding protein
BrdU	5-bromo-2'-deoxyuridine
BSA	bovine serum albumin
Ca <sup>2+</sup>	calcium
CaCo2	carcinom Colon 2
CFP	cyan fluorescent protein
CGD	chronic granumaltous disease
CHOP	C/EBP-homologous protein
DAB	Diaminobenzidine
DCF	5-(and-6)-chloromethyl-2',7'-dichlorodihydrofluorescein diacetate (H2DCFDA)
DEPC	diethylpyrocarbonate
DHE	dihydroethidium
DMEM	Dulbecco's modified Eagle medium
DMSO	dimethylsulfoxide

DTT	dithiothreitol
DUOX	dual oxidase
Ea.Hy926	endothelial alike hybridoma 926
EC	endothelial cells
ECAM	endothelial cellular adhesion molecules
eIF2 $\alpha$	eukariotic initiation factor 2 $\alpha$
eNOS	endothelial nitric oxide synthase
EPO	erythropoietin
ER	endoplasmic reticulum
ERK	p41/42 extracellular signal regulated kinase
ET-1	endothelin 1
ETA	endothelin receptor A
ETB	endothelin receptor B
GAPs	GTPase activating proteins
GDIs	guanine nucleotide exchange inhibitors
GEFs	guanine nucleotide exchange factors
GFP	green fluorescence protein
GPR	G protein-coupled receptors
GPx	glutathion peroxidase
GTT	guanidinethiocyanate
h	hours
H <sub>2</sub> O <sub>2</sub>	hydrogenperoxide
HAT	hypoxanthine, aminopterin, thymidin
HBSS	Hank's balanced salt solution
HEK293	human embryonic kidney 293 cells
HIF-1	hypoxia inducible factor-1

HMEC	human microvascular endothelial cells
HRE	hypoxia-responsive elements
hU-II	human urotensin-II
HUVEC	human umbilical vein endothelial cells
ICAM-1	intercellular adhesion molecule
IGF-1	insulin-like growth factor
IL1- $\alpha$	interleukin-1 $\alpha$
IRE1	inositol requiring element 1
JNK	c-jun N-terminal kinase
LDL	low density lipoprotein
L-NAME	N- $\omega$ -nitro-L-arginine methyl ester
LPS	lipopolysaccharides
MAPK	mitogen activated protein kinases
MEK1	mitogen activated protein kinase kinase 1
MF	microsomal fraction
min	minutes
MOPS	3-(N-morpholino)propanesulfonic acid
mRNA	messenger RNA
NAC	N-acetyl-cysteine
NADPH	Nicotinamide adenine dinucleotide phosphate
NO	nitric oxide
NOX1-5	NADPH oxidase 1 - 5
NOXA1	NADPH oxidase activator 1
NOXO1	NADPH oxidase organizer 1
O <sub>2</sub> <sup>-•</sup>	superoxide anion radical
OH <sup>•</sup>	hydroxyl radicals

ONOO-	peroxynitrite
oxLDL	oxidated low density lipoprotein
PAF	platelet activation factor
PAGE	polyacrylamide gel electrophoresis
PASMC	pulmonary arterial smooth muscle cells
PBS	phosphate-buffered saline
PCR	Polymerase chain reaction
PDGF	platelet derived growth factor
PDI	protein disulfide isomerase
PERK	PKRC endoplasmatic reticulum kinase
PGI <sub>2</sub>	prostaglandin I <sub>2</sub> or prostacyclin
PH	pulmonary hypertension
-phox	phagocytic oxidase
PI3K	phosphatidyl-inositol-(3) kinase
PKB	protein kinase B
PMN	polymorphonuclear leukocytes
PP1	protein phosphatase 1
PTP1B	protein tyrosine phosphatase 1 B
qPCR	quantitative PCR
RH123	rhodamine123
ROS	reactive oxygen species
RT-PCR	reverse transcription polymerase chain reaction
SDS	Sodium dodecyl sulfate
SDS-PAGE	Sodium dodecyl sulfate polyacrylamide gel electrophoresis
siCtr	nonspecific siRNA
siRNA	small interfering RNA

SOD	superoxide dismutase
TCL	total cell lysate
TEMED	Tetramethylethylenediamine
TF	tissue factor
TGF- $\beta$	transforming growth factor $\beta$
TMB	tetramethyl-benzidine
TNF $\alpha$	tumor necrosis factor $\alpha$
Tris	tris(hydroxymethyl)aminomethane
UPR	unfolded protein response
VEGF	vascular endothelial growth factor
VSMC	vascular smooth muscle cells
XBP1	X-box binding protein 1
YFP	yellow fluorescent protein

## 7.2 List of figures

Fig. 1	Schematic overview about the progression of atherosclerosis.	3
Fig. 2	Reactive oxygen and reactive nitrogen species in vascular cells.	5
Fig. 3	Schematic overview of the structure and activation of the phagocytic NADPH oxidase.	6
Fig. 4	Schematic overview of the NOX homologues NOX1 to NOX5.	8
Fig. 5	Schematic overview of NOXO1 and NOXA1 in comparison with their homologues p47phox and p67phox.	9
Fig. 6	Schematic overview of the unfolded protein response (UPR).	10
Fig. 7	Activation of ATF4 and XBP1 by unfolded protein response.	11
Fig. 8	Luciferase reporter plasmid maps.	24
Fig. 9	Principle of gene silencing using the siStrike system.	25
Fig. 10	Schematic overview over the TOPO cloning principle.	30
Fig. 11	Structure of 5-(and-6)- chloromethyl-2',7'- dichlorodihydrofluorescein diacetate, acetyl ester (CM-H2DCFDA).	45
Fig. 12	Structure of the dihydroethidium.	46
Fig. 13	Schematic overview of the working principle of the polymerase chain reaction (PCR).	56
Fig. 14	NOX1, NOX2, NOX4 and p22phox mRNA and protein are expressed in endothelial cells.	70
Fig. 15	Different NOX5 splice variants are expressed in endothelial cells.	71
Fig. 16	Different NOX5 proteins are expressed in endothelial cells.	73
Fig. 17	p22phox and NOX5 are expressed in the vessel wall.	74
Fig. 18	NOXA1 mRNA is expressed in endothelial cells and HEPG2 cells.	75
Fig. 19	NOXO1 mRNA is expressed in endothelial cells and HEPG2 cells.	76

- Fig. 20 NOX2 and NOX4 colocalize in an intracellular compartment in endothelial cells, but only NOX2 colocalizes with f-actin. 78
- Fig. 21 NOX2, NOX4 but not NOX1 are intracellularly localized in endothelial cells. 79
- Fig. 22 p22phox, NOX2 and NOX4 are expressed in the endoplasmic reticulum of endothelial cells. 80
- Fig. 23 p22phox, but not NOX2 and NOX4 are localized in the endoplasmic reticulum of cervix carcinoma cells. 81
- Fig. 24 NOX5 variants are expressed in an ER like compartment in endothelial cells. 82
- Fig. 25 Bimolecular fluorescence studies show an interaction between NOX2, NOX4, NOX5S or NOX5 $\beta$  and p22phox. 83
- Fig. 26 p22phox coimmunoprecipitates with NOX2, NOX4, NOX5S and NOX5 $\beta$ . 85
- Fig. 27 p22phox, NOX2, NOX4 and NOX5 are downregulated by specific siRNA. 86
- Fig. 28 p22phox, NOX2, NOX4 and NOX5 modulate ROS generation of endothelial cells. 87
- Fig. 29 p22phox is not required for NOX5S- or NOX5 $\beta$ -mediated intracellular ROS production in endothelial cells. 88
- Fig. 30 Calcium increases NOX5 dependent ROS generation in endothelial cells. 89
- Fig. 31 p22phox, NOX2, NOX4 and NOX5 modulate the proliferation of endothelial cells. 90
- Fig. 32 The p38 MAP kinase contributes to the proliferative response mediated by NOX2 and NOX4. 91
- Fig. 33 NOX1 does not contribute to basal ROS generation and proliferation of endothelial cells. 92
- Fig. 34 NOX2 and NOX5 are regulated by thrombin in endothelial cells. 94

Fig. 35	NOX2 and NOX5 mediates thrombin-induced ROS generation in endothelial cells.	95
Fig. 36	NOX2 and NOX5 mediates thrombin induced proliferation and tube formation in endothelial cells.	96
Fig. 37	Protein disulfide isomerase is associated with NOX4 and increased ROS generation in endothelial cells.	97
Fig. 38	ER-stress induces ROS generation via p22phox in endothelial cells.	98
Fig. 39	ER-stress increases p22phox mRNA and protein levels in endothelial cells.	99
Fig. 40	Thapsigargin induces XBP1 and ATF4 activation in endothelial cells.	100
Fig. 41	ATF4 and XBP1 mediates ROS generation under thapsigargin stimulation in endothelial cells.	101
Fig. 42	ATF4 and XBP1 mediates p22phox expression under thapsigargin stimulation in endothelial cells.	102
Fig. 43	ER-stress and ATF4 activates p22phox promoter in endothelial cells.	103
Fig. 44	ER-stress activates a p22phox enhancer element via ATF4 and XBP1 in endothelial cells	104

## 7.3 Curriculum vitae

### Persönliche Daten

Name	Andreas Petry
Geburtsdatum	06. Dezember 1978
Geburtsort	Berlin
Staatsangehörigkeit	deutsch
Familienstand	ledig

### Hochschule

2004-2009	Dissertation zum Dr. rer. nat. am Lehrstuhl für Pharmazeutische Biologie an der Ludwig-Maximilians-Universität München, unter der Betreuung von Frau Prof. Dr. Angelika Vollmar, in der Experimentellen Kinderkardiologie bei Frau Prof. Dr. Agnes Görlach am Deutschen Herzzentrum München des Freistaates Bayern, Klinik an der Technischen Universität München
2002-2003	Diplomarbeit im Fach Genetik am Chemotherapeutischen Forschungsinstitut Georg-Speyer-Haus, Frankfurt am Main
09/2002	Diplomprüfung Biologie
09/2000	Vordiplomprüfung Biologie
1998-2003	Studium der Biologie an der Johann Wolfgang Goethe-Universität Frankfurt am Main

1998-2003                      Studium der Informatik an der Johann Wolfgang  
Goethe-Universität Frankfurt am Main

### **Schule**

1989-1998                      Gymnasium Bischof-Neumann-Schule, Königstein im  
Taunus, Abschluss: Allgemeine Hochschulreife

1985-1989                      Grundschule Max-von-Gagernschule, Kelkheim am  
Taunus

### **Berufsausbildung und Tätigkeiten**

seit 09/2003                      wissenschaftlicher Mitarbeiter in der Experimentellen  
Kinderkardiologie bei Frau PD Dr. Agnes Görlach am  
Deutschen Herzzentrum München des Freistaates  
Bayern, Klinik an der Technischen Universität  
München

### **Auszeichnungen und Förderungen**

2009                              Reisestipendium der GlaxoSmithKline Stiftung für „88<sup>th</sup>  
Annual Meeting of the German Physiological Society  
2009“, Gießen, 22.03.2009 – 25.03.2009

2008                              Reisestipendium der GlaxoSmithKline Stiftung für  
“Annual Meeting of the Society for Microcirculation &  
Vascular Biology (GfMVB) 2008“, Aachen, 25.09.2008  
– 27.09.2008

2006-2007                      Stipendiat im Graduiertenkolleg 438 „Vaskuläre  
Biologie in der Medizin“

- 03/2006 Finalist bei der "YOUNG FEPS poster award session" auf dem "Joint Meeting of The German Physiologic Society and The European Federation of Physiologic Societies 2006" in München. Titel der Posterpräsentation: "Multiple NOX proteins mediate the proliferative response in endothelial cells".  
Publiziert in: Journal of Vascular Research 2006;43: 571-571
- 2005 Reisestipendium der GlaxosmithKline Stiftung für „3<sup>rd</sup> European Meeting on Vascular Biology and Medicine 2005", Hamburg, Germany, 28.09.2005 – 30.09.2005
- 2004-2005 Stipendiat im Graduiertenkolleg 438 "Vaskuläre Biologie in der Medizin"
- 2004-2007 Kollegiat im Graduiertenkolleg 438 "Vaskuläre Biologie in der Medizin"
- 2004 Reisestipendium der GlaxoSmithKline Stiftung für "American Heart Association - Scientific Sessions 2004", New Orleans, LA, 07.11.2004 – 10.11.2004
- 09/2000 Vorgeschlagen als Stipendiant zur Förderung durch die „Studienstiftung des deutschen Volkes“ aufgrund der erbrachten Leistungen in der Vordiplomprüfung Biologie

## 7.4 Publications

### Manuscripts

Petry A, Djordjevic T, Weitnauer M, Kietzmann T, Hess J, Görlach A. NOX2 and NOX4 mediate proliferative response in endothelial cells. *Antioxidants & Redox Signaling*, 8:1473-1484, 2006

BelAiba RS\*, Djordjevic T\*, Petry A\*, Diemer K, Bonello S, Banfi B, Hess J, Pogrebniak A, Bickel C, Görlach A. NOX5 variants are functionally active in endothelial cells. *Free Radical Biology & Medicine*, 42:446-459, 2007, \*contributed equally to this manuscript.

Diebold I, Djordjevic T, Petry A, Hatzelmann A, Tenor H, Hess J, Görlach A. Phosphodiesterase 2 mediates redox-sensitive endothelial cell proliferation and angiogenesis by thrombin via Rac1 and NADPH oxidase 2. *Circulation Research*, 104:1169-1177, 2009

### Published Abstracts

Djordjevic T, BelAiba R, Diebold I, Bonello S, Petry A, Bickel C, Kietzmann T, Hess J, Görlach A: Rac controls the expression of the HIF target gene PAI-1 in response to thrombin in vascular cells. *Pflugers Archiv-European Journal of Physiology*, 447:S69, 2004

Bickel C, Pogrebniak A, Diemer K, Bonello S, Petry A, BelAiba R, Acker H, Hess J, Görlach A: Human vascular cells express a distinct NOX5 isoform: Role in the generation of reactive oxygen species and the proliferative response. *Cardiology in the Young*, 14:50, 2004

Bickel C, Petry A, Djordjevic T, Diemer K, Pogrebniak A, Bonello S, BelAiba RS, Hess J, Acker H, Görlach A: Human vascular cells express a distinct NOX5 isoform: Role in the generation of reactive oxygen species and the proliferative responses. *Circulation*, 110; III-157, 2004

Djordjevic T, Petry A, Bickel C, Bonello S, BelAiba RS, Hess J, Acker H, Pfeilschifter J, Görlach A: Interaction of p22phox with NOX2 or NOX4 results in ROS production and proliferation of endothelial cells. *Circulation*, 110:III-284, 2004

Bonello S, Petry A, Belaiba RS, Zaehring C, Hess J, Djordjevic T, Görlach A: Human HIF-3 $\alpha$  is an inhibitor of the HIF pathway in endothelial cells. *Circulation*, 110:III-214, 2004

Petry A, Djordjevic T, Bickel C, Bonello S, BelAiba RS, Pfeilschifter J, Hess J, Görlach A. Interaction of p22phox with NOX2 or NOX4 results in ROS production and proliferation of endothelial cells. *Pflugers Archiv-European Journal of Physiology*, 449, S1, S26, 2005

Bickel C, Petry A, Djordjevic T, Diemer K, Pogrebniak A, Bonello S, BelAiba RS, Acker H, Hess J, Görlach A. Endothelial cells express a distinct, functionally active NOX5 isoform. *Pflugers Archiv-European Journal of Physiology*, 449, S1, S26, 2005

Bonello S, Petry A, BelAiba RS, Djordjevic T, Zähringer C, Hess J, Görlach A. HIF3 $\alpha$  inhibits the hypoxic response in vascular cells. *Pflugers Archiv-European Journal of Physiology*, 449, S1, S40, 2005

Petry A, Djordjevic T, Bickel C, Bonello S, BelAiba RS, Pfeilschifter J, Hess J, Görlach A: Reactive oxygen species upregulate NOX4, but not NOX2, in endothelial cells. *Journal of Vascular Research*, 42/S2, 2005

Görlach A, Bickel C, Petry A, Djordjevic T, BelAiba RS, Diemer K, Bonello S, Acker H, Pogrebniak A, Hess J. A NOX5 isoform is functionally active in human endothelial cells". *Journal of Vascular Research* 42, II/39, 2005

Bonello S, Petry A, Belaiba RS, Zaehring C, Djordjevic T, Hess J, Görlach A. Human HIF-3 $\alpha$  is a novel inhibitor of angiogenesis. *Journal of Vascular Research* 42, II/46, 2005

Petry A, Djordjevic T, Weitnauer M, BelAiba RS, Hess J, Görlach A. Multiple NOX proteins mediate the proliferative response in endothelial cells. *Acta Physiologica*, 86, 1, 141, 2006

Djordjevic T, Petry A, Weitnauer M, BelAiba RS, Hess J, Görlach A. Endothelial proliferation is mediated by multiple NOX proteins. *Cardiology in the Young*, 16/2,32, 2006

Petry A, Djordjevic T, Weitnauer M, BelAiba RS, Diemer K, Hess J, Görlach A. Multiple NOX Proteins Mediate the Proliferative Response in Endothelial Cells. *J Vasc Res* 43:533-580, 2006

Bonello S, BelAiba R, Petry A, Djordjevic T, Zähringer C, Görlach A. HIF3  $\alpha$  is a negative modulator of the hypoxic response in endothelial cells. *J Vasc Res* 43(1):49-50, 2006

Djordjevic T, Petry A, BelAiba RS, Hess J, Görlach A. Urotensin-II stimulates NOX2- and NOX4-dependent angiogenesis. *Acta Physiologica*, 191, 2007

Diebold I, Petry A, Burger M, Djordjevic T, Hess J, Görlach A. FoxO3 Mediates Urotensin-II-induced MMP2 Expression In Pulmonary Artery Smooth Muscle Cells. *Circulation*, 116: II\_109, 2007

Djordjevic T, Petry A, Schäfer N, Weitnauer M, Hess J, Görlach A. Urotensin-II activates Rac and ROS production in pulmonary artery smooth muscle cells involving GPR14 and Gai proteins. *Circulation*, 116: II, 2007

Diebold I, Petry A, Burger M, Hess J, Görlach A. FoxO3 mediates MMP-2 expression by urotensin-II. *Acta Physiol*, 192, S663, 2008

Diebold I, Petry A, Burger M, Hess J, Görlach A. FoxO3 regulates urotensin-II induced MMP2 expression in pulmonary artery smooth muscle cells. *European Heart Journal*, 29, 235, 2008.

Diebold I, Petry A, Weitnauer M, Hess J, Görlach A. Urotensin-II activates Rac1 and ROS production in pulmonary artery smooth muscle cells involving Gai proteins. *Cardiology in the young*, 18 (1):20.2008.

Diebold I, Petry A, Burger M, Hess J, Görlach A. FoxO3 mediates urotensin-II-induced matrix metalloproteinase-2 (MMP-2) in pulmonary vascular smooth muscle cells, *Cardiology in the young*, 18(1), 2008

Diebold I, Djordjevic T, Petry A, Hatzelmann A, Tenor, H, Hess J, Görlach A. PDE2 mediates redox-sensitive endothelial cell proliferation and angiogenesis by thrombin via Rac1 and NOX2 *Acta Physiol*, 193, 2009

Petry A, Diebold I, Schäfer N, Hess J, Görlach A. Thrombin activates NOX1 involving G $\alpha_i$  and Rac1 in pulmonary artery smooth muscle cells *Acta Physiol*, 193, 2009

## Presentations at international conferences

### Oral communications

Petry A, Djordjevic T, Bickel C, Bonello S, BelAiba RS, Pfeilschifter J, Hess J, Görlach A. Interaction of p22phox with NOX2 or NOX4 results in ROS production and proliferation of endothelial cells. 84th Annual Meeting of the German Physiological Society, Göttingen, 06.03-09.03.05.

Petry A, Djordjevic T, Bickel C, Bonello S, BelAiba RS, Pfeilschifter J, Hess J, Görlach A. Interaction of p22phox with NOX2 or NOX4. Graduiertenkollegs "Vascular Biology in Medicine", Herrsching a. Ammersee, 12.03. – 13.03.05.

Petry A, Djordjevic T, Bickel C, Bonello S, BelAiba RS, Pfeilschifter J, Hess J, Görlach A. Reactive oxygen species upregulate NOX4, but not NOX2, in endothelial cells. *Journal of Vascular Research*, Vol. 42/S2, 2005. 3<sup>rd</sup> European Meeting on Vascular Biology and Medicine, Hamburg, Germany, 28.09.05 – 30.09.05.

Petry A, Djordjevic T, Weitnauer M, BelAiba RS, Hess J, Görlach A. Multiple NOX proteins mediate the proliferative response in endothelial cells. 4. Symposium des DFG Graduiertenkollegs "Vascular Biology in Medicine", Herrsching a. Ammersee, 10.11. – 11.11.07.

Petry A, Djordjevic T, Weitnauer M, BelAiba RS, Hess J, Görlach A. Multiple NOX proteins mediate the proliferative response in endothelial cells. *Acta Physiologica* 2006; Volume 186, Supplement 650 :PM07A-7. Joint Meeting of The German Society of Physiology and The Federation of European Physiological Societies 2006, Munich, 26.03.2006-29.03.2006

Petry A, Diebold I, Schafer N, Hess J, Gørlach A. Thrombin activates NOX1 involving Gi and Rac1 in pulmonary artery smooth muscle cells. The 88th Annual Meeting of The German Physiological Society, Giessen, 22.03.2009-25.03.2009

Petry A, Diebold I, Schäfer N, Hess J, Gørlach A. Thrombin activates NOX1 involving  $G\alpha_i$  and Rac1 in pulmonary artery smooth muscle cells. 75. Jahrestagung der Deutschen Gesellschaft für Kardiologie, Mannheim, 16.04.2009 – 18.04.2009

### Poster presentations

Petry A, Djordjevic T, BelAiba RS, Bonello S, Acker H, Hess J, Gørlach A: The NADPH oxidase subunit p22phox is regulated by a redox-sensitive pathway in endothelial cells. 4th International Conference on Peroxynitrite and Reactive Nitrogen Species in Biology and Medicine, University of Konstanz, 27.07.04 – 31.07.04.

Djordjevic T, Petry A, Bickel C, Bonello S, BelAiba RS, Acker H, Pfeilschifter J, Gørlach A: Interaction of P22phox With NOX2 Or NOX4 Results in ROS Production And Proliferation Of Endothelial Cells. Supplement to Circulation Vol. 110/17; American Heart Association, Scientific Sessions 2004, New Orleans LA, 07.11.04 – 10.11.04.

Petry A, DjordjevicT, Weitnauer M, BelAiba RS, Hess J, Gørlach A: Multiple NOX proteins mediate the proliferative response in endothelial cells. The German Society of Physiology, Joint Meeting, München, 26.03 - 29.03.06.

Petry A, Djordjevic T, Weitnauer M, BelAiba RS, Diemer K, Hess J, Gørlach A. Multiple NOX Proteins Mediate the Proliferative Response in Endothelial Cells. J Vasc Res 2006;43:533-580; Annual Meeting of the German Society for Microcirculation and Vascular Biology. Munich, Germany, 12.10. – 14.10.06.

Petry A, Diebold I, Schäfer N, Hess J, Gørlach A: Thrombin activates NOX1 involving  $G\alpha_i$  and Rac1 in pulmonary artery smooth muscle cells. Annual Meeting of the German Society for Microcirculation and Vascular Biology. Aachen, Germany, 25.09.08 – 27.09.08.

### Invited talks

A. Petry, T. Djordjevic, M. Weitnauer, R.S. BelAiba, J. Hess, A. Gørlach: Multiple NOX proteins mediate the proliferative response in endothelial cells. I. Beritashvili Physiological Institute, Georgian Academy of Sciences, Tbilisi, Georgia, 04.04.07.

## 7.5 Acknowledgements

First and foremost, I want to thank Prof. Dr. Agnes Görlach for providing the opportunity to perform this PhD thesis in her laboratories in Munich at the German Heart Center Munich. I am very thankful for her professional and personal support and the long, fruitful and inspiring discussions.

I am also very grateful to my supervisor at the Ludwig-Maximilians-Universität München, Prof. Dr. Angelika Vollmar who accepted me as an external PhD student. To her go many thanks for support and discussions during the different progress stages of my thesis.

I am very grateful to my former colleague Dr. Talija Djordjevic for her guiding, advice, kind support and motivating discussions especially in the initial stage of my work who initiates me in the art of ROS measurements as well as many other methods. I am indebted to her as well as to my former colleagues Dr. R. Siham Bel Aiba and Kerstin Diemer for kindly performing NOX5 RT-PCRs, angiogenesis assays and especially the immunohistochemistry assays.

All the work of my thesis could not be done without all the grateful help and hard work of all the other current and former members of the research group of Prof. Dr. A. Görlach. Many thanks go to all of the ExKK for their collaborative support and stimulating discussions: Sabine Becht, Christian Bickel, Steve Bonello, Karel Chalupsky, Isabel Diebold, Johanna Ebner, Monika Fuchs, Korinna Griesser, Shang You He, Damir Kracun, Renaud Quillet, Florian Rieß, Gaby Römer, Michaela

Rößner, Tomasz Rzymiski, Karim Sabrane, Thomas Schwend, Amrei Steinhoff, Michael Weitnauer, Stefan Würth and Christian Zähringer.

I am also thankful to the AG Maßberg for helpful support of supplies, to the members of AG Koch for nice discussions to bring one on other thoughts and to the “morning-coffee round” Monika, Birgit, Sabine and Christina.

Deepest thanks go to all who invested time and effort in helping me in correcting and finalizing this work, especially Cristina Valcu, Katharina Reger, Andrea Buchstaller and my dear friend Silke Karl, without your help this work would never be done, thank you all so much! Many thanks also for all the chocolates, cookies and strange fruits!

I also want to thank my friends for their encouragement, especially Patrick, Eva, Steffi and Claudia for giving moral support and always having an open ear, and of course I want to thank the little “Quälgeist” Karin for motivating and for her friendship.

Eventually, I want to thank my family for all their love and constant support provided throughout my entire life.

## 7.6 Overview of used cloning PCR programs

### p22phoxYN:

Enzyme	Pfu (Bioron)	
Total volume	50 $\mu$ l	
Buffer (10x)	5 $\mu$ l	
F-primer (10pmol/ $\mu$ l)	1 $\mu$ l	
R-primer (10pmol/ $\mu$ l)	1 $\mu$ l	
dNTP (5mmol/ $\mu$ l)	2 $\mu$ l	
Template	25 ng	
Enzyme	1 $\mu$ l	
Add H <sub>2</sub> O	50 $\mu$ l	
Template	pcDNA6CFPp22phox	
Temperature ( $^{\circ}$ C)	Time (min)	Cycles
94	1:00	1
94	1:00	27
55	1:00	
72	1:00	
72	5:00	1
8	$\infty$	1

### NOX2YC, NOX5SYC

Enzyme	HF Kit (Roche)	
Total volume	25 $\mu$ l	
Buffer (10x)	5 $\mu$ l	
F-primer (10pmol/ $\mu$ l)	0.5 $\mu$ l	
R-primer (10pmol/ $\mu$ l)	0.5 $\mu$ l	
dNTP (5mmol/ $\mu$ l)	1.5 $\mu$ l	
Template	25 ng	
Enzyme	0.4 $\mu$ l	
Add H <sub>2</sub> O	25 $\mu$ l	
Template	pcDNA6CFPgp91phox pGEX3xNOX5S	

Temperature (°C)	Time (min)	Cycles
95	1:00	1
95	1:00	27
59	1:00	
72	1:45	
72	7:00	1
8	∞	1

### pEGFP-NOX4, pEYFP-NOX4

Enzyme	HF Kit (Roche)
Total volume	25 µl
Buffer (10x)	5 µl
F-primer (10pmol/µl)	0.5 µl
R-primer (10pmol/µl)	0.5 µl
dNTP (5mmol/µl)	1.5 µl
Template	0.3 µg
Enzyme	0.4 µl
Add H <sub>2</sub> O	25 µl

Template pCMV-NOX4YC

Temperature (°C)	Time (min)	Cycles
95	1:00	1
95	1:00	26
59	1:00	
72	2:10	
72	7:00	1
8	∞	1